19 Fluorescence Sensing

Fluorescence sensing of chemical and biochemical analytes is an active area of research.[1–8] These efforts are driven by the desire to eliminate the use of radioactive tracers, which are costly to use and dispose of. There is also a need for rapid and low-cost testing methods for a wide range of clinical, bioprocess, and environmental applications. During the past decade numerous methods based on high-sensitivity fluorescence detection have been introduced, including DNA sequencing, DNA fragment analysis, fluorescence staining of gels following electrophoretic separation, and a variety of fluorescence immunoassays. Many of these analytical applications can be traced to the early reports by Undenfriend and coworkers,[9] which anticipated many of today's applications of fluorescence. The more recent monographs[6–8] have summarized the numerous analytical applications of fluorescence.

Why is fluorescence rather than absorption used for high-sensitivity detection? Fluorescence is more sensitive because of the different ways of measuring absorbance and fluorescence. Light absorbance is measured as the difference in intensity between light passing through the reference and the sample. In fluorescence the intensity is measured directly, without comparison with a reference beam. Consider a 10^{-10} M solution of a substance with a molar extinction coefficient of 10^5 M^{-1} cm^{-1}. The absorbance will be 10^{-5} per cm, which is equivalent to a percentage transmission of 99.9977%. Even with exceptional optics and electronics, it will be very difficult to detect the small percentage of absorbed light, 0.0023%. Even if the electronics allow measurement of such a low optical density, the cuvettes will show some variability in transmission and surface reflection, which will probably exceed the intensity difference due to an absorbance of 10^{-5}. In contrast, fluorescence detection at 10^{-10} M is readily accomplished with most fluorometers. This advantage is due to measurement of the fluorescence relative to a dark background, as compared to the bright reference beam in an absorbance measurement. It is relatively easy to detect low levels of light, and the electronic impulses due to single photons are measurable with most photomultiplier tubes.

In this chapter we describe the various approaches to fluorescence sensing, which include essentially all the phenomenon discussed in previous chapters. Fluorescence sensing is described mostly within the framework of the medical applications, but it is clear that fluorescence detection is also widely used in biochemical, chemical, environmental and forensic analysis.

19.1. OPTICAL CLINICAL CHEMISTRY AND SPECTRAL OBSERVABLE

One long-range goal of fluorescence sensing is noninvasive monitoring of clinically relevant species and physiological parameters (Figure 19.1). A suitable portable device would measure the clinical values of interest, then store and/or transmit them to the physician. At present we are rather distant from the ultimate goal of noninvasive testing with devices similar to cell phones. The limitation is not in optics or electronics, but rather due to the lack of stable and biocompatible methods of in-vivo sensing. It is already possible to measure fluorescence through skin, and the measurements can accurately return pH and ion concentrations. In the near term we are likely to see devices similar to PDAs (Figure 19.2) that contain the chemistry and optics needed to perform clinical assays using body fluid samples. Such portable devices would find widespread usefulness, especially in emergency situations. The sensor array could be exposed to blood, and the results would be immediately available. This concept of rapid point-of-care clinical chemistry is driving the rapid development of numerous fluorescence sensing devices. In the following sections we describe the principles of fluorescence sensing, and illustrate how such devices can provide analytical data.

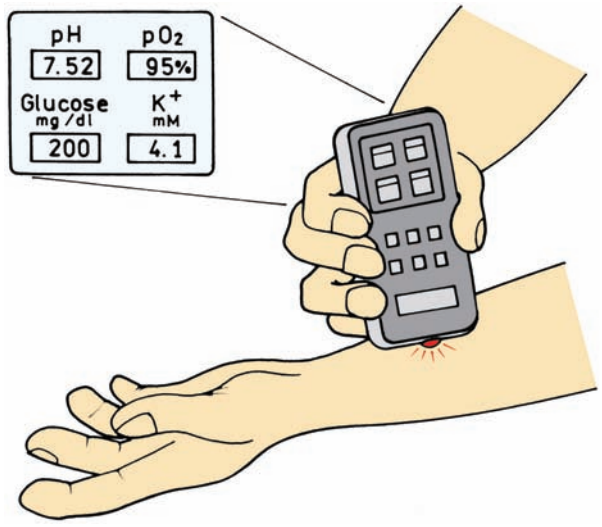

Figure 19.1. Optical clinical chemistry and noninvasive monitoring of physiological parameters.

19.2. SPECTRAL OBSERVABLES FOR FLUORESCENCE SENSING

The fluorescence intensity can be used to measure the concentration of the fluorescent species. In the present chapter sensing is understood in a different context. The goal is to measure the concentration of some analyte, not the amount of fluorophore. In the case of blood gases these analytes are pH, pCO_2, and pO_2. Blood electrolytes include Na^+, K^+, Ca^{2+}, Mg^{2+} and Cl^-, and many additional analytes that are measured in the clinical laboratory.[10,11] Fluorescence sensing requires a change in a spectral property response to the analyte. Changes can occur in the intensity, excitation spectrum, emission spectrum, anisotropy, or lifetime of the sensing probe.

The most direct sensing method is when the fluorescence intensity of the probe changes in response to the analyte (Figure 19.3, left). Such changes often occur for fluorophores that are subject to collisional quenching by a relevant species, such as oxygen. While conceptually simple, collisional quenching is only useful with a few clinically relevant analytes. It is often inconvenient or unreliable to use intensity changes, which can occur for a wide variety of reasons. For instance, the use of fiber optics is desirable as a means to locate the sensor at the site of interest, and to have the light source and detector remotely located.[12] However, it is difficult to perform quantitation intensity measurements through fibers. Fluorescence microscopy is another instance where intensity measurements are difficult. It is not possible to control the fluorophore concentration at each location in the cell, and the local probe concentration changes continually due to diffusion and/or photobleaching. For such applications it is important to use measurements which are independent of fluorophore concentration. This can be accomplished using wavelength-ratiometric probes (Figure 19.3), which display shifts in the absorption or emission spectra upon binding of the analyte. Wavelength-ratiometric probes are desirable because the ratios are independent of the probe concentration. The analyte concentration can then be determined from the ratio of fluorescent intensities measured at two excitation or emission wavelengths.

Another ratiometric method is fluorescence polarization or anisotropy. In this case the analyte causes a change in the anisotropy of the label. Anisotropy measurements are

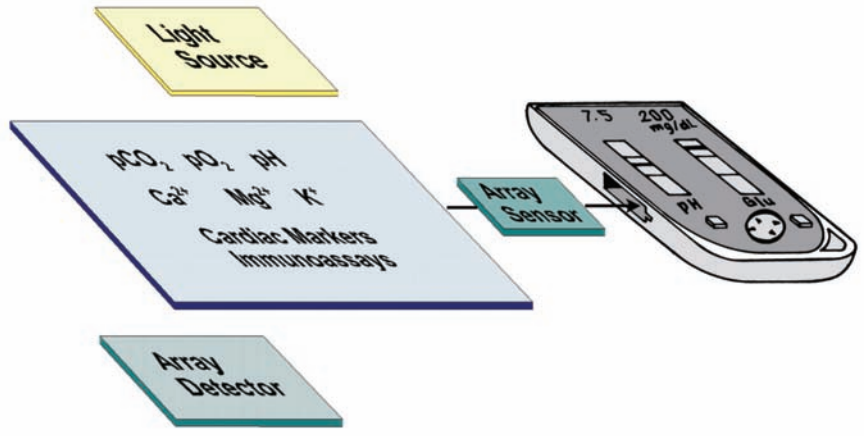

Figure 19.2. Fluorescence sensor for point-of-care testing.

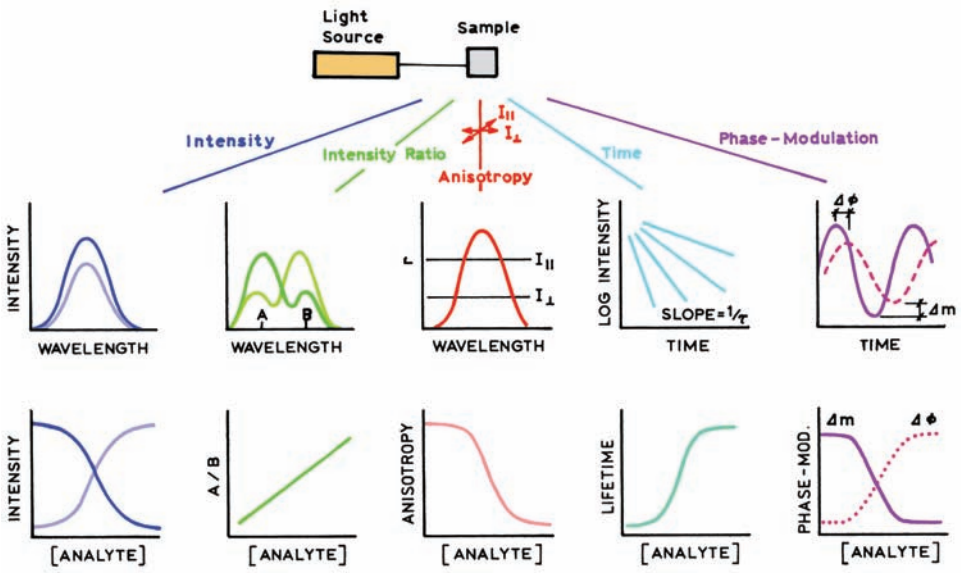

Figure 19.3. Spectral observables for fluorescence sensing. From left to right, sensing is performed using intensities, intensity ratios, anisotropies, time-domain lifetimes, and phase-modulation measurements.

frequently used in competitive immunoassays, in which the actual analyte displaces labeled analyte that is bound to specific antibody. This results in a decrease in the anisotropy. Anisotropy values are calculated using the ratio of polarized intensity measurements. The use of an intensity ratio makes the anisotropy measurements independent of fluorophore concentration as long as the measurements are not distorted by autofluorescence or poor signal-to-noise.

Fluorescence lifetimes can also be used for sensing (Figure 19.3). The lifetimes can be measured using either time-domain (TD) or frequency-domain (FD) methods. A few years ago lifetime measurements were regarded as too complex for sensing applications. However, advances in electrooptics technology now make it feasible to perform nanosecond decay time measurements using small inexpensive instruments. The use of lifetimes for sensing may be the next step in making sensors that display the long-term stability needed in real-world applications.[13–16]

19.2.1. Optical Properties of Tissues

The design of fluorescence probes for clinical applications is determined in part by the optical properties of water and tissues.[17] In general, the autofluorescence from tissues or any biological sample is lower for longer excitation wavelengths. The use of longer wavelengths also avoids light absorption by hemoglobin and melanin (Figure 19.4). In the past there has been a limited number of fluorophores that emit at long wavelengths. At present there is a growing number of fluorophores that emit between 700 and 1000 nm. This range is useful because water absorption increases above 1000 nm. The region of low absorption from 600 to 1000 nm is sometimes called the therapeutic range. Fortunately, a variety of lasers and solid-state lasers are available for excitation in this range of wavelengths.

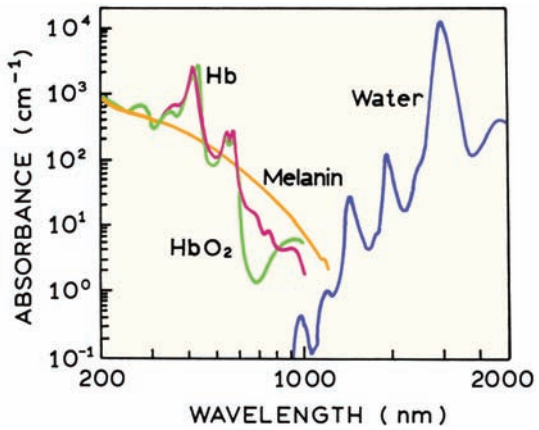

Figure 19.4. Optical absorbance of tissues and water. Hb, hemoglobin. Revised and reprinted with permission from [17]. Copyright © 1996, Annual Reviews.

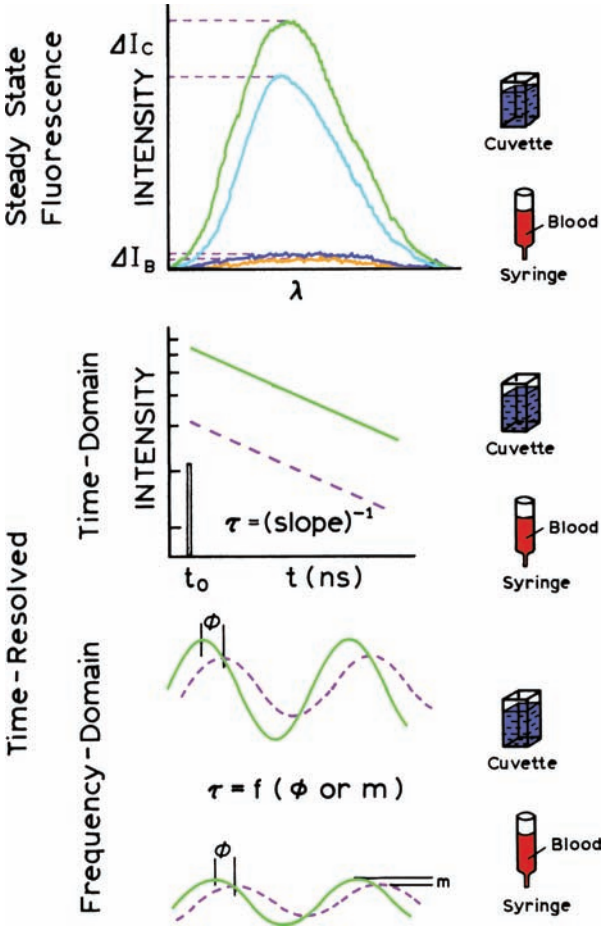

Figure 19.5. Intensity, time-domain, and frequency-domain sensing. In the top panel ΔI_B is that obtained from measurements of blood in a syringe and ΔI_C the value observed from a cuvette.

19.2.2. Lifetime-Based Sensing

Prior to describing the various mechanisms of sensing, it is useful to expand on the use of decay-time measurements for sensing (Figure 19.5). In the research laboratory, where clean cuvettes and optical surfaces are easy to maintain, intensity measurements can be accurate and reproducible (top panel in Figure 19.5). However, suppose that the sample is blood, which is contained in a translucent syringe. The intensity will be decreased by the absorbance of the blood and by the scattering properties of the syringe, and it may be difficult to obtain a reliable intensity-based calibration. Now consider lifetime instead of intensity measurements (middle panel in Figure 19.5). If the intensity is large enough to measure, the intensity decay is the same independent of attenuation of the signal. Similarly, if the lifetime is measured by phase or modulation (bottom panel), the values are expected to be independent of intensity.

Lifetime-based sensing is a means to avoid the difficulties of quantitative intensity measurements. Consider a sensing fluorophore placed on the end of an optical fiber that is used for oceanographic studies. The fiber will be flexing while being towed by the ship, resulting in intensity fluctuations. Additionally, the probe may be leaking from the tip, resulting in decreases in intensity. Quantitative intensity measurements would clearly be difficult under these conditions. Lifetime measurements have already been used for an oceanographic fiber optic oxygen sensor.[18]

19.3. MECHANISMS OF SENSING

Any phenomenon that results in a change of fluorescence intensity, wavelength, anisotropy, or lifetime can be used for sensing. The simplest mechanism to understand is collisional quenching, where the fluorophore is quenched by the analyte (Figure 19.6). Collisional quenching results in a decrease in the intensity or lifetime of the fluorophore, either of which can be used to determine the analyte concentration. Static quenching can also be used for sensing, but the lifetime would not change.

Resonance energy transfer (RET) is perhaps the most general and valuable phenomenon for fluorescence sensors (Figure 19.6, right). Any process that brings the donor and acceptor into close proximity will result in a decrease in the donor intensity and/or decay time. Since energy transfer acts over macromolecular distances, it can be used to detect association of proteins as occurs in immunoassays. However, the applications of RET are not limited to detection of protein association. RET has also been used as the basis for pH and cation sensors. Sensors were developed that contain acceptors whose absorption spectra are dependent on pH. A change in pH results in a change in absorbance of the acceptor, which in turn alters the donor intensity.

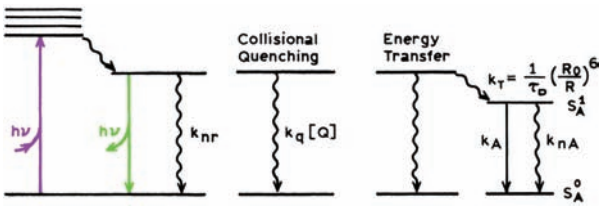

Figure 19.6. Modified Jablonski diagram for the processes of absorption and fluorescence emission (left), dynamic quenching (middle), and resonance energy transfer (RET) (right).

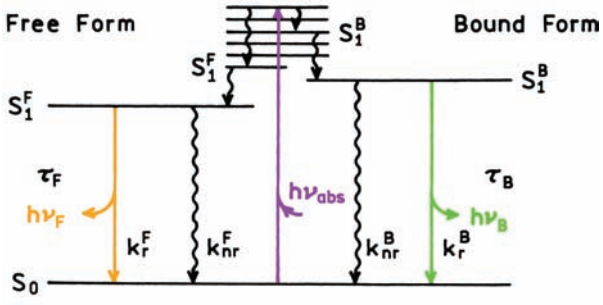

Figure 19.7. Jablonski diagram for the free (F) and bound (B) forms of a sensing probe. From [13].

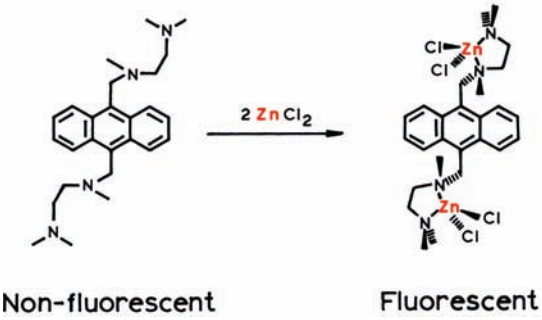

Figure 19.8. A zinc probe based on photoinduced electron transfer. Revised from [21].

Another mechanism for sensing is available when the fluorophore can exist in two states, if the fractions in each state depend on the analyte concentration (Figure 19.7). Typically there is equilibrium between the fluorophore free in solution and the fluorophore bound to analyte. One form can be nonfluorescent, in which case emission is only seen in the absence or presence of analyte, depending on which form is fluorescent. Probes that act in this manner are not wavelength-ratiometric or lifetime probes. Alternatively, both forms may be fluorescent but display different quantum yields or emission spectra. This type of behavior is often seen for pH probes, where ionization of the probe results in distinct absorption and/or emission spectra. Spectral shifts are also seen for probes that bind specific cations such as calcium. Such probes allow wavelength-ratiometric measurements. In this case the change in intensity or shift in the emission spectrum is used to determine the analyte concentration. Probes that bind specific analytes are often referred to as probes of analyte recognition.[19]

There are many mechanisms that can be used to design probes that exhibit changes in fluorescence in response to analytes. Fluorescence probes can form twisted intramolecular charge-transfer (TICT) states.[20] Another mechanism is photoinduced electron transfer (PET), which has been used to develop sensors for metal ions.[21–23] These sensors often rely on the well known quenching by amines due to PET. Figure 19.8 shows a PET-based zinc sensor. In the absence of zinc the anthracene is quenched by exciplex formation with the amino groups. Upon binding of zinc, the nitrogen lone pair of electrons is no longer available for PET. As a result charge transfer no longer occurs, and the anthracene becomes fluorescent.[21] While the mechanism of this particular sensor is understood, this is not true of all sensors. In many cases spectral changes are seen but the mechanism is not certain. In the following sections we describe examples of each type of sensor (collisional, RET or analyte recognition).

19.4. SENSING BY COLLISIONAL QUENCHING

19.4.1. Oxygen Sensing

Use of collisional quenching as the sensing mechanism requires the fluorescent probe to be sensitive to quenching by the desired analyte. Collisional quenching results in a decrease in intensity and lifetime, which is described by the Stern-Volmer equation:

$$\frac{F_0}{F} = \frac{\tau_0}{\tau} = 1 + k_q\tau_0[Q] = 1 + K[Q] \qquad (19.1)$$

In this equation $F_0(\tau_0)$ and $F(\tau)$ are the intensities (lifetimes) in the absence and presence of the quencher, respectively, K is the Stern-Volmer quenching constant, and k_q is the bimolecular quenching constant. The most obvious application of collisional quenching is oxygen sensing. In order to obtain sensitivity to low concentrations of oxygen, fluorophores are typically chosen that have long lifetimes in the absence of oxygen (τ_0). Long lifetimes are a property of transition metal complexes[24] (Chapter 20), and such complexes have been frequently used in oxygen sensors.[25–31] For use as an oxygen sensor the metal–ligand complexes (MLCs) are usually dissolved in silicone, in which oxygen is rather soluble and freely diffusing. The silicone also serves as a barrier to prevent other interfering molecules from interactions with the fluorophores and affect the intensity or lifetime.

The high sensitivity of the long-lifetime MLCs to oxygen is shown by the Stern-Volmer plots (Figure 19.9). The compound $[Ru(Ph_2phen)_3]^{2+}$ is more strongly quenched

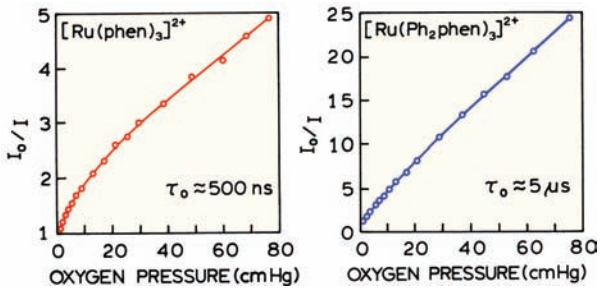

Figure 19.9. Stern-Volmer plots for oxygen quenching of $[Ru(phen)_3]^{2+}$ and $[Ru(Ph_2phen)_3]^{2+}$ in GE RTV 118 silicon. Phen is 1,10-phenanthroline; ph_2phen is 4,7-diphenyl-1,10-phenanthroline. Revised from [24].

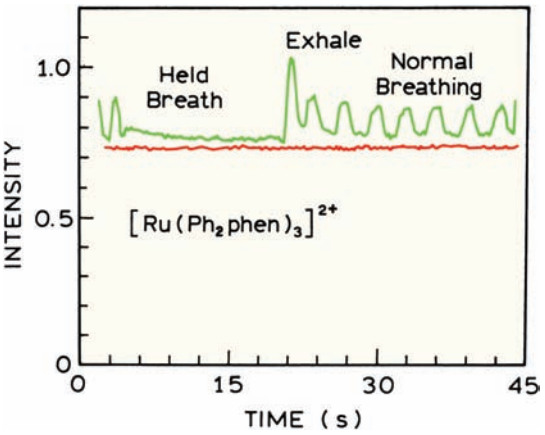

Figure 19.10. Luminescence intensity of an oxygen sensor with $[Ru(Ph_2phen)_3]^{2+}$ as the probe, when exposed to breathing. Revised from [24].

than $[Ru(phen)_3]^{2+}$. The difference in sensitivity is due to the longer unquenched lifetime (τ_0) of the diphenyl derivative, and thus the larger Stern-Volmer quenching constant (eq. 19.1). These long-lifetime probes have been used in real-time oxygen sensors. For example, Figure 19.10 shows the intensity of $[Ru(Ph_2phen)_3]^{2+}$ in silicone while exposed to exhaled air. The intensity increases with each exhale because of the lower O_2 and higher CO_2 content of the exhaled air. The higher intensity on the first exhale after the breath was held is due to the lower O_2 content in the air that was retained longer in the lungs. The oxygen sensitivity of the sensor can be adjusted by selecting probes with different lifetimes or by modifying the chemical composition of the supporting media. The sensitivity to oxygen can be increased by using MLCs with longer lifetimes, some of which are as long as 50 μs.[32]

19.4.2. Lifetime-Based Sensing of Oxygen

For practical sensing applications the device must be simple and inexpensive, which is possible using the long-lifetime MLCs. The oxygen-sensitive MLCs in Figure 19.9 absorb near 450 nm, and are thus easily excited with blue light-emitting diodes (LEDs). One simple oxygen sensor device is shown in Figure 19.11. Because of the long decay times and simple instrumentation, oxygen sensors were used to demonstrate the stability of phase-angle sensing in the presence of large-amplitude intensity fluctuations.[33] The intensity was varied by waving fingers in the light path, resulting in fivefold changes in intensity (Figure 19.11). In contrast to the measured intensities measurements, the phase angles remained constant.

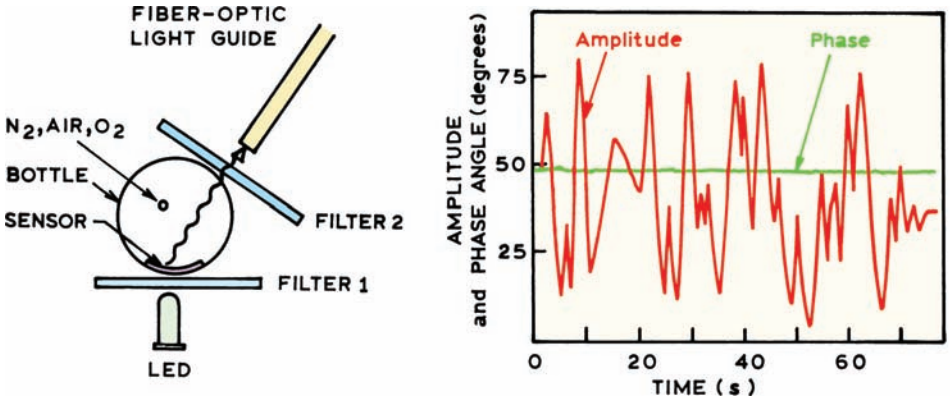

Figure 19.11. Phase-angle stability with intensity fluctuations measured with an oxygen-sensing device. The amplitude of the incident light was varied by waving fingers between the LED and the sensor. Revised from [33].

Lifetime-based sensing is valuable for probes that are subject to collisional quenching and do not display wavelength-ratiometric behavior. The capability for ratiometric measurements can be designed into oxygen sensors by including a nanosecond-lifetime fluorophore in the supporting media. This fluorophore can provide a reference that is not sensitive to the oxygen concentration. For in-vivo applications MLCs are known to have longer absorption and emission wavelengths.[34] These MLCs have been used to measure lifetimes and oxygen concentrations through skin.[35]

19.4.3. Mechanism of Oxygen Selectivity

An important consideration for any sensor is selectivity. For oxygen, the selectivity is provided by a unique combination of the fluorophore and the supporting media. Almost all fluorophores are collisionally quenched by oxygen, so that no fluorophore is completely specific for oxygen. However, the extent of quenching is proportional to the unquenched lifetime τ_0 (eq. 19.1). For fluorophores in aqueous solution with decay times under 5 ns, the extent of quenching by dissolved oxygen from the atmosphere is negligible. Hence, one reason for the apparent oxygen selectivity of $[Ru(Ph_2phen)_3]^{2+}$ is its long lifetime near 5 µs, which results in extensive quenching by atmospheric oxygen.

Selectivity of the MLC oxygen sensor is also due to the silicone support. Silicone is impermeable to most polar species, so most possible interferants cannot penetrate the silicon to interact with the probe. Fortunately, oxygen dissolves readily in silicon, so that the support is uniquely permeable to the desired analyte. Finally, there are no other substances in air which act as collisional quenchers. NO is also a quencher but is not usually found in the air. Hence, the sensor is selective for O_2 because of a combination of the long lifetime of the MLC probe and the exclusion of potential interferants from the nonpolar silicone support.

19.4.4. Other Oxygen Sensors

While $[Ru(Ph_2phen)_3]^{2+}$ is the most commonly used fluorophore in oxygen sensors, other probes are available. Almost any long-lived fluorophore can be used as an oxygen sensor, particularly when dissolved in an organic solvent. Because of the long decay times, phosphorescence can be used to detect oxygen. For many applications, such as oxygen sensing in blood or through skin, it is useful to have probes that can be excited with red or NIR wavelengths. Several porphyrin derivatives are known that display oxygen-sensitive phosphorescence.[36–37] One example is platinum (II) octaethylporphyrin ketone (Figure 19.12), which can be excited at 600 nm. This molecule shows a surprisingly large Stokes shift, with the emission maximum at 758 nm. The lifetime of 61.4 µs results in oxygen-sensitive emission even when the probe is embedded in polystyrene.

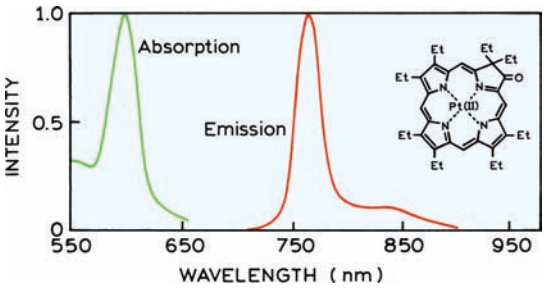

Figure 19.12. Absorption and emission spectra of a phosphorescent porphyrin ketone. Revised and reprinted with permission from [36]. Copyright © 1995, American Chemical Society.

Simple instrumentation can be constructed for lifetime-based sensing with long-lifetime emitters. Figure 19.13 (top) shows a schematic for a simple device for lifetime-based sensing of oxygen.[38] The fluorophore is platinum (II)

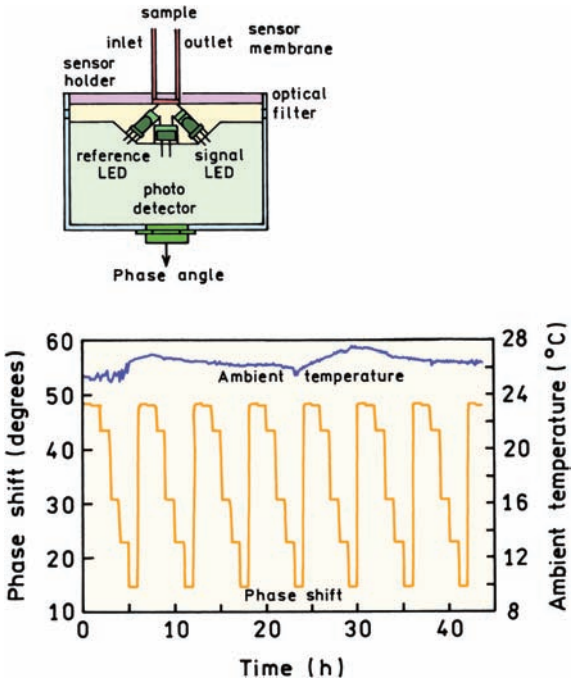

Figure 19.13. Lifetime-based sensing of oxygen using platinum (II) octaethylporphyrin ketone in a polymer membrane. The light modulation frequency is 3907 Hz. The gaseous oxygen concentrations were 0, 0.1, 5.1, 9.96, and 20.55%. Revised from [39].

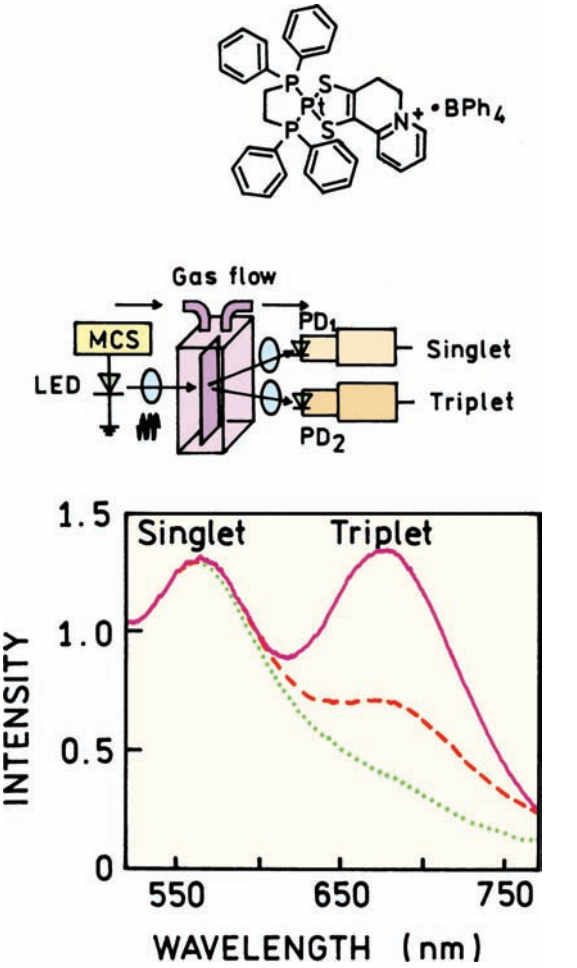

Figure 19.14. Oxygen sensing using a platinum complex in a polymeric film. Revised from [39].

octaethylporphyrin ketone in a polymer film, which displays an unquenched lifetime in the range of 40–60 μs. The excitation source is an amplitude-modulated LED. The electronics measures the phase angle of the emission relative to the excitation, using separate detectors for the excitation and emission. The phase angles are highly sensitive to the oxygen concentration, and are stable over long periods of time. Reasonable amounts of photobleaching or continuity drifts would not affect the phase angle measurements.

Wavelength-ratiometric measurements are usually not possible with collisonally quenched probes. One interesting exception is the platinum complex shown in Figure 19.14. This compound displays both a singlet emission near 560 nm and a triplet emission near 670 nm, with lifetimes of 0.5 ns and 14 μs, respectively.[39] The emission intensity of the long-lived emission is sensitive to oxygen and the short lifetime emission is not sensitive to oxygen (lower panel). A simple solid-state device can be used to measure the ratios of emission intensities at 560 and 670 nm, and thus the oxygen concentration.

19.4.5. Lifetime Imaging of Oxygen

Molecules that display dual emission (Figure 19.14) are highly unusual, and there are not many opportunities for wavelength-ratiometric oxygen sensing. One method to make measurements that are mostly independent of intensity is to use fluorescence lifetime imaging microscopy (FLIM),[40–41] which is described in Chapter 22. In FLIM the contrast in the image is based on the lifetime at each point in the sample and not on the emission intensity. Figure 19.15 shows images of bronchial epithelial cells labeled with $[Ru(bpy)_3]^{2+}$, which in the oxygen-free samples displays a lifetime near 600 ns.[42–43] The intensity image on the left reveals the local concentration and/or quantum yield of the probe in the cells. The image on the right shows the lifetimes in each region of the sample. The lifetimes are essentially constant which indicates the oxygen concentration is constant throughout the cells. These lifetime images were calculated from images taken with a gated image intensifier and CCD camera.

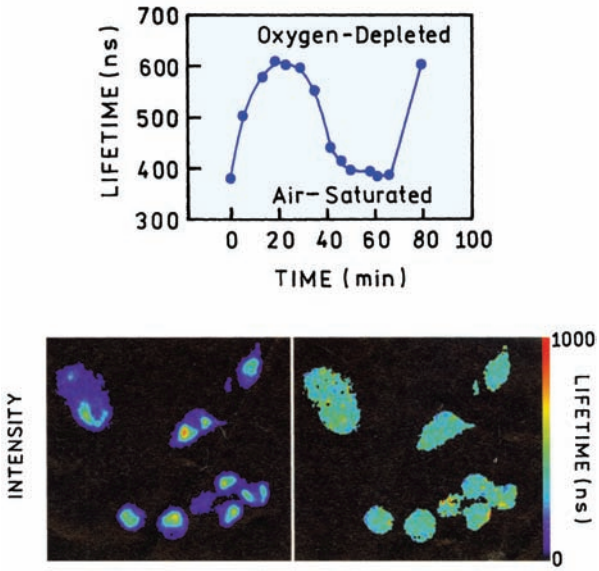

Figure 19.15. Fluorescence intensity and lifetime images of human bronchial epithelia cells labeled with $[Ru(bpy)_3]Cl_2$. Lifetime images were obtained using a gated image intensifier and a CCD camera. From [43].

Table 19.1. Spectral Properties of Representative Chloride Probes[a]

Compound[b]	λ_{abs} (nm)	λ_{em} (nm)	Quantum yield	K (M^{-1})
SPQ[c]	318/345	450	0.69	118[d]
SPA	–	–	–	5
Lucigenin	368/955	506	0.67	390
MACA	364/422	500	0.64	225
MAMC	366/424	517	0.24	160

[a]From [49].
[b]Abbreviations: lucigenin, N,N,N-dimethyl-9,9'-bisacridium nitrate; SPQ, 6-methoxy-*N*-(3-sulfopropyl)quinolinium; SPA, N-sulfopropylacridium; MACA, N-methylacridium-9-carboxamide; MAMC, N-methylacridium-9-methylcarboxylate.
[c]The unquenched lifetime of SPQ is 26 ns.
[d]The Stern-Volmer constant in cells is 13 M^{-1}. From [51].

19.4.6. Chloride Sensors

It is well known that heavy atoms like bromine and iodine act as collisional quenchers. For sensing applications chloride is more important because it is prevalent in biological systems. However, chloride is a less effective quencher, and relatively few fluorophores are quenched by chloride. A hint for developing chloride-sensitive probes was available from the knowledge that quinine is quenched by chloride. Quinine contains a quinolinium ring, which can be used to make a variety of chloride-sensitive probes.[44–48] Representative structures are shown in Figure 19.16. It is evident from the Stern-Volmer plots in Figure 19.17 that the quinolines are not equally sensitive to chloride, and that the quenching constant depends on the chemical structure (Table 19.1).

These chloride-sensitive probes can be used to measure chloride transport across cell membranes (Figure 19.18). Erythrocyte ghosts are the membranes from red blood cells

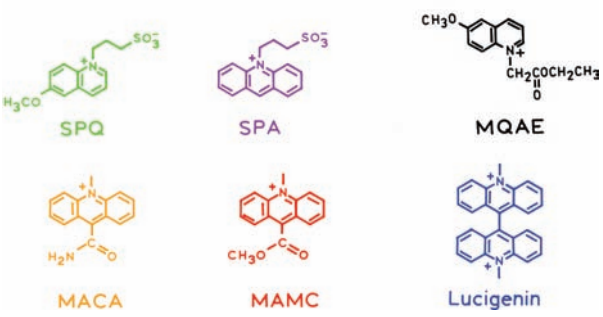

Figure 19.16. Representative chloride probes. These probes are collisionally quenched by chloride (Table 19.1). Revised and reprinted with permission from [49]. Copyright © 1994, Academic Press Inc.

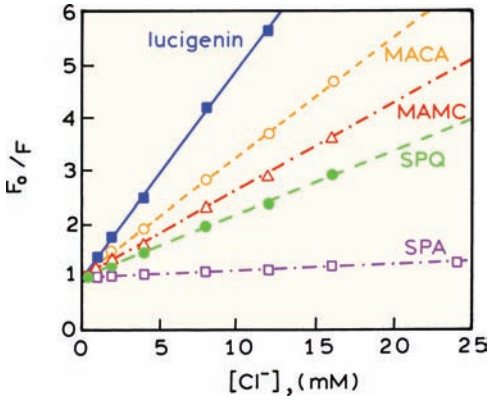

Figure 19.17. Stern-Volmer plots for chloride quenching of SPQ, SPA, lucigenin, MACA, and MAMC. See Table 19.1. Revised and reprinted with permission from [49]. Copyright © 1994, Academic Press Inc.

following removal of the intracellular contents. The ghosts were loaded with SPQ and 100 mM chloride. The ghosts were then diluted into a solution of 66 mM K_2SO_4. Sulfate does not quench SPQ. When diluted into sulfate-containing buffer the intensity of SPQ increased due to efflux of the chloride. This transport is due to an anion exchange pathway. Chloride transport could be blocked by dihydro-4,4'-diisothiocyanostilbene-2,2'-disulfonic acid (H_2DIDS), which is an inhibitor of anion transport. Hence, the chloride probes can be used for physiological studies of ion transport.

The chloride probes are subject to interference. They are also quenched by bromide, iodide, and thiocyanate.[50]

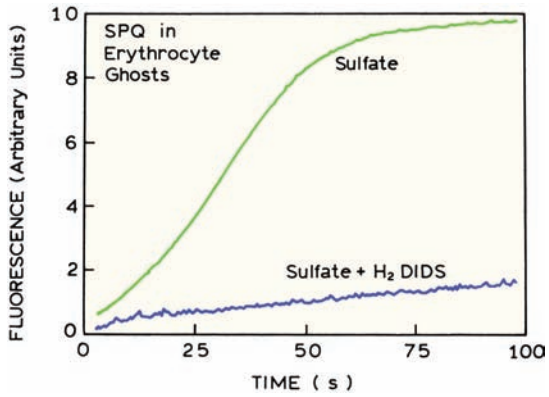

Figure 19.18. Fluorescence intensity of SPQ in erythrocyte ghosts as a function of time, reflecting chloride transport from the erythrocyte ghosts. The two curves are for SPQ-containing erythrocyte ghosts diluted into sulfate-containing buffer in the absence and in the presence of an anion-transport inhibitor (H_2DIDs). Revised and reprinted with permission from [46]. Copyright © 1987, American Chemical Society.

Perhaps more importantly, SPQ is quenched by free amines, which can distort measurements in amine-containing buffers. In fact, the Stern-Volmer quenching constant of SPQ in aqueous solution is 118 M^{-1}, whereas in cells the quenching constant is near 13 M^{-1}. This decrease has been attributed to quenching of SPQ by non-chloride anions and proteins in cells.[51] Quenching of SPQ by amines was turned into an opportunity, by using the quenching caused by the amine buffers as an indicator of pH.[50] As the pH increases, more of the buffer is in the free amine form, resulting in a decrease in the intensity of SPQ. A disadvantage of the chlorine probes is that they are not ratiometric probes. Some of the probes leak out of cells, decreasing the intensity and preventing accurate measurements of the chloride concentration. The quinoline probes have been made into wavelength-ratiometric probes by linking them to a chloride-insensitive fluorophore using dextran or a flexible chain.[52–53]

19.4.7. Lifetime Imaging of Chloride Concentrations

The need for covalently linked chloride-sensitive and -insensitive probes can be avoided by lifetime imaging. Since chloride is a collisional quencher, the decreases in lifetime are proportional to the decreases in intensity (Figure 19.17). FLIM of the chloride probe 6-methoxy-quinolyl acetoethyl ester (MQAE) was used to determine the concentrations of chloride in olfactory epithelium.[54] In this tissue the olfactory sensory neurons penetrate through supporting epithelial cells, terminating in dendritic knobs (Figure 19.19). The transduction mechanism for olfactory signal transduction involves an influx of calcium and an efflux of chloride. For this to occur the olfactory dendrites must accumulate higher concentrations of chloride than the surrounding tissue. Lifetime measurements of MQAE in this tissue revealed a shorter lifetime of MQAE in the dendrite knob than in the supporting cells, which indicates a higher chloride concentration in the knobs. Lifetime images were obtained using laser scanning microscopy and two-photon excitation (Chapter 18). Intensity decays were recorded by TCSPC at each point in the image. A calibration curve for the lifetime at various chloride concentrations was determined using a similar tissue and ionophore to control the intracellular chloride concentrations. Using this calibration it was possible to use the lifetime image to create a chloride concentration image in the olfactory tissue. This image shows higher chloride concentrations in the dendrites than in the surrounding tissue. This experiment was made possible by the advances in TCSPC (Chapter 4) and multiphoton microscopy.

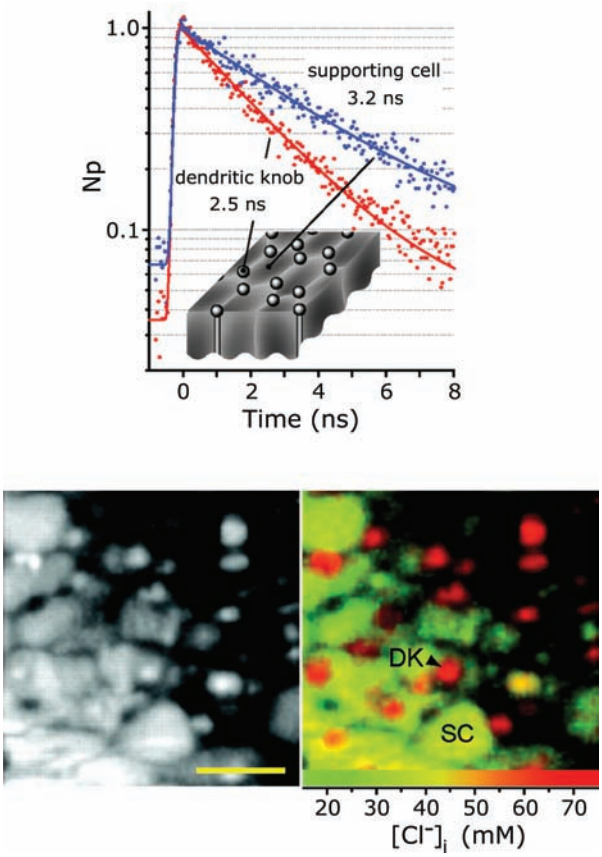

Figure 19.19. **Top**: Intensity decays of MQAE in the ends of the neuronal sensing cells (dendritic knob) or in the epithelial supporting cells. **Bottom**: The lower panels show the intensity (left) and chloride concentration image (right) of the olfactory epithelium. Reprinted with permission from [54]. Copyright © 2004, Journal of Neuroscience.

19.4.8. Other Collisional Quenchers

A wide variety of molecules can act as quenchers (Chapter 8), and they permit developments of sensors based on collisional quenching. Benzo(b)fluoranthene was found to be highly sensitive to sulfur dioxide.[55] Oxygen interfered with the measurements but was 26-fold less efficient as a quencher than SO_2. Halogenated anesthetics are known to quench protein fluorescence and can be detected by collisional quenching of anthracene and perylene.[56] Carbazole is quenched by a wide variety of chlorinated hydrocarbons.[57] NO, which serves as a signal for blood vessel dilation, is

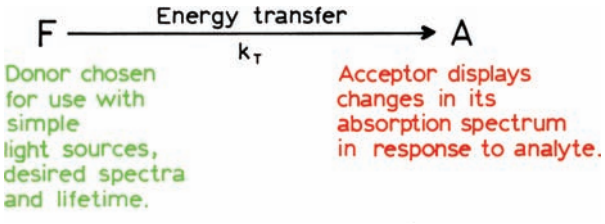

Figure 19.20. Principle of energy-transfer sensing.

also a collisional quencher.[58–59] However, physiologically relevant concentrations of NO are too low for significant collisional quenching. Fluorescent probes of NO usually react chemically with NO.[60–62]

19.5. ENERGY-TRANSFER SENSING

Resonance energy transfer (RET) offers many opportunities and advantages for fluorescence sensing. Energy transfer occurs whenever the donor and acceptor are within the Förster distance. Changes in energy transfer can occur due to changes in analyte proximity, or due to analyte-dependent changes in the absorption spectrum of acceptor (Figure 19.20). A significant advantage of RET-based sensing is that it simplifies the design of the fluorophore. For collisional quenching, or analyte recognition probes (Section 19.8), the probe must be specifically sensitive to these analytes. It is frequently difficult to obtain the desired sensitivity and fluorescence spectral properties in the same molecule. However, if RET is used, the donor and acceptor can be separate molecules (Figure 19.20). The donor can be selected for use with the desired light source, and need not be intrinsically sensitive to the analyte. The acceptor can be chosen to display a change in absorption in response to the analyte. Alternatively, an affinity sensor can be based on a changing concentration of acceptor around the donor due to the association reaction.

19.5.1. pH and pCO_2 Sensing by Energy Transfer

A wide variety of pH indicators are available from analytical chemistry. Since indicators are intended for visual observation, they display pH-dependent absorption spectra with absorption at visible wavelengths. These indicators have formed the basis for a number of RET-pH/pCO_2 sensors. One of the earliest reports used eosin as the donor and phenol red as the acceptor.[63] Phenol red was selected because it displays a pK_a near 7, and the basic forms absorb

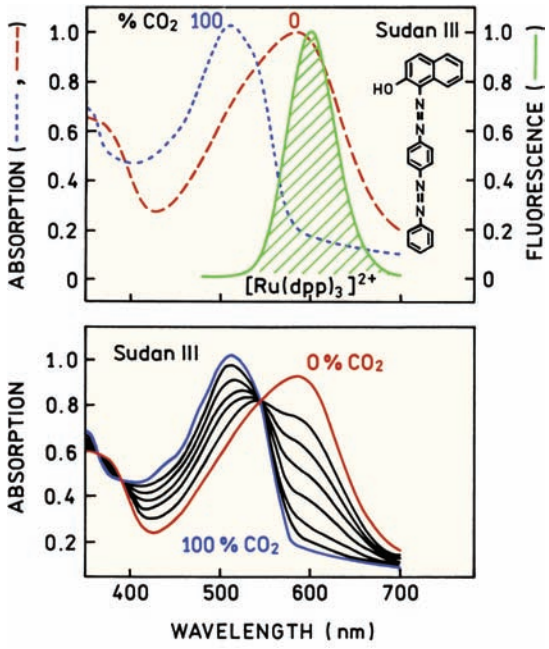

Figure 19.21. **Top**: Absorption spectra of Sudan III in the sensing matrix in the absence (0%) and presence (100%) of CO_2. The emission spectrum is for $[Ru(dpp)_3]^{2+}$. **Bottom**: CO_2-dependent absorption spectra of Sudan III. Revised from [69].

at 546 nm where eosin emits. Consequently, the eosin intensity decreased as the pH increased. In the case of this particular sensor it was not certain whether the decreased intensity was due to RET or to an inner filter effect, but it is clear that RET is a useful mechanism as the basis for designing sensors.

This same basic idea was used to create lifetime-based sensors for pH, pCO_2,[64–69] and ammonia.[70–73] Spectra for a representative sensor are shown in Figure 19.21. The donor was $[Ru(dpp)_3]^{2+}$, where dpp is 4,7-diphenyl-1,10-phenanthroline.[69] This donor was chosen for its long decay time, allowing lifetime measurements with an amplitude-modulated LED at 20 kHz. The acceptor was Sudan III, which displayed a CO_2-dependent absorption spectrum. This dependence on CO_2 was due to changes in pH in the polymeric media that contained the donor, acceptor, and buffering components. At low partial pressure of CO_2 the pH is high and Sudan III absorbs at the emission wavelength of the donor. As the partial pressure of CO_2 increases the long-wavelength absorption of Sudan III decreases.

This RET sensor could be used to measure the partial pressure of CO_2 (Figure 19.22). The apparent lifetime was measured from the phase angle of the $[Ru(dpp)_3]^{2+}$ emission. As the partial pressure of CO_2 increased the phase

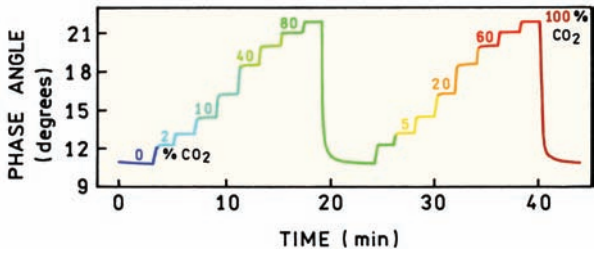

Figure 19.22. CO_2-dependent phase angles of $[Ru(dpp)_3]^{2+}$ in the sensor matrix containing Sudan III. The output of the LED was modulated at 20 kHz. Revised from [69].

angle increased, indicating an increase in the mean lifetime of $[Ru(dpp)_3]^{2+}$. The change in phase angle or lifetime showed that the partial pressure of CO_2 affected the extent of RET because inner filter effects are not expected to alter the lifetimes.

A critical point in sensor design is the support containing the probes. For the pCO_2 sensor, the support consisted of silica gel and ethylcellulose (EC). The EC contained tetraoctylammonium hydroxide (TOAH) which served as a phase transfer agent for the CO_2. These details are mentioned to show that careful consideration of the support and actual use of the sensor is needed to result in a useful device. Depending on the support and analyte it may be necessary to use phase transfer agents to facilitate uptake of the analyte into the supporting media.[74] Another important technique for fabricating sensors is the use of sol gels. The basic idea is the hydrolysis of tetraethylorthosilicate (TEOS, $Si(OC_2H_5)_4$) in a mixture of water and ethanol. As TEOS is hydrolyzed, it forms silica (SiO_2). Monoliths and glass films of silica can be formed at low temperatures with mild conditions. The porosity of the sol gels can be controlled, and fluorophores or even enzymes can be trapped within the sol gel matrix.[75–76] The result is a solid sensor which contains the trapped molecules.

19.5.2. Glucose Sensing by Energy Transfer

Control of blood glucose is crucial for the long-term health of diabetics.[77] Present methods to measure glucose require fresh blood, which is obtained by a finger stick. This procedure is painful and inconvenient, making it difficult to determine the blood glucose as frequently as is needed. Erratic blood glucose levels due to diabetes are responsible for adverse long-term problems of blindness and heart disease. These effects are thought to be due to glycosylation of protein in blood vessels. Consequently, there have been

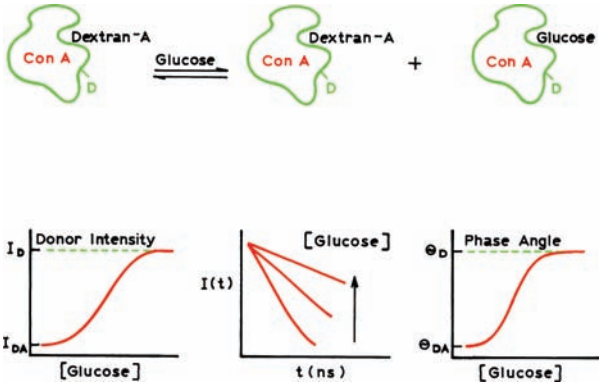

Figure 19.23. Glucose sensing by resonance energy transfer. Revised from [78].

numerous efforts to develop noninvasive methods to measure blood glucose.

Because of the medical need there have been continued efforts to develop a noninvasive means to measure blood glucose and to develop fluorescence methods to detect glucose. These have often been based on the glucose-binding protein concanavalin A (ConA) and a polysaccharide, typically dextran, which serves as a competitive ligand for glucose (Figure 19.23).[78–79] Typically, the ConA is labeled with

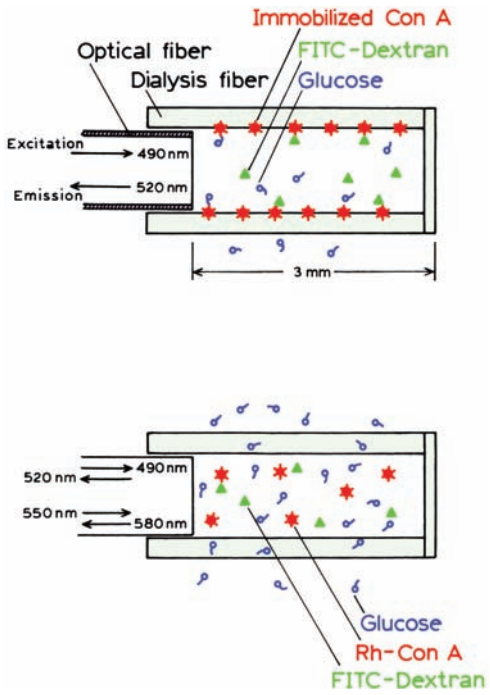

Figure 19.24. Resonance energy transfer sensor for glucose. Revised from [80].

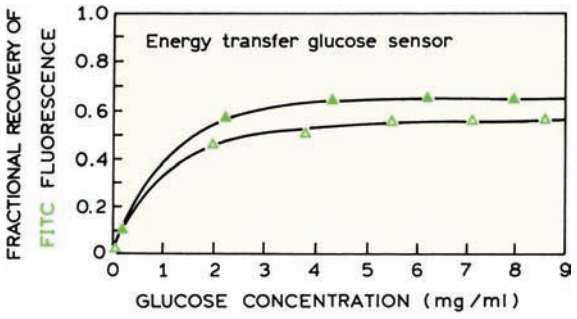

Figure 19.25. Recovery of FITC fluorescence during glucose titration for two weight ratios of Rh-ConA/FITC-dextran, 217 (▲) and 870 w/w (△). Revised from [81].

a donor (D) and the dextran with an acceptor (A), but the labels can be reversed. Binding of D-ConA to A-dextran results in a decrease in donor intensity or lifetime. The glucose in the sample competes for the glucose binding sites on D-ConA, releasing D-ConA from the acceptor. The intensity decay time and phase angles of the donor are thus expected to increase with increasing glucose concentration.

This principle was used in the first reports of glucose sensing by fluorescence intensities.[79–81] A fiber-optic glucose sensor was made using FITC-labeled dextran and rhodamine-labeled ConA (Figure 19.24). The acceptor could be directly excited as a control measurement to determine the amount of Rh-ConA. The response of this glucose sensor is shown in Figure 19.25. The donor and acceptor were placed on the dextran and ConA, respectively. The donor fluorescence was not completely recovered at high concentrations of glucose. This lack of complete reversibility is a problem that plagues ConA-based glucose sensors to the present day. It is hoped that these problems can be solved using alternative glucose binding proteins, especially those that have a single glucose binding site and may be less prone to irreversible associations. It seems probable that site-directed mutagenesis will be used to modify the glucose-binding proteins to obtain the desired glucose affinity and specificity.

As might be expected, lifetime-based sensing has been applied to glucose, and has been accomplished using nanosecond probes,[82] long-lifetimes probes,[83] and laser-diode-excitable probes.[84] The problem of reversibility has been addressed by using sugar-labeled proteins in an attempt to minimize crosslinking and aggregation of the multivalent ConA. Such glucose sensors are occasionally fully reversible,[84] but there is reluctance to depend on a system where reversibility is difficult to obtain.

19.5.3. Ion Sensing by Energy Transfer

Wavelength-ratiometric probes are available for Ca^{2+} and Mg^{2+}, but the performance of similar probes for Na^+ and K^+ is inadequate (Section 19.8.3). It is difficult to design probes for K^+ and Na^+ with the desired binding constant and selectivity, and that also display adequate spectral changes. These difficulties can be understood by considering a sensor for K^+. In blood the concentrations of K^+ and Na^+ are near 4.5 and 120 mM, respectively. A probe for K^+ must be able to bind K^+ selectively, and not be saturated by a 25-fold excess of Na^+. Given the similar chemical properties of Na^+ and K^+, and the smaller size of Na^+, such selectivity is difficult to achieve. These problems can be alleviated to some extent by making use of ionophores like valinomycin that display high selectivity for K^+. Valinomycin is a cyclic molecule that unfortunately does not contain any useful chromophoric groups. Consequently, one has to develop a sensor that transduces the binding of K^+ to result in a fluorescence spectral change.

One method to develop a K^+ sensor is to use a dye that displays a change in its absorption spectrum on ionization.[85] The sensor was fabricated using polyvinyl chloride, valinomycin, plus fluorescent beads (FluoSpheresJ, Molecular Probes, Eugene, OR). The acceptor is shown in Figure 19.26. When K^+ enters the membrane, KFU-111 loses a proton resulting is an increase in absorbance at 650 nm. This absorbance overlaps with the emission spectra of the FluoSpheresJ, resulting in a decreased intensity (Figure 19.27). As the K^+ concentration is increased the FluoSphere intensity is progressively decreased (Figure 19.28).

Examination of Figure 19.27 reveals that the emission spectrum is distorted at higher concentrations of K^+. This indicates that the mechanism of K^+ sensing is not energy transfer, but rather is an inner filter effect due to KFU-111, as was stated by the authors.[85] In this particular sensor there was no opportunity for the fluorophore and absorption dye to interact, as the fluorophores were in the beads, and thus distant from the absorber. The important point is that spectral overlap does not imply that the mechanism is resonance energy transfer. Potassium sensors using valinomycin but other donors such as rhodamine and cyanine dyes have also been reported.[86–87] For the cyanine donor 1,1'-dioctadecyl-3,3,3',3'-tetramethylindodicarbocyanine perchlorate [$DiIC_{18}(5)$], lifetime measurements demonstrated that RET was the dominant mechanism for K^+ sensing.[87] One difficulty with RET sensing is that the extent of energy transfer depends strongly on acceptor concentration, so that the sensors require frequent calibration. This problem can poten-

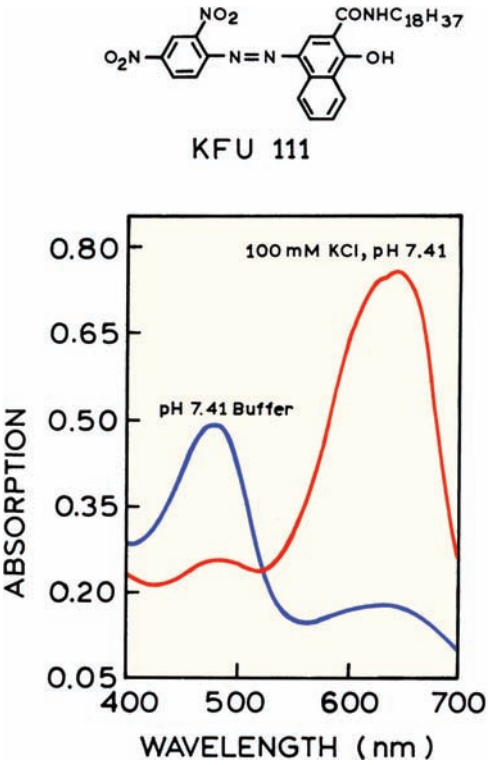

Figure 19.26. Absorption spectra of 4-((2',4'-dinitrophenyl)azo)-2-((octadecylamino)carbon-yl-l-naphthol (KFU 111) in a plasticized PVC membrane containing potassium tetrakis(4-chlorophyenyl)borate (PTCB) and valinomycin, in contact with a 100 mM aqueous solution of KCl at pH 7.41, and with potassium-free buffer at pH 7.41. Revised and reprinted with permission from [85]. Copyright © 1993, American Chemical Society.

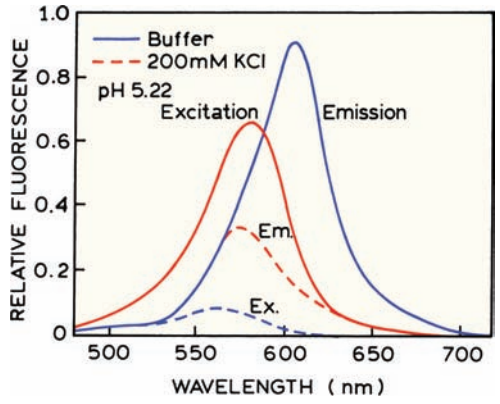

Figure 19.27. Excitation and emission spectra of FluoSphereJ particles contained in the plasticized PVC membrane containing PTCB, valinomycin, and KFU 111 contacted with a 200 mM KCl solution at pH 5.22 (dashed) and with plain buffer of pH 5.22 (solid). The emission spectrum of the FluoSpheres in the presence of K^+ is distorted due to the inner filter effect caused by the blue form of the absorber dye. Revised and reprinted with permission from [85]. Copyright © 1993, American Chemical Society.

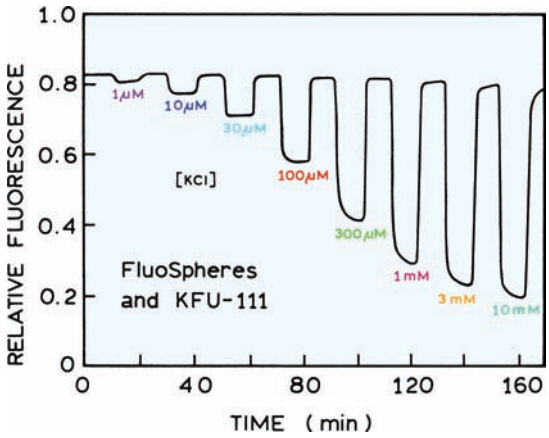

Figure 19.28. Response time, relative signal change, and reversibility of the potassium sensor in the presence of dye KFU 111 in the membrane; pH 5.82, excitation/emission wavelengths set to 560/605 nm. The sensor did not respond to potassium without KFU 11. Revised and reprinted with permission from [85]. Copyright © 1993, American Chemical Society.

tially be circumvented by using covalently linked donors and acceptors.

19.5.4. Theory for Energy Transfer Sensing

The theory for sensing by energy transfer is complex and depends on the nature of the sensor. There are two limiting cases—unlinked donors and acceptors distributed randomly in space, and covalently linked donor-acceptor pairs. Suppose the donor–acceptor pair is not linked and that the acceptor can exist in two forms with different absorption spectra and Förster distances (R_{01} and R_{02}). The intensity decay is given by

$$I_{DA}(t) = I_0 \exp\left[-\frac{t}{\tau_D} - 2(\gamma_1 + \gamma_2)\sqrt{\frac{t}{\tau_D}} \right] \qquad (19.2)$$

where τ_D is the donor decay time and γ_1 and α_2 are functions of the acceptor concentration, and are related to R_{01} and R_{02}, as described in Chapter 15 (eqs. 15.1–15.3). Alternatively, the donor and acceptor may be covalently linked. In this the intensity decay is given by

$$I_{DA}(t) = I_D\left[g_1 \int_0^\infty P(r) \exp\left(\frac{t}{\tau_{DA1}}\right) dr \right.$$

$$\left. + (1 - g_1) \int_0^\infty P(r) \exp\left(\frac{t}{\tau_{DA2}}\right) dr \right] \qquad (19.3)$$

where

$$\frac{1}{\tau_{DAi}} = \frac{1}{\tau_D} + \frac{1}{\tau_D}\left(\frac{R_{0i}}{r}\right)^6 \qquad (19.4)$$

$P(r)$ is the distance distribution, and g_1 and $(1 - g_1)$ are the fractional intensities of each form at $t = 0$. The transfer efficiency (E) can be calculated by

$$E = 1 - \frac{F_{DA}}{F_D} = 1 - \frac{\int_0^\infty I_{DA}(t)\,dt}{\int_0^\infty I_D(t)\,dt} \qquad (19.5)$$

where $I_D(t)$ is an intensity decay of the donor with no acceptors; F_D and F_{DA} are the relative intensities of the donor in the absence and presence of acceptor. These general expressions can be used to simulate the expected performance of an energy-transfer sensor using known or estimated parameter values.[13]

19.6. TWO-STATE pH SENSORS

19.6.1. Optical Detection of Blood Gases

The phrase "blood gases" refers to the measurement of pH, pCO_2, and pO_2 in arterial blood. Optical detection of blood gases is a longstanding goal of optical sensing. Blood-gas measurements are frequently performed on patients in the intensive care unit, premature infants, and trauma victims. Since the status of such patients changes rapidly, it is important to obtain the blood gas results as quickly as possible. While the status of optical detection of blood gases is evolving rapidly, many of the currently used methods do not satisfy the needs of intensive care and emergency health care situations where the blood gases are changing rapidly.[88–89]

Determination of blood gases is difficult, time-consuming, and expensive. Measuring a blood gas requires taking a sample of arterial blood, placing it on ice, and transporting it to a central laboratory. At the central laboratory the pH is measured using an electrode, and O_2 and CO_2 by the Clark and Severinghaus electrodes, respectively. Even for a stat request, it is difficult to obtain the blood-gas report in less than 30 minutes, by which time the patient's status is often quite different. Additionally, handling of blood by health-care workers is undesirable with regard to the risk of acquired immunodeficiency syndrome (AIDS) and other infectious diseases.

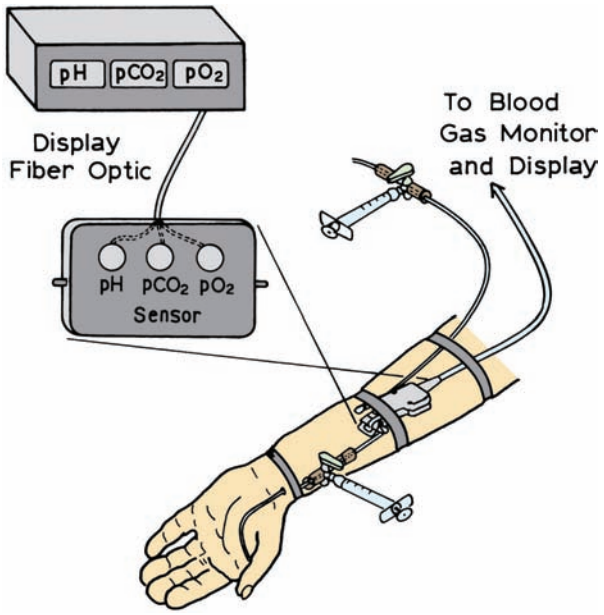

Figure 19.29. Arterial blood-gas sensor. Revised from [89].

How can optical sensing of blood gases improve on this situation? One approach is shown in Figure 19.29.[89] The sensor chemistry is a cassette that is attached to an arterial line. When needed, blood is drawn into the cassette, and the blood gases are determined by appropriate fluorescent sensors. Oxygen could be determined using $[Ru(Ph_2phen)_3]^{2+}$, and pH can be measured using HPTS or other pH-sensitive fluorophores (Section 19.6.2).[90] The ability to measure pH also allows pCO_2 to be measured using the bicarbonate couple.[91] This is accomplished by measuring the pH of a bicarbonate solution that is exposed to the CO_2. The concentration of dissolved CO_2 alters the extent of bicarbonate dissociation and hence the pH. With the use of such a device the blood-gas measurements could be made without loss or handling of blood and the results can be available immediately. Such instruments have been developed,[92–93] but improvements in performance are desirable. This idea of clinical chemistry using fiber optics originates with the early work of D. W. Lubbers and colleagues.[94] In the long term it is hoped that blood gases can be determined noninvasively, as shown in Figure 19.1, or with a simple point-of-care device (Figure 19.2).

19.6.2. pH Sensors

Fluoresceins: Fluorescein was one of the earliest pH sensors.[95–96] Fluorescein and other pH-sensitive probes have

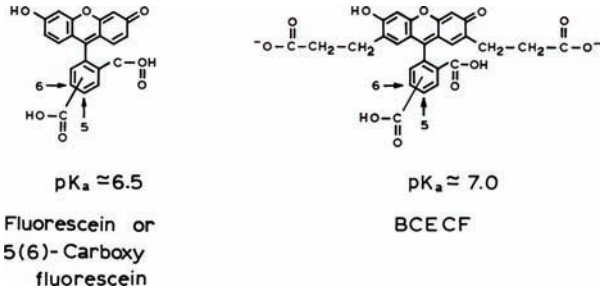

Figure 19.30. Fluorescein-type pH probes.

also been used to measure pCO_2 by the bicarbonate couple.[97–98] One early use of fluorescein was to determine intracellular pH values. However, fluorescein leaks rapidly from cells, so highly charged derivatives are often used, such as 5(6)-carboxyfluorescein or 2',7'-bis(2-carboxyethyl)-5(6)-carboxyfluorescein (BCECF) (Figure 19.30). Fluorescein displays a complex pH-dependent equilibrium, and emission from the various ionic forms[99–102] (Figure 19.31). The lactone form is usually found in organic solvents and is not formed in aqueous solutions above pH 5. Only the two high-pH anionic forms are fluorescent (Figure 19.31).

Fluorescein is a moderately useful excitation wavelength-ratiometric probe. The absorption spectrum shifts to higher wavelengths with a pK_a near 6.5 (Figure 19.32). These absorption and emission spectral changes are due to the equilibrium between the two fluorescent forms of fluorescein—the monoanion and dianion forms (Figure 19.31). These spectral changes allow wavelength-ratiometric pH measurements with two excitation wavelengths near 450 and 495 nm. The intensity ratio increases with increasing pH (Figure 19.33). The data in Figure 19.33 are for fluorescein linked to dextran, which was used to prevent the fluorescein from leaking out of the cells.

One disadvantage of fluorescein is that its pK_a is near 6.5, whereas the cytosolic pH of cells is in the range of 6.8 to 7.4. Hence, it is desirable to have a higher pK_a for accurate pH measurement. BCECF (Figure 19.30) was developed[103] to have spectral properties similar to those of fluo-

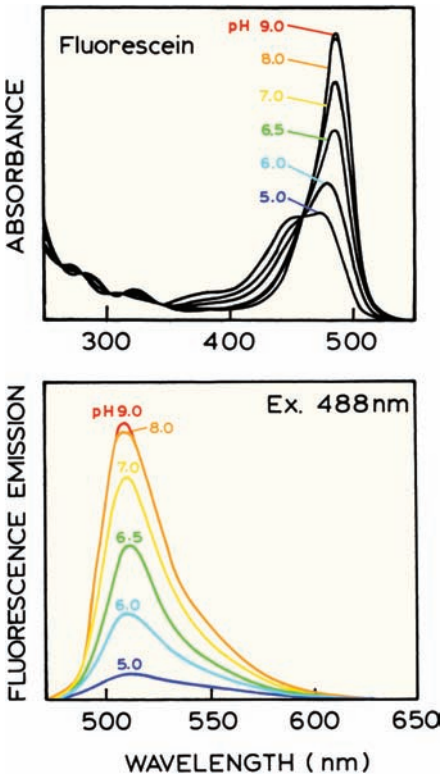

Figure 19.32. Absorption and emission spectra of fluorescein. Data from [100].

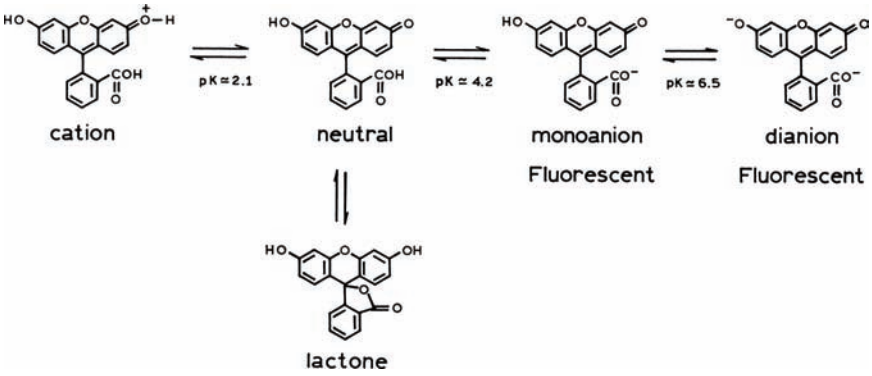

Figure 19.31. pH-dependent ionization of fluorescein. Only the monoanion and dianion forms of fluorescein are fluorescent.

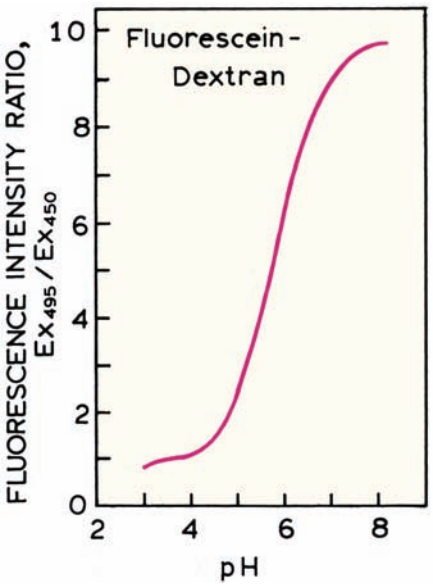

Figure 19.33. Wavelength-ratiometric pH calibration for fluorescein linked to dextran. Revised from [95].

rescein, but to have a higher pK_a near 7.0 (Table 19.2). This illustrates an important aspect of all sensing probes: the pK_a value or the analyte dissociation constant must be comparable to the concentration of the analyte to be measured. However, it can be difficult to adjust a pK_a value or dissociation constant. Additionally, the affinities observed in solution may be quite different from the values needed in a sensor, where the probe may bind to proteins or membranes or the probe may be present in a polymeric support. Significant development is often needed to adapt a sensor for use in a clinical application.

HPTS, A Wavelength-Ratiometric pH Sensor: A disadvantage of fluorescein as a sensor is that it is difficult to use as a wavelength-ratiometric probe. This is because the absorption and emission intensity is low for 450-nm excitation (Figure 19.32). The pH probe 8-hydroxypyrene-1,3,6-trisulfonate (HPTS)[104–107] displays more favorable properties as a wavelength-ratiometric probe. The sulfonate groups are for solubility in water and the hydroxyl group provides sensitivity to pH. Excitation and emission spectra of HPTS show a strong dependence on pH (Figure 19.34). As the pH is increased HPTS shows an increase in absorbance at 450 nm, and a decrease in absorbance below 420 nm. These changes are due to the pH-dependent ionization of the hydroxyl group. The emission spectrum is independent of pH, suggesting that emission occurs only from the ionized form of HPTS. Conveniently, the apparent pK_a of HPTS is near 7.5, making it useful for clinical measurements that need to be most accurate from 7.3 to 7.5 (Table 19.2). HPTS has also been used as a CO_2 sensor when dissolved in the appropriate bicarbonate solution.[108]

Table 19.2. Spectral and Lifetime Properties of pH Probes

Probe[b]	Excitation $\lambda_B(\lambda_A)$ [nm]	Emission $\lambda_B(\lambda_A)$ [nm]	Q_B (Q_A)	Lifetime (ns)[a] $\bar{\tau}_B$ ($\bar{\tau}_A$)	pK_A
BCECF	503 (484)	528 (514)	~0.7	4.49 (3.17)	7.0
SNAFL-1	539 (510)	616 (542)	0.093 (0.33)	1.19 (3.74)	7.7
C. SNAFL-1	540 (508)	623 (543)	0.075 (0.32)	1.11 (3.67)	7.8
C. SNAFL-2	547 (514)	623 (545)	0.054 (0.43)	0.94 (4.60)	7.7
C. SNARF-1	576 (549)	638 (585)	0.091 (0.047)	1.51 (0.52)	7.5
C. SNARF-2	579 (552)	633 (583)	0.110 (0.022)	1.55 (0.33)	7.7
C. SNARF-6	557 (524)	635 (559)	0.053 (0.42)	1.03 (4.51)	7.6
C. SNARF-X	575 (570)	630 (600)	0.160 (0.07)	2.59 (1.79)	7.9
Resorufin	571 (484)	528 (514)	NA[c]	2.92 (0.45)	~5.7
HPTS	454 (403)	511	NA	N/A	7.3
$[Ru(deabpy)(bpy)_2]^{2+}$	450 (452)	615 (650)	NA	380 (235)	7.5
Oregon-Green	489 (506)	526	0.65 (0.22)	4.37 (2.47)	1.8
DM-Nerf	497 (510)	527 (536)	0.88 (0.37)	3.98 (2.50)	1.6
Cl-Nerf	504 (514)	540	0.78 (0.19)	4.00 (1.71)	2.3

[a] $\bar{\tau}_A$ and $\bar{\tau}_B$ refer to the mean lifetimes of the acid and base forms, respectively.
[b] Abbreviations: BCECF, 2',7'-bis(2-carboxyethyl)-5(6)-carboxyfluorescein; bpy, 2,2'-bipyridine; HPTS, 8-hydroxypyrene-1,3,6-trisulfonate; deabpy, 4,4'-diethylaminomethyl-2,2'-bipyridine; bpy, 2,2'-bipyridine.
[c] NA: Not available.

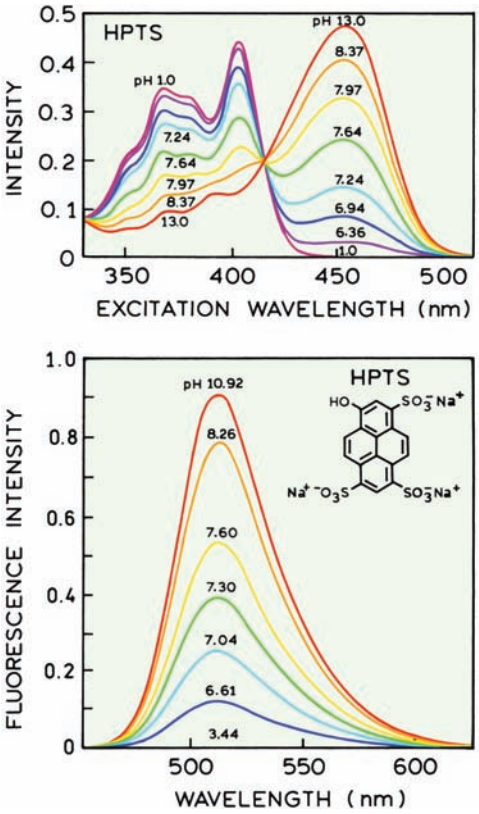

Figure 19.34. **Top**: Excitation spectra of the pH probe 1-hydroxypyrene-3,6,8-trisulfonate (HPTS) in 0.07 M phosphate buffer at various pH values. **Bottom**: Emission spectra of HPTS when excited at 454 nm. Revised from [105].

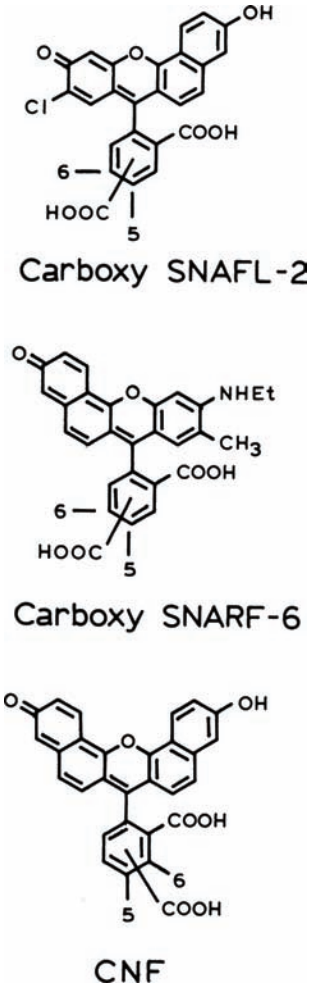

Figure 19.35. Wavelength-ratiometric pH sensors. Carboxy SNAFL-2 is a seminaphthofluorescein, carboxy SNARF-6 is a seminaphthorhodafluor, and CNF is 5-(and 6-)carboxy-naphthofluorescein.

One possible disadvantage of HPTS is that it undergoes ionization in the excited state, rather than at ground-state equilibrium. The fact that HPTS undergoes an excited-state reaction can be recognized by noting that the excitation spectra are comparable to the absorption spectra of both the phenol and phenolate forms, but that there is only a single long-wavelength emission spectrum (Figure 19.34). The phenol form emits at shorter wavelengths and is only seen in highly acidic media. The presence of excited-state ionization is also indicated by a higher apparent pK_A in pure water than in buffers.[105] It is known that the pK_A values of the hydroxyl group for the ground- and excited-state HPTS are 7.3 and 1.4, respectively,[106] so that HPTS molecules in the protonated state will tend to undergo ionization upon excitation. It seems that any excited-state process will be dependent on the details of the local probe environment. Under most conditions excited-state ionization of HPTS is complete prior to emission, so that only the phenolate emission is observed. Nonetheless, for sensing purposes we prefer probes that display a ground-state pK_a near 7.5. One disadvantage of HPTS has been the relatively short excitation wavelength, particularly for the acid form. However, availability of blue light-emitting diodes (Chapter 2) may result in increased use of HPTS.

SNAFL and SNARF pH Probes: A family of improved pH probes became available in 1991.[109] These dyes are referred to as seminaphthofluoresceins (SNAFLs) or seminaphthorhodafluors (SNARFs). Representative structures are shown in Figure 19.35. A favorable feature of these probes is that they display shifts in both their absorption and emission spectra with a pK_A from 7.6 to 7.9 (Figure 19.36). Also, the absorption and emission wavelengths are reasonably long, so that both forms of the probes can be excited with visible wavelengths near 540 nm (Table 19.2).

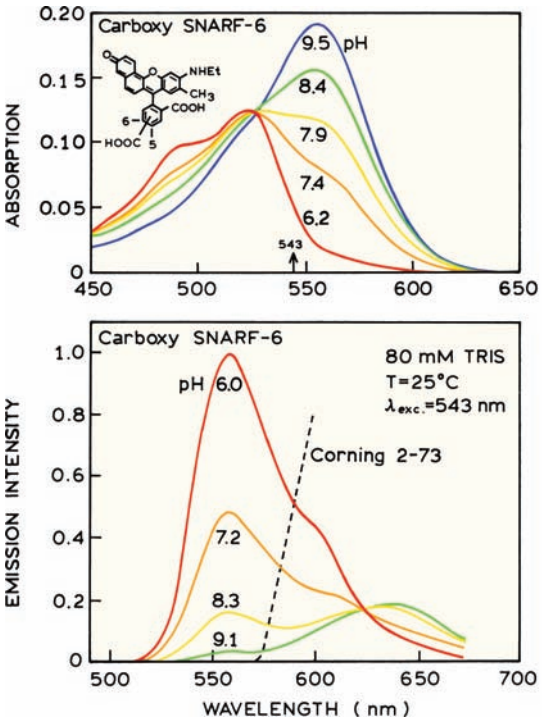

Figure 19.36. pH-dependent absorption (top) and emission spectra (bottom) of carboxy SNARF-6. The dashed line shows the transmission cutoff of the long-pass filter used for the phase and modulation measurements. Revised and reprinted with permission from [110]. Copyright © 1993, American Chemical Society.

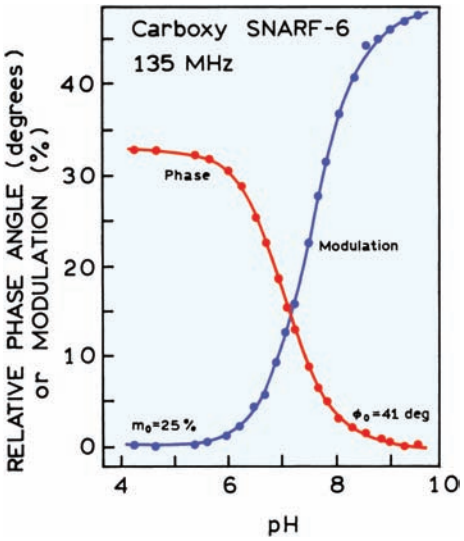

Figure 19.37. pH-dependent phase and modulation of carboxy SNARF-6 when excited at 543 nm with a green He-Ne laser. The phase values are relative to the value at high pH, $\phi_0 = 41°$. The modulation values are relative to the value at low pH, $m_0 = 0.25$. Revised and reprinted with permission from [110]. Copyright © 1993, American Chemical Society.

The spectral shifts (Figure 19.36) allow the SNAFLs and SNARFs to be used as either excitation or emission wavelength-ratiometric probes.

The fact that both the acid and base forms of the probe are fluorescent allows their use as lifetime probes. If only one form was fluorescent then the lifetime would not change with pH. The pH-dependent phase and modulation data of carboxy SNARF-6 shows a strong dependence on pH (Figure 19.37). The decay time of the base form is less than that of the acid form. The decay times at pH 4.9 and 9.3 are 4.51 and 0.95 ns, respectively.[110] pH sensing based on lifetimes can provide stable measurements for extended periods of time. However, it is important to recognize that lifetime measurements, like intensity ratio measurements, can be affected by interactions of the probes with biological macromolecules. The intensity decays of carboxy SNARF-1 were found to be sensitive to the presence of serum albumin, or intracellular proteins.[111]

There is continued development of new pH probes[112–113] and sensors.[114–116] For clinical applications, longer wavelengths are usually preferable. This was accomplished with the SNAFL probes by introduction of an additional benzyl ring into the parent structure (Figure 19.35). This carboxynaphthofluorescein (CNF)[118] shows shifts in the absorption and emission spectra with pH (Figure 19.38). pH probes have been developed using cyanine dyes[119] and a pH sensor excitable at 795 nm has been described.[120–121] This carboxy carbocyanine dye shows a decrease in intensity near pH 8.5, but does not display spectral shifts, except at short wavelengths near 435 nm. UV-excitable pH probes with multiple pK_A values from 1.7 to 9.0 have also been described.[122] For clinical applications with simple instruments it can be valuable to have long-lifetime pH probes. A pH-sensitive ruthenium metal–ligand complex with a decay time near 300 ns has been reported with a pK_A value near 7.5.[123] Additionally, a pH-dependent lanthanide has also been reported.[124] Given the continuing need for pH measurements, additional advances in practical pH sensors can be expected.

19.7. PHOTOINDUCED ELECTRON TRANSFER (PET) PROBES FOR METAL IONS AND ANION SENSORS

In the previous section we saw how probes could be designed based on reversible ionization of a group in conjuga-

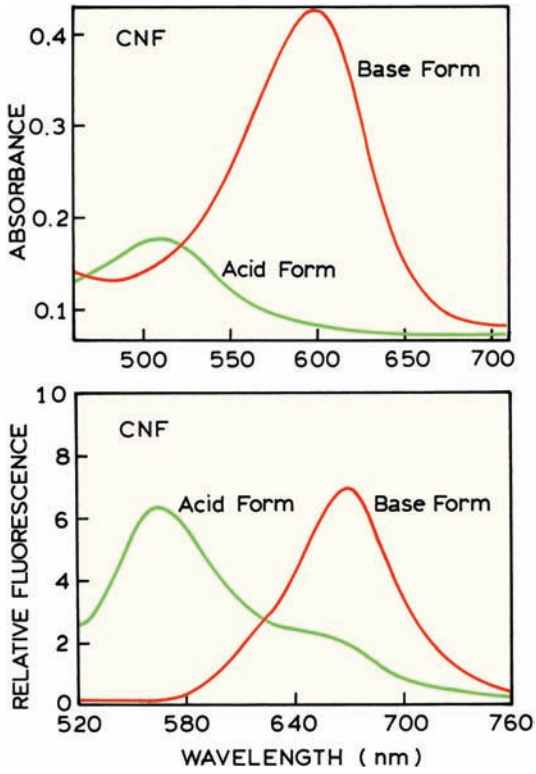

Figure 19.38. Absorption (top) and emission spectra (bottom) of the acid and base form of carboxynaphthofluorescein (CNF). Revised and reprinted with permission from [117]. Copyright © 2001, American Chemical Society.

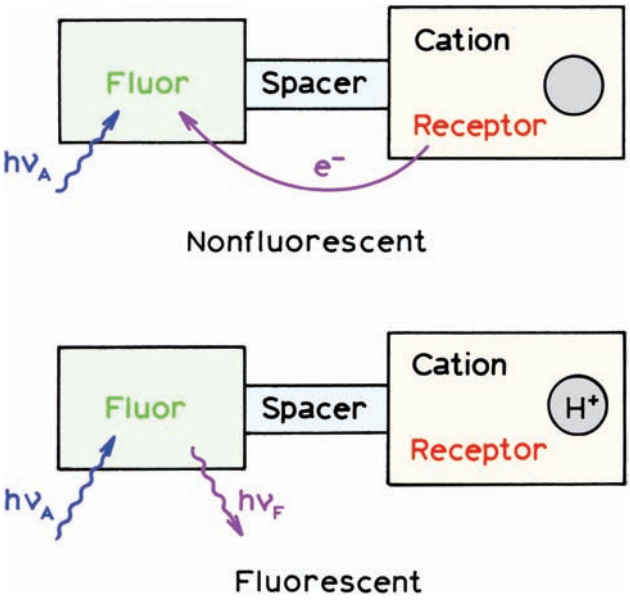

Figure 19.39. Chemical sensing based on photoinduced electron transfer.

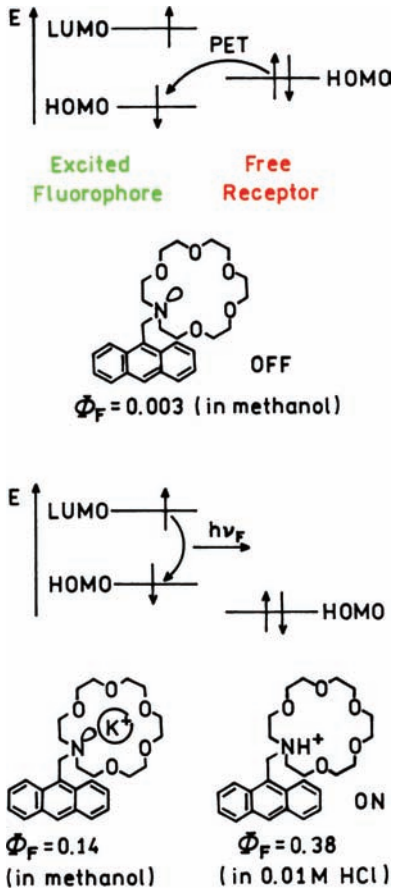

Figure 19.40. Molecular orbital energy and a typical structure for a PET sensor. Revised from [128].

tion with the aromatic ring (Figure 19.39). Another mechanism for sensors is the quenching interaction of a linked side chain with the fluorophore. The origin of these probes can be traced to the early studies of exciplex formation of amines with aromatic hydrocarbons. This phenomenon has been exploited to develop sensors based on quenching of fluorophores by amines.[125–128] The basic idea is that quenching by amines requires the lone pair of electrons localized on the nitrogen (Figure 19.40). When the fluorophore is in the excited state these lone pair electrons are in a higher-energy orbital (HOMO, top) than the energy of the vacancy left by the excited electron. Hence, an electron from the nitrogen enters this lower-energy orbital, effectively quenching the fluorescence. If the lone electron pair binds a proton or a cation the energy of this pair is lowered (bottom). Electron transfer is then inhibited and the fluorophore is not quenched. Such probes are said to undergo

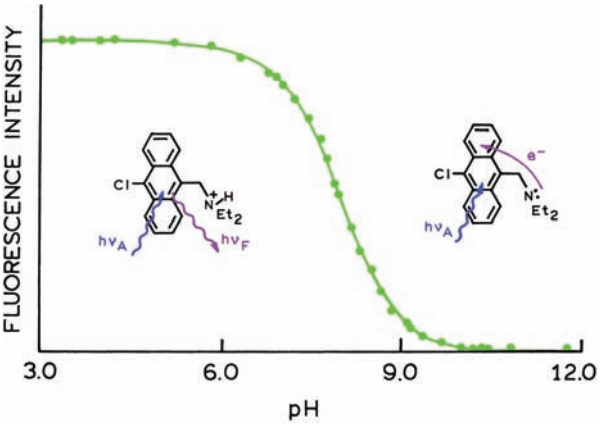

Figure 19.41. pH-dependent fluorescence of 9-chloro-10-(diethylaminomethyl)anthracene. Revised and reprinted with permission from [126]. Copyright © 1989, American Chemical Society.

photoinduced electron transfer (PET), which is the light-induced transfer of electrons from the nitrogen into the aromatic ring. A simple example of a PET sensor is the alkylamino anthracene shown in Figure 19.41. At low pH the amino group is protonated and does not quench the anthracene. As the pH is increased, the amino group becomes unprotonated, and the fluorescence decreases due to PET.

This use of PET has been extended to create sensors for metal ions[129–131] and for nonmetal anions.[132–136] As an example, Figure 19.42 shows an anthracene derivative with an aminoalkyl side chain which binds phosphate. Hydrogen bonding of phosphate to the amino groups results in increased anthracene fluorescence. A similar approach was used to create an anthracene derivative that displays increased fluorescence when bound to citrate (Figure 19.43). The structures of these phosphate and citrate probes illustrate the rational design of fluorophores based on known principles. Unfortunately, PET mechanism may not be extendable to long-wavelength probes because quenching by amines becomes inefficient at long wavelengths.

19.8. PROBES OF ANALYTE RECOGNITION

Extensive efforts have been directed toward the design and synthesis of fluorescent probes for cations: Na^+, K^+, Mg^{2+} and especially Ca^{2+}. These efforts can be traced to the discovery of crown ethers and their ability to form complexes with metal ions,[137–139] and subsequent work to create more complex structures to bind a variety of small molecules. The greatest effort has been in synthesis of probes for cal-

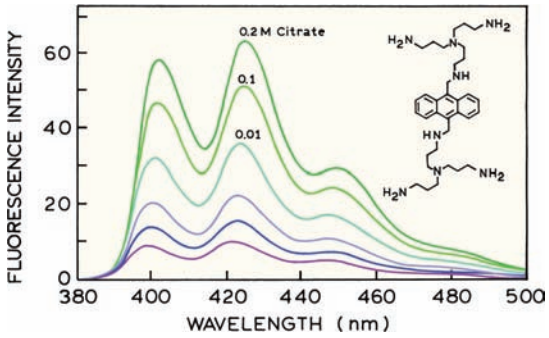

Figure 19.43. Emission spectra of an alkylaminoanthracene derivative in the presence of various amounts of citrate at pH 6. From bottom to top, [Citrate] = 0, 0.1, 1, 10 mM, 0.1 M, 0.2 M. Revised from [134].

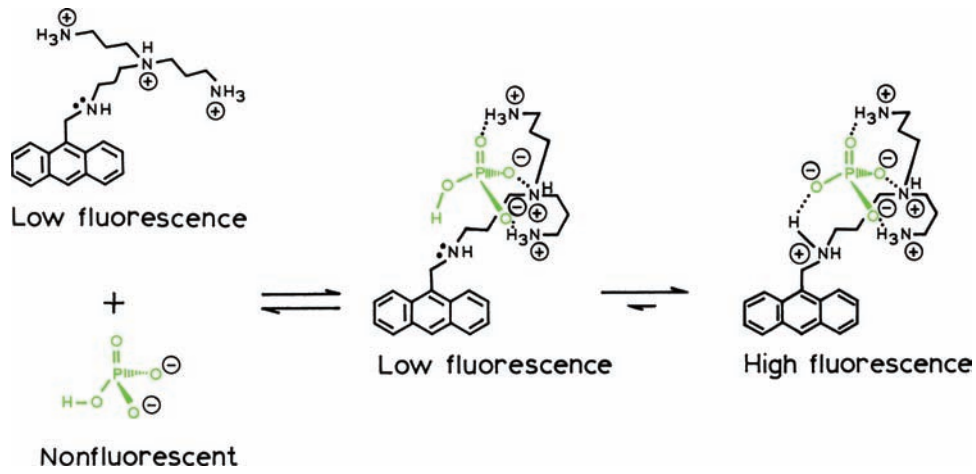

Figure 19.42. Phosphate sensing with an alkylamino anthracene derivative. Revised and reprinted with permission from [134]. Copyright © 1989, American Chemical Society.

Table 19.3. Typical Analyte Concentrations in Blood Serum and in Resting Cells

Analyte	In blood serum (mM)	In resting cells (mM)
H^+	34–45 nM	10–1000 nM
(pH)	(7.35–7.46)	(6–8)
Na^+	135–148	4–10
K^+	3.5–5.3	100–140
Li^+	0–2	–
Mg^{2+}	–	0.5–2
Ca^{2+}	4.5–5.5	50–200 nM
Cl^-	95–110	5–100
HCO_3^-	23–30	–
CO_2	4–7 (% Atm)	–
O_2	8–16 (% Atm)	–

cium, and entire books have been devoted to calcium probes.[140] Much of this work can be traced to the development of intracellular cation probes by Tsien and colleagues.[141–143] Since these initial publications many additional cation probes have been developed. It is not possible to completely describe this extensive area of research. Instead we describe the most commonly used cation sensors, and the strength and weaknesses of existing probes.

19.8.1. Specificity of Cation Probes

A survey of the literature reveals that a large number of diverse structures can chelate cations. However, a dominant use of these probes is imaging of intracellular cations. In this case the indicators have to be sensitive to the intracellular concentrations of cations or anions (Table 19.3). These concentrations define the affinity needed by the chelators for the cation and the degree of discrimination required against other cations. For example, a probe for K^+ in blood is not useful unless it does not bind Na^+ at its physiological concentration of 140 mM. Also, it is desirable to have a means for trapping the probes within cells. These criteria suggest a group of chelators that are useful for intracellular probes. The azacrown ethers have suitable affinity constants for Na^+ and K^+, APTRA is a chelator for Mg^{2+}, and BAPTA is a suitable chelator for Ca^{2+} (Figure 19.44). These are the dominant chelation groups used in intracellular cation probes.

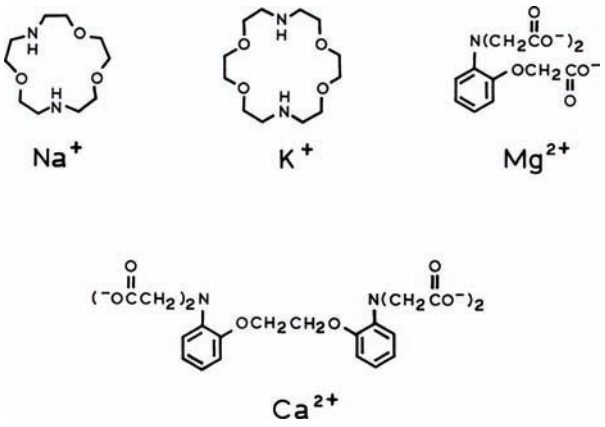

Figure 19.44. Chelating groups for Na^+, K^+, Mg^{2+}, and Ca^{2+}.

19.8.2. Theory of Analyte Recognition Sensing

Suppose the probe can exist in two states, free (P_F) and bound (P_B) to the analyte (A). If the binding stoichiometry is 1 to 1, the dissociation reaction is given by

$$AP_B \rightleftharpoons A + P_F \tag{19.6}$$

and the dissociation constant is defined as

$$K_D = \frac{[P_F]}{[AP_B]}[A] \tag{19.7}$$

The relative concentrations of the free and bound form of the probes are given by

$$K_D = \frac{[P_F]}{[AP_B]}[A] \tag{19.8}$$

$$\frac{[AP_B]}{[P]} = \frac{[A]}{K_D + [A]} \tag{19.9}$$

where [P] is the total concentrations of indicator ($[P] = [P_F] + [AP_B]$).

These equations can be used to calculate the relative amounts of free and bound probes as the analyte concentration is increased (Figure 19.45). The range of analyte concentrations that can be measured are those for which there exist significant amounts of each form of the probe. The analyte concentration range over which a probe can be used is determined by the dissociation constant, K_D (Figure 19.45). This is a critical factor in using probes that bind specific analytes. The binding constant of the probe must be comparable to analyte concentration. The useful range of analyte concentrations is typically restricted to $0.1K_D < [A] < 10K_D$. Concentrations lower than $0.1K_D$ and higher than

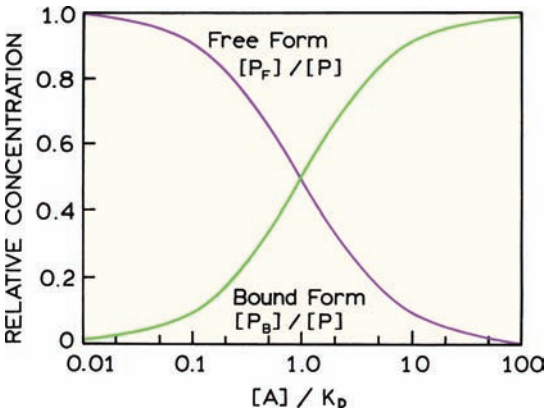

Figure 19.45. Relations between analyte concentration ([A]), dissociation constant (K_D) of the analyte-probe complex, and relative concentrations of the free (P_F) and bound (P_B) forms of the probe.

$10K_D$ will produce little change in the observed signal. In the use of fluorescence sensing probes, and eqs. 19.6–19.9, we are assuming that the analyte is present in much greater concentration than the probe. Otherwise, the probe itself becomes a buffer for the analyte and distorts the analyte concentration.

Intensity-Based Sensing: There are a number of probes that display changes in intensity but do not display spectral shifts. Such probes include the calcium probes Calcium Green[J], Fluro-3, and Rhod-2. In these cases the analyte concentration can be obtained from

$$[\mathrm{A}] = K_D \frac{F - F_{min}}{F_{max} - F} \tag{19.10}$$

where F_{min} is the fluorescence intensity when indicator is in the free form, F_{max} is the intensity when the indicator is totally complexed, and F is the intensity when indicator is partially complexed by analyte. Changes in the fluorescence intensity are typically due to different quantum yields of the free and complexed forms, rather than differences in the absorption spectrum. The changes in quantum yield have been explained as due to formation of twisted internal charge-transfer (TICT) states or to changes in the extent of PET.

In order to determine the analyte concentration using eq. 19.10, all intensities must be determined with the same instrumental configuration, the same optical path length, and the same probe concentration. These requirements are often hard to satisfy, especially in microscopy when observing cells. Measurement of F_{max} and F_{min} requires lysing the cells and titrating the released indicator, or using ionophores to saturate the indicator. These calibration methods do not compensate for dye loss due to photobleaching or leakage during the experiment, and can also alter the spatial distribution of the probe. For this reason it is desirable to have methods that are independent of probe concentration. This is possible using wavelength-ratiometric probes or lifetime-based sensing.

Wavelength-Ratiometric Probes: Many probes display spectral shifts in their absorption or emission spectra upon binding analytes. In these cases the analyte concentrations can be determined from a ratio of intensities, independent of the overall probe concentration. For excitation-ratiometric probes the analyte concentration can be determined by[143]

$$[\mathrm{A}] = K_D \left(\frac{R - R_{min}}{R_{max} - R} \right) \left(\frac{S_F(\lambda_2)}{S_B(\lambda_2)} \right) \tag{19.11}$$

where $R = F(\lambda_1)/F(\lambda_2)$ is the ratio of intensities for the two excitation wavelengths λ_1 and λ_2. R_{min} and R_{max} are the ratios for the free and the complexed probe, respectively. For an excitation wavelength-ratiometric probe the value of $S_F(\lambda_2)$ and $S_B(\lambda_2)$ are related to the extinction coefficients and quantum yields of the probe excited at λ_2:

$$\left(\frac{S_F(\lambda_2)}{S_B(\lambda_2)} \right) = \frac{\varepsilon_F \Phi_F}{\varepsilon_B \Phi_B} \tag{19.12}$$

For an emission wavelength-ratiometric probe one can use eq. 19.11 with the values of $S_F(\lambda_2)$ and $S_B(\lambda_2)$. They are related to the relative intensities of the free and bound forms of the probe:

$$\frac{S_F(\lambda_2)}{S_B(\lambda_2)} = \frac{F_F}{F_B} \tag{19.13}$$

Unlike intensity-based measurements, use of wavelength-ratiometric probes and eq. 19.11 makes the measurements independent of probe concentration.

19.8.3. Sodium and Potassium Probes

Typical Na^+ and K^+ probes are shown in Figure 19.46, and all of these contain azacrown groups or a closely related structure. The first reported probes[141] were sodium-binding benzofuran isophthalate (SBFI) for Na^+ and potassium-

Table 19.4. Spectral and Lifetime Properties of Mg^{2+}, Na^+, and K^+ Probes

Probe[b]	Excitation[a] λ_F (λ_B) [nm]	Emission λ_F (λ_B) [nm]	Q_F (Q_B)	Lifetime (ns) [a] $\bar{\tau}_F$ ($\bar{\tau}_B$)	K_D (mM)
Mg^{2+} Probes					
Mag-Quin-1	348 (335)	499 (490)	0.0015 (0.009)	0.57 (10.3)	6.7
Mag-Quin-2	353 (337)	487 (493)	0.003 (0.07)	0.84 (8.16)	0.8
Mag-Fura-2	369 (330)	511 (491)	0.24 (0.30)	1.64 (1.72)	1.9
Mag-Fura-5	369 (332)	505 (482)	NA[c]	2.52 (2.39)	2.3
Mag-Indo-1	349 (330)	480 (417)	0.36 (0.59)	1.71 (1.90)	2.7
Mag-Fura-Red	483 (427)	659 (631)	0.012 (0.007)	0.38 (0.35)	2.5
Mg Green	506	532	0.04 (0.42)	0.98 (3.63)	1.0
Mg Orange	550	575	0.13 (0.34)	1.06 (2.15)	3.9
Na^+ Probes					
SBFI	348 (335)	499 (490)	0.045 (0.083)	0.27 (0.47)	3.8
SBFO	354 (343)	515 (500)	0.14 (0.44)	1.45 (2.09)	31.0
Na Green	506	535	7-fold[d]	1.14 (2.38)	6.0
K^+ Probes					
PBFI	336 (338)	557 (507)	0.24 (0.72)	0.47 (0.72)	5.1
CD 222	396 (363)	480 (467)	3.7-fold	0.17 (0.71)	0.9

[a]F and B refer to the free and cation-bound forms of the probes, respectively.
[b]Abbreviations: SBFI, sodium-binding benzofuran isophthalate; SBFO, sodium-binding benzofuran oxazole; PBFI, potassium-binding benzofuran isophthalate.
[c]NA: not available.
[d]$Q_B/Q_F = 7$.

binding benzofuran isophthalate (PBFI) for K^+ (Table 19.4). While designed to be excitation wavelength-ratiometric probes, these probes suffer several disadvantages. They require UV excitation, which results in substantial amounts of autofluorescence from cells. The excitation spectra show only minor changes in shape upon binding of Na^+ and K^+ to these probes (Figure 19.47). Apparently, the charge densities of these singly charged cations are not suf-

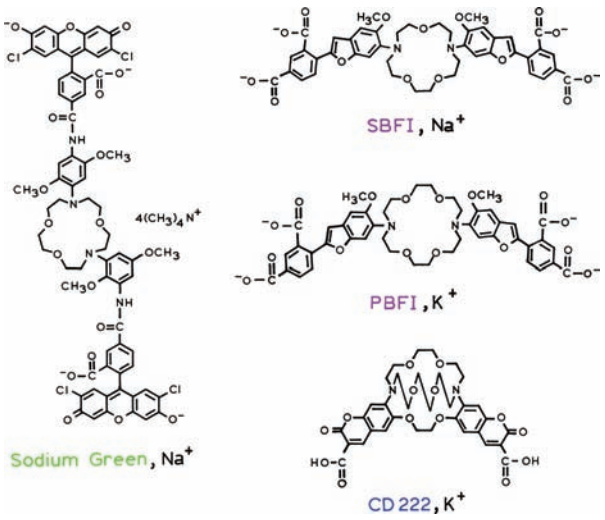

Figure 19.46. Representative Na^+ and K^+ probes. Sodium Green is a trademark of Molecular Probes Inc.

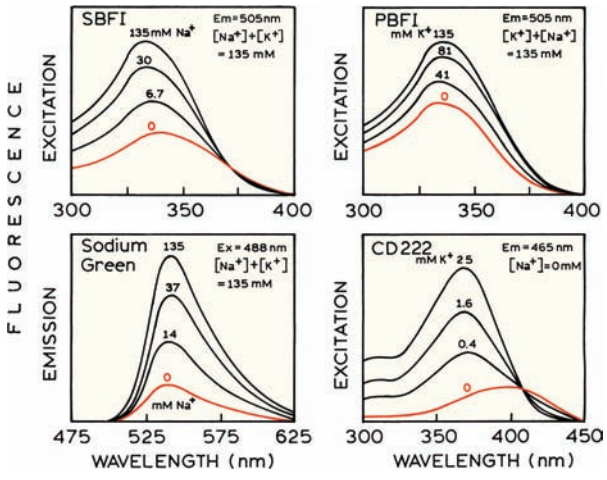

Figure 19.47. Excitation (SBFI, PBFI and CD 222) and emission (Sodium Green) spectra of Na^+ and K^+ probes in the presence of various concentrations of the ions. Sodium Green is a trademark of Molecular Probes Inc. Data from [144].

ficient to result in substantial spectral shifts. In support of this hypothesis, one notices that PBFI, which binds the larger K^+ ion, shows a smaller spectral shift than that seen for binding for Na^+ and SBFI.

A coumarin-based probe is available for K^+: CD222. This probe has a more complex chelating group (Figure 19.46) that is directly connected to the coumarin fluorophore.[145–146] This probe can be excited at longer wavelengths than SBFI and PBFI, and displays larger spectral shifts (Figure 19.47). The dissociation constant for K^+ binding to CD222 is near 1 mM (Table 19.4). This probe is useful for measurements of extracellular K^+, but the binding is too strong for measurements of intracellular K^+ (Table 19.3). The apparent K_D of CD222 for K^+ is increased in the presence of Na^+. As a result, CD222 may be useful for measurements of extracellular K^+ in blood in the concentration range 3–6 mM.[147] Several other probes with a coumarin fluorophore and a chelator for K^+ have been described.[148–150] Given the availability of blue and UV LEDs, these probes may soon find use in simple clinical devices.

In an effort to avoid cellular autofluorescence, several Na^+ and K^+ probes have been developed for longer excitation wavelength. One of these probes is Sodium Green™, which is a sodium-specific azacrown conjugated on both nitrogens to a dichlorofluorescein (Figure 19.46). Sodium Green can be excited at 488 nm, and displays increasing intensity in the presence of increasing concentrations of Na^+ (Figure 19.47). Unfortunately, Sodium Green does not display any spectral shifts, so that wavelength-ratiometric measurements are not possible. Furthermore, the analogous probe for potassium has not been reported, so that K^+ probes are limited in number.

The inability to develop wavelength-ratiometric probes for Na^+ and K^+, particularly with long excitation and emission wavelengths, illustrates an advantage of lifetime-based sensing. Sodium Green was found to display a multi-exponential decay, with lifetimes of 1.1 and 2.4 ns in the absence and presence of Na^+, respectively.[151] The phase and modulation values (Figure 19.48) are independent of total intensity, allowing the concentration of Na^+ to be determined even if the probe concentration is unknown. Cation-dependent decay times of SBFI and PBFI have been reported. Unfortunately, SBFI, PBFI, and similar probes display only modest changes in lifetime,[152–154] so that these probes do not seem suitable for lifetime-based sensing of Na^+ or K^+. CD222 does display useful changes in lifetime in response to K^+, even in the presence of large amounts of Na^+. In this case, lifetime-based sensing of K^+ using CD222 at the concentration present in blood appears to be possible. In contrast, CD222 does not allow wavelength-ratiometric measurements of K^+ in the presence of 100 mM sodium.[147]

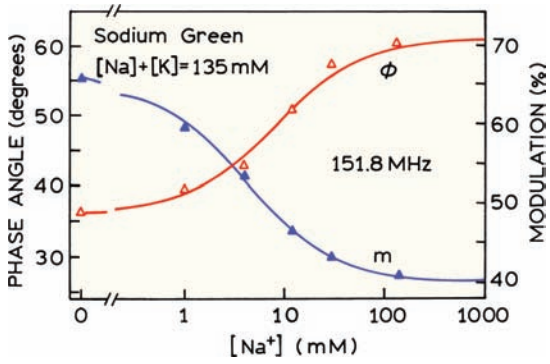

Figure 19.48. Sodium-dependent phase (ϕ) and modulation (*m*) of Sodium Green. Excitation was at 514 nm, and emission was observed above 530 nm. Data from [151].

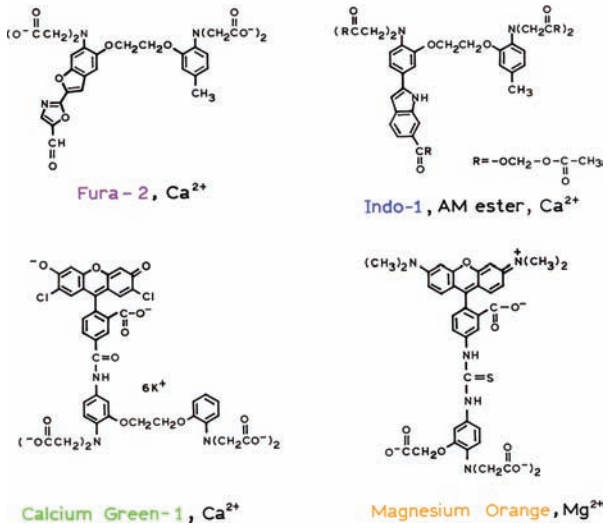

Figure 19.49. Representative Ca^{2+} and Mg^{2+} probes.

19.8.4. Calcium and Magnesium Probes

Calcium probes are perhaps the most widely used intracellular indicators (Figure 19.49). These indicators are based on the BAPTA chelator, which binds Ca^{2+} with affinities near 100 nM (Table 19.5). These probes are suitable for measurements of intracellular Ca^{2+}, but bind Ca^{2+} too tightly for measurement of Ca^{2+} in blood or serum, which is near 5 mM (Table 19.3). These probes are often used in fluorescence microscopy, where the local probe concentration is

Table 19.5. Spectral and Lifetime Properties of Ca^{2+} Probes

Probe	Excitation [a] λ_F (λ_B) [nm]	Emission $\lambda_F(\lambda_B)$ [nm]	$Q_F(Q_B)$	Lifetime (ns) [a] $\bar{\tau}_F$ ($\bar{\tau}_B$)	K_D (nM)
Quin-2	356 (336)	500 (503)	0.03 (0.14)	1.35 (11.6)	60.0
Fura-2	362 (335)	518 (510)	0.23 (0.49)	1.09 (1.68)	145.0
Indo-1	349 (331)	482 (398)	0.38 (0.56)	1.40 (1.66)	230.0
Fura Red	472 (436)	657 (637)	Low QY [b]	0.12 (0.11)	140.0
BTC [c]	464 (401)	531	NA [d]	0.71 (1.38)	
Fluo-3	504	526	40-fold	0.04 (1.28)	390
Rhod-2	550	581	100-fold	NA	570
Ca Green	506	534	0.06 (0.75)	0.92 (3.60)	190
Ca Orange	555	576	0.11 (0.33)	1.20 (2.31)	185
Ca Crimson	588	611	0.18 (0.53)	2.55 (4.11)	185
Ca Green-2	505	536	~100-fold[e]	NA	550
Ca Green-5N	506	536	~30-fold	NA	14,000
Ca Orange-5N	549	582	~5-fold	NA	20,000
Oregon Green					
BAPTA-1	494	523	~14-fold	0.73 (4.0)	170
BAPTA-2	494	523	35-fold	NA	580
BAPTA-5N	494	521	NA	NA	20,000

[a]F and B refer to the Ca^{2+} free and Ca^{2+}-bound forms of the probes, respectively.
[b]Low quantum yield.
[c]BTC, coumarin benzothiazole-based indicator.
[d]NA: not available.
[e]The term x-fold refers to the relative increase in fluorescence upon cation binding.

unknown. The salt forms of these dyes (Figure 19.49) do not diffuse across cell membranes, so that the cells need to be labeled by microinjection or electrophoration. BAPTA-based probes are also available with esterified carboxy groups, the so-called acetoxymethyl esters (AM esters). Figure 19.49 shows the AM ester of Indo-1. In this form the dyes are less polar and passively diffuse across cell membranes. Once inside the cell the AM esters are cleaved by intracellular esterases, and the negatively charged probe is trapped in the cells.

Fura-2 and Indo-1 are both wavelength-ratiometric probes. Fura-2 displays a large shift in its absorption spectrum upon binding Ca^{2+}, and is thus used with two excitation wavelengths (Figure 19.50).[155] Indo-1 displays a shift in its emission spectrum upon binding Ca^{2+}. Indo-1 can be used with two emission wavelengths, and a single excitation wavelength. Thus Indo-1 is preferred when using laser excitation sources, such as in a laser scanning microscope, where it is difficult to get two different excitation wavelengths.

Like the Na^+ and K^+ probes, Fura-2 and Indo-1 absorb in the UV. This is a disadvantage because of cellular autofluorescence and because it is difficult to obtain microscope optics with high-UV transmission. Hence it is desirable to develop calcium probes with longer excitation and emission wavelengths. Coumarin[156] and styryl-based[157] calcium probes have been developed but have not yet been widely used. The excitation spectra of one such probe are shown in Figure 19.51. These probes allow excitation up to 520 nm, but wavelength-ratiometric measurements require a second excitation wavelength below 430 nm.

Calcium probes based on fluoresceins and rhodamines are also available.[158–159] These probes typically have a BAPTA group linked to the fluorophore, rather than being part of the fluorophore. We refer to such probes as conjugate probes. One example is Calcium Green-1^J (Figure 19.49), which shows an approximately eight-fold increase in fluorescence upon binding calcium (Figure 19.50). Calcium Green-1^J is just one member of a series of conjugate probes for Ca^{2+} that display a range of emission wavelengths. Because Calcium Green-1 does not display a spectral shift it cannot be used for wavelength-ratiometric measurements. However, the lifetimes of the Calcium Green^J series all increase on Ca^{2+} binding, allowing the calcium

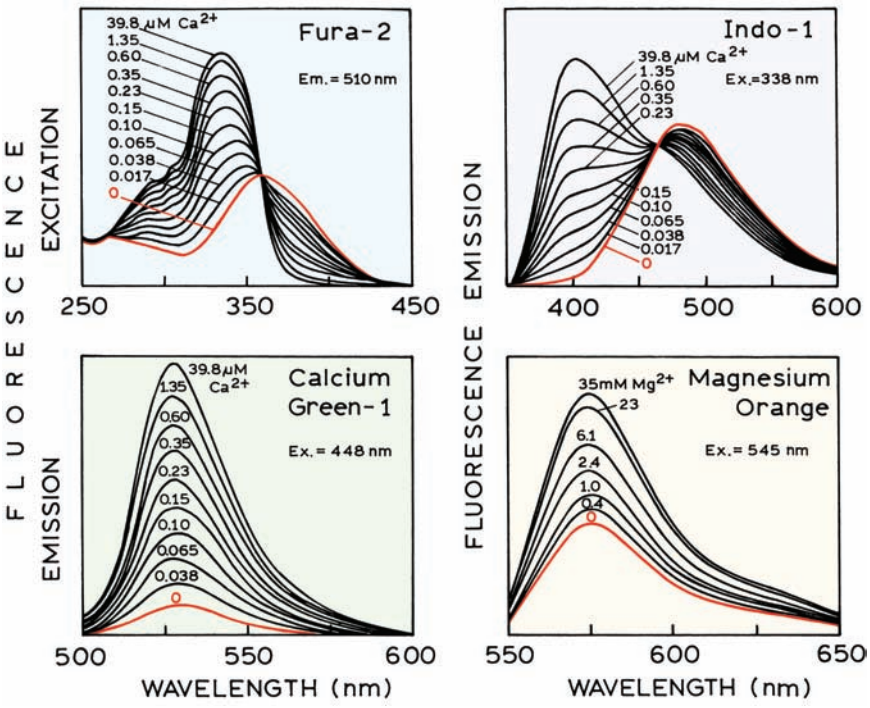

Figure 19.50. Excitation (Fura-2) and emission spectra (Indo-1, Calcium Green-1 and Magnesium Orange) of Ca^{2+} and Mg^{2+} probes in the presence of various concentrations of the ion. Revised from [142] and [144].

concentration to be determined from the lifetimes.[160–161] One of the first calcium probes, Quin-2, displays a tenfold increase in lifetime when bound to calcium.[162–163] However, Quin-2 requires UV excitation and displays a low quantum yield, so that it is now used less frequently. Recently, Ca^{2+} probes based on squaraines have been reported, allowing excitation wavelengths as long as 635 nm.[164–165]

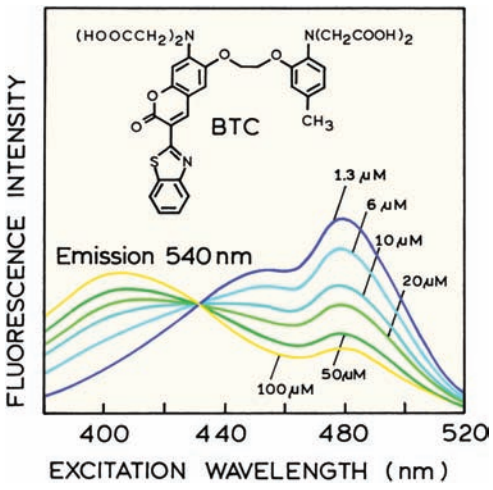

Figure 19.51. Excitation spectra of the coumarin benzothiazole-based indicator (BTC) lithium salt in Ca^{2+} solutions with concentrations ranging from 1.3 to 100 μM $CaCl_2$. Revised from [156].

While the use of the calcium probes seems straightforward, calibration is difficult when such probes are located within cells.[166–170] When used as intracellular indicators, the calcium probes are typically calibrated in the presence of other intracellular ions at their expected concentrations.[171] It is difficult to maintain nanomolar Ca^{2+} concentrations in the calibration solutions, and the probes themselves can alter the overall Ca^{2+} concentration. For this reason, calcium buffers have been developed and are commercially available. And, finally, the probe may interact with intracellular macromolecules, or by phototransformation during illumination in the microscope, resulting in altered behavior compared to the calibration data.[166,172]

Calcium probes have also been developed using aza-crown ethers as the chelator rather than BAPTA.[173–177] However, these probes have been mostly studied in organic solvents and used to study the effects of Ca^{2+} on electron transfer. Magnesium-sensitive probes are available (Table 19.4),[176–184] and some have been characterized as lifetime probes.[184] These probes typically have the APTRA chelator, rather than BAPTA, as can be seen for the calcium probe

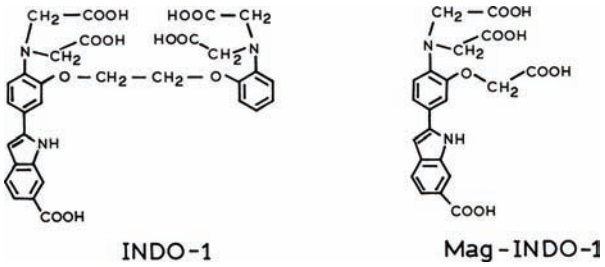

Figure 19.52. Chemical structures of the calcium probe of Indo-1 and the magnesium probe Mag-Indo-1. Data from [181].

Indo-1, and the analogous magnesium probe Mag-Indo-1 (Figure 19.52).

19.8.5. Probes for Intracellular Zinc

In recent years there has been increased interest in zinc. It is well known that zinc if bound to a number of enzymes and plays a structural role in zinc finger proteins. At present there is interest in the possible rate of zinc in plaque formation in Alzheimer's disease, post-ischemic toxicity, and as a neurotransmitter.[185] A number of zinc-sensitive fluorophores are now available.[186–189] Most of these probes contain the chelating group shown for Zinpry-1 (Figure 19.53). These probes show increases in fluorescence in the presence of zinc, which is probably due to a decrease in the amount of PET quenching in the zinc-bound form. The dissociation constants of these probes are near 1 to 3 nM. The

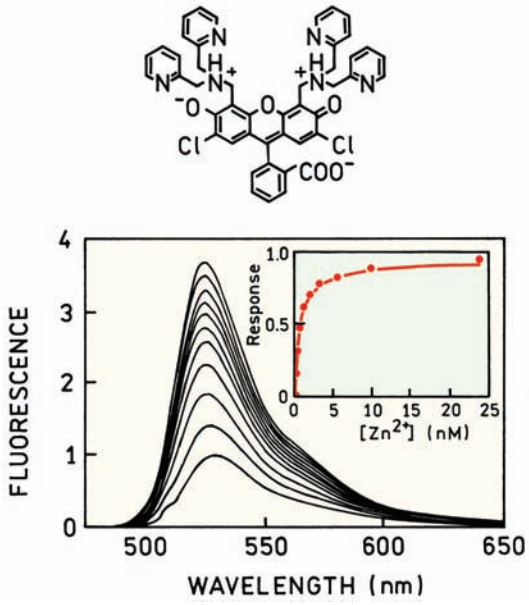

Figure 19.53. Chemical structure and emission spectra of Zinpyr-1. Reprinted with permission from [186]. Copyright © 2000, American Chemical Society.

levels of free zinc in cells may be in the picomolar range, so that zinc probes with higher affinity are needed.[190–191]

19.9. GLUCOSE-SENSITIVE FLUOROPHORES

The principles of analyte recognition have been used to develop fluorophores that are sensitive to glucose. There is

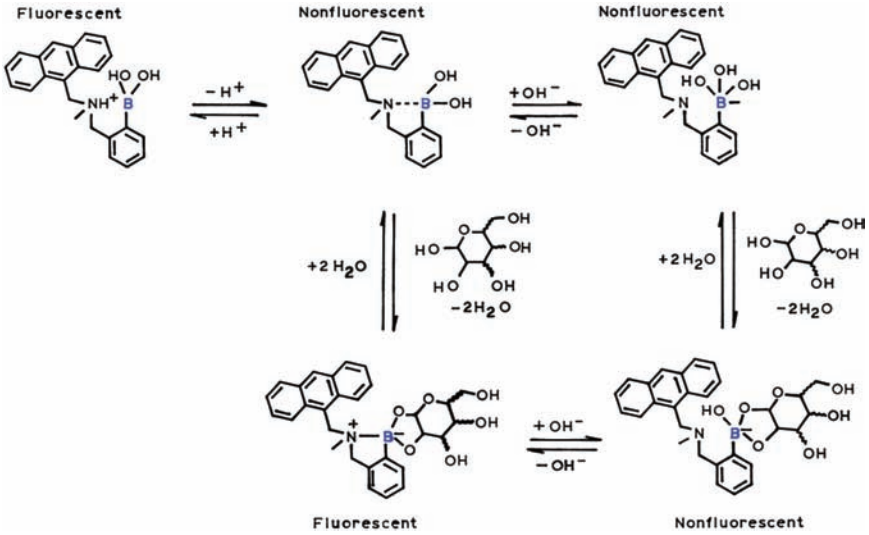

Figure 19.54. Glucose sensor based on photoinduced electron transfer. Revised from [194].

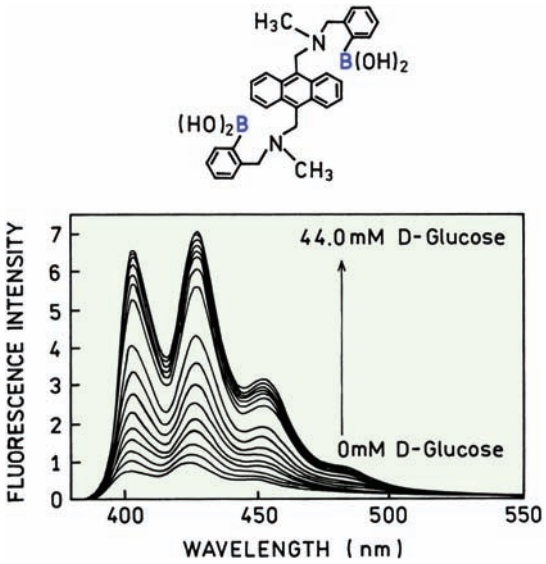

Figure 19.55. Glucose-dependent emission spectra of the shown structure. From [196].

vast literature on this topic,[192–193] from which we have selected several examples. These probes use boronic acid as part of the fluorophore. Boron forms complexes with diols, which has been used for decades for oxidation of sugars. Complexation of sugars to boron-containing fluorophores can result in changes in the emission intensity.[194–195] For the probe shown in Figure 19.54 complexation of sugars to the boron influences the extent of photoinduced electron transfer from the amino group. Depending on pH and sugar concentration, the anthracene group is either fluorescent or nonfluorescent. Figure 19.55 shows emission spectra of a similar probe. Addition of glucose results in an eight-fold increase in intensity.

A disadvantage of the probe shown in Figure 19.55 is that it is not wavelength ratiometric. Wavelength-ratiometric probes for glucose are now known.[197–200] One example is shown in Figure 19.56. This probe does not display PET quenching. Instead, complexation with glucose affects the extent of charge transfer from the amino group to the boronic acid. Upon binding of sugar there is more electron density on the boron, which decreases the extent of charge transfer and results in a blue shift in the emission spectra. Fructose usually gives the largest spectral change with such probes because it is the most reducing sugar. A difficulty with boronic acid fluorophores (BAFs) is to obtain a sugar-dependent spectral change at physiological pH. Many BAFs show sugar-dependent spectral changes only at pH 8 or higher. Several BAFs are now known that are sensitive at pH 7.5.[201–202]

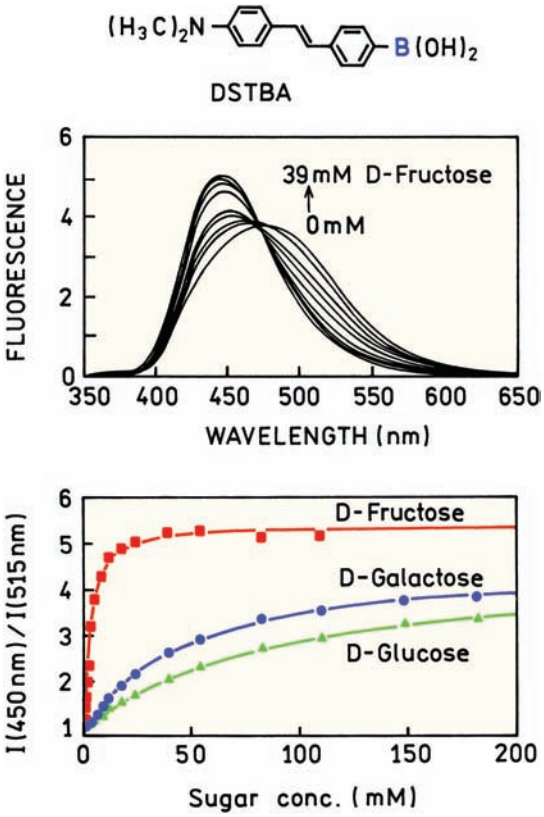

Figure 19.56. Emission spectra and wavelength ratios of the saccharide-sensitive probe DSTBA. Reprinted with permission from [200]. Copyright © 2001, American Chemical Society.

19.10. PROTEIN SENSORS

Another approach to sensing is to use proteins that bind the analyte of interest.[203–209] The usual approach is to express the recombinant protein with a single-cysteine residue for labeling. The probe is usually selected to be sensitive to solvent polarity, and the cysteine residue is positioned close to the binding site. Binding of the analyte to the protein may result in a change in the environment around the probe and a change in its fluorescence intensity. Protein sensors have been made for glucose,[210–212] maltose,[213–214] and other analytes.[215–218] Protein sensors are frequently based on the periplasmic protein from *E. coli*. These proteins provide the chemotactic signals needed by the bacterium to move toward nutrients. These signaling proteins have two domains.[219] The binding site is located between the domains that usually move closer together upon ligand binding.

Figure 19.57 shows an example of an engineered protein for glucose sensing. This protein sensor is based on the

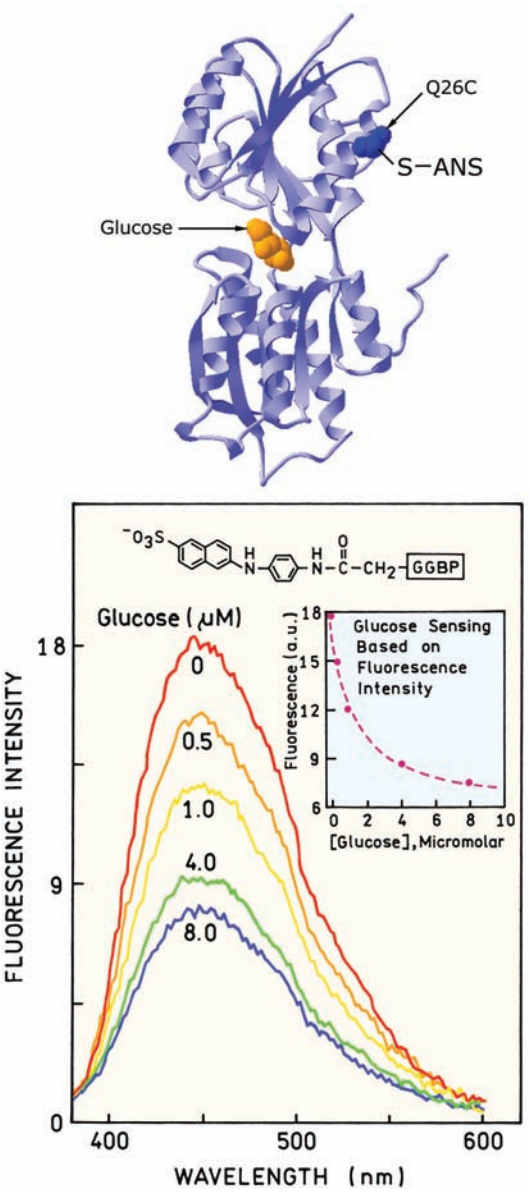

Figure 19.57. Protein sensor for glucose based on the glucose–galactose binding protein from *E. coli*. From [212].

glucose-galactose binding protein (GGBP) from *E. coli*. The wild-type protein contains no cysteine residues. GGBP was mutated by insertion of a single-cysteine residue at position 26, which was labeled with a sulfhydryl-reactive analogue of ANS. Upon addition of glucose the ANS intensity decreases about twofold. This decrease probably occurs because glucose binding brings the two domains closer together. The ANS is distant from the glucose-binding site and probably becomes more exposed to water when the domains move closer together.

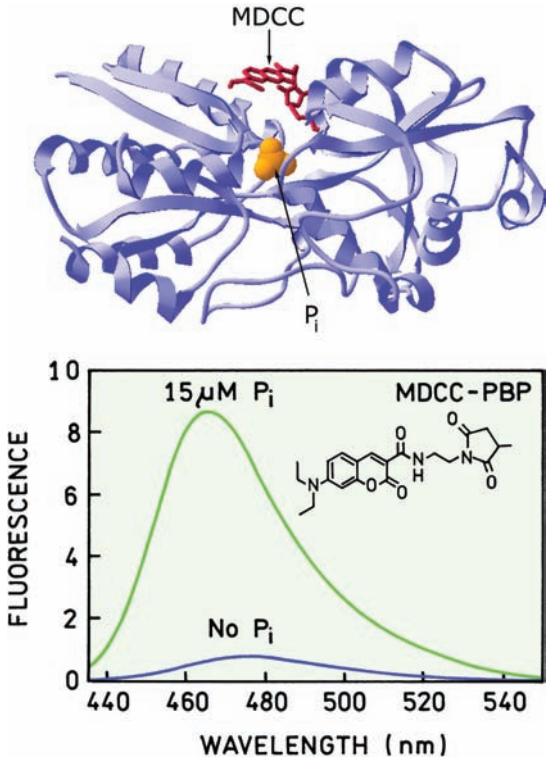

Figure 19.58. Emission spectra (bottom) of a coumarin-labeled phosphate binding protein from *E. coli* (top) in the absence and presence of 15 μM phosphate. Revised and reprinted with permission from [214]. Copyright © 1998, American Chemical Society.

A different periplasmic protein from *E. coli* was used to make a protein sensor for phosphate.[214–215] In one of these sensors a cysteine residue was inserted at residue 197 and labeled with a coumarin derivative (Figure 19.58). In this case binding of the phosphate ligand resulted in a dramatic increase in fluorescence intensity that is probably the result of shielding the fluorophore from water.

19.10.1. Protein Sensors Based on RET

The large intensity change displayed by the phosphate sensor (Figure 19.58) is exceptional. Most protein sensors display smaller changes of 1.5- to 2-fold, comparable to that shown for the glucose sensor in Figure 19.57. The scientific literature does not contain many reports of experiments which did not work, but it is likely that many laboratories attempted to make protein sensors using the periplasmic proteins and RET. It was logical to speculate that the changing distance between the domains would result in a change in RET between donors and acceptors positioned on opposite domains. Few such reports have appeared, probably

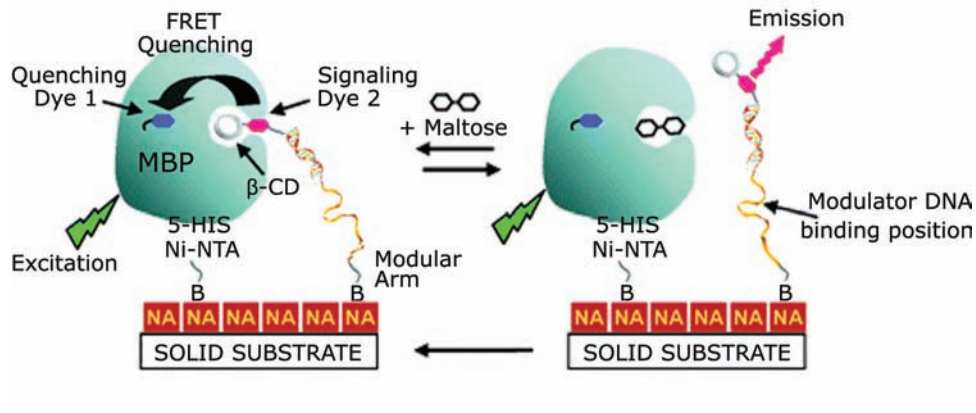

Figure 19.59. Schematic of a surface-bound maltose sensor based on the maltose-binding protein from *E. coli* and RET. Reprinted with permission from [220]. Copyright © 2004, American Chemical Society.

because the changes in distance have not been large enough to result in large changes in the transfer efficiency.

This problem of a limited change in intensity was solved by the use of RET between surface-bound reagents (Figure 19.59). This example also illustrates the increasingly sophisticated chemistry of sensors. This maltose sensor is based on the maltose-binding protein (MBP) from *E. coli*. The protein is bound to a NeutrAvidin surface by a biotinylated linker. MBP is labeled with a nonfluorescent acceptor QSY7. The donor is Cy3.5, which is also bound to the surface by a specialized linker (Figure 19.60). This linker contains a cyclodextrin that binds to MBP as well as the Cy3.5 donor. These components are bound to the surface by a biotinylated DNA linker arm that contains regions of single- and double-stranded DNA. The single-stranded region is present to allow changes in rigidity of the DNA by binding of a complementary sequence called modulator DNA. When both MBP and the linker are bound to the surface the

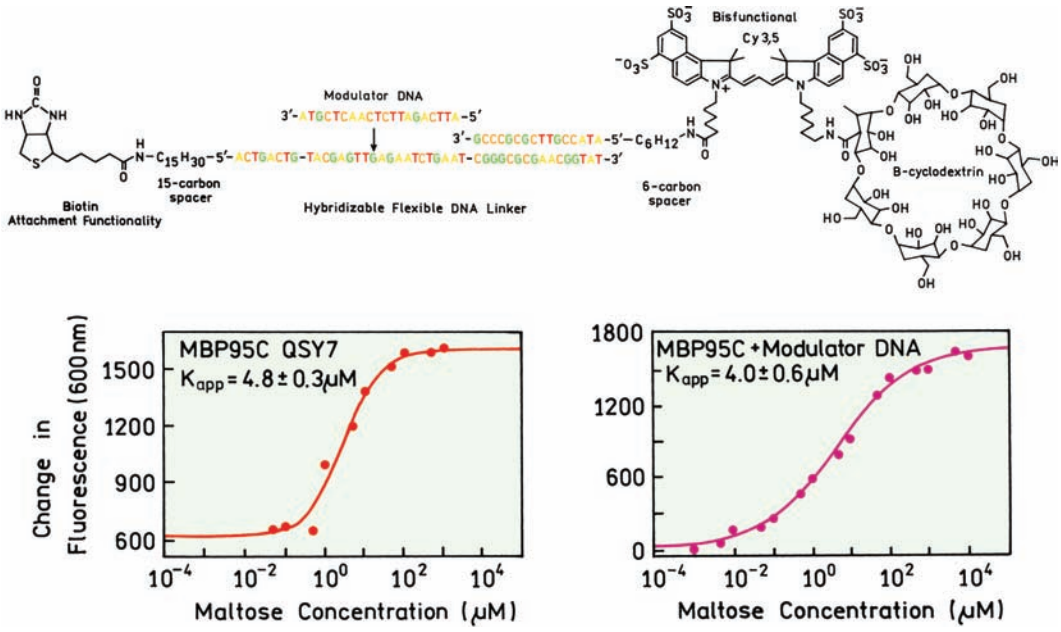

Figure 19.60. Linker arm containing the Cy3.5 donor and the cyclodextrin ligand. The fluorophore is bound to the surface via a biotinylated DNA oligomer with a single stranded region for binding of modulator DNA. The lower panels show the change in donor intensity of the sensor (Figure 19.58) in response to maltose. Revised and reprinted with permission from [220]. Copyright © 2004, American Chemical Society.

donor is quenched because the cyclodextrin binds to the protein that brings the Cy3.5 in close proximity to the QSY7 acceptor. Since QSY7 is nonfluorescent it is also called a quencher. Addition of maltose displaces cyclodextrin from MBP, resulting in an increased donor intensity (Figure 19.59). The extent of binding and, more importantly, the extent of RET could be increased by binding of the modulator DNA. These results describe a general strategy for surface-bound sensors that are adjustable and yield large changes in intensity. This approach is likely to be used in sensors for a wide variety of analytes.

19.11. GFP SENSORS

In Chapter 3 we described the ability of GFP to undergo internal reactions to create its own chromophore. This chromophore is contained with a β-barrel structure and is usually not sensitive to the surrounding solution conditions. GFP, its mutants, and the red coral proteins can be expressed in a wide variety of cells and organisms.[221] Hence, it would be useful if these proteins could be engineered to become sensitive to desired analytes. This has been accomplished in several ways, including the use of RET and modification of the protein structure so that the chromophore becomes sensitive to the analyte.

19.11.1. GFP Sensors Using RET

Since RET is a through-space phenomenon it can be used to modify the spectral properties of the GFP chromophore. GFP sensors based on RET have been developed for several analytes, such as calcium,[222–225] protein phosphorylation,[225–226] histone methylation,[227] and others.[228–230] The basic idea for these sensors is to make linked donor–acceptor GFP pairs where the conformation of the linker changes in response to the analyte.

Figure 13.22 in Chapter 13 shows a GFP-RET sensor for protein phosphorylation.[225] Cyan fluorescent protein (CFP) and yellow fluorescent protein (YFP) are used as the donor–acceptor pair. CFP and YFP are linked by a peptide that is a substrate for protein kinase. The linker also contains a phosphorylation recognition domain that binds the phosphorylated peptide. Binding of the phosphopeptide to the recognition domain is expected to bring the GFPs closer together, resulting in an increase in energy transfer. The lower panel shows fluorescence ratio images of CHO cells that express the sensor. When the cells are treated with insulin the donor intensity at 480 nm decreases relative to

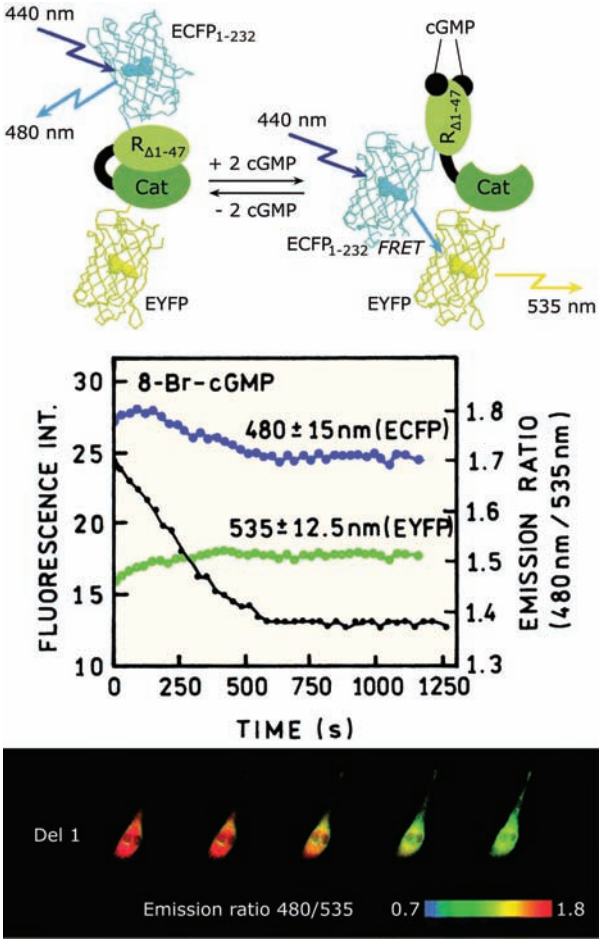

Figure 19.61. GFP-RET sensor for cGMP. Top: Schematic of sensor. Middle: Spectral response of sensor. Bottom: Ratio images of CHO cells expressing the GFP sensor. Revised and reprinted with permission from [230]. Copyright © 2000, American Chemical Society.

the acceptor emission at 535 nm. This result shows that cells can be grown and express protein sensors designed to detect a specific analyte or enzymatic activity.

Another example of a GFP-RET sensor is shown in Figure 19.61. The donor is enhanced cyan fluorescent protein (ECFP) and the acceptor enhanced yellow fluorescent protein (EYFP). The donor and acceptor are linked by the catalytic and regulating domains of cGMP-dependent protein kinase (PK). The PK was modified by removal of residues 1 to 47 (Δ1–47), which are responsible for dimerization of this PK, insuring that the sensor is a monomer within the cell. This sensor was expressed in CHO cells. The cells were treated with 8-Br-cGMP, which is a phosphodiesterase-resistant analogue of cGMP. This treatment results in a decrease in donor emission at 480 nm and a

slight increase in acceptor emission at 535 nm (middle panel). The ratio of donor-to-acceptor emission of the intracellular protein shows that the extent of RET increases in response to 8-Br-cGMP. Apparently, binding of cGMP or 8-Br-cGMP brings the donor and acceptor closer together.

19.11.2. Intrinsic GFP Sensors

In the previous two examples RET was used as the transducer mechanism. RET was used because the chromophore in GFP is usually shielded from the solvent. RET was also used to obtain a wavelength-ratiometric sensor that is needed to provide a quantitative interpretation of intracellular fluorescence. Mutant GFPs have been identified that are sensitive to chloride (Section 8.14.3) and pH. These proteins typically do not display shifts in their emission spectra[231–234] and cannot be used as emission-ratiometric probes. Some of the pH-sensitive GFP mutants display changes in absorption with pH, but excitation-ratiometric probes are less convenient than emission-ratiometric probes in fluorescence microscopy.

An emission wavelength-ratiometric pH-sensitive GFP is now available.[235] The absorption spectrum is sensitive to pH; more importantly, the emission spectra are also sensitive to pH (Figure 19.62). This sensitivity is not due to RET, but to ionization of a tyrosine side chain. As might be expected the longer-wavelength absorption and emission occurs at higher pH where the tyrosine is ionized. This protein can be used for estimation of intracellular pH. Figure 19.63 shows images of fibroblasts transfected with the gene for this GFP. The transfected cells show emission from the blue emission near 460 nm (top panel) and the green emission near 515 nm (middle panel). These two emissions are seen to be co-localized from the overlay with the light image (lower panel).

In summary, it is now possible to grow cells, and probably organisms, that express GFPs with sensitivity to a wide variety of ions and biomolecules.

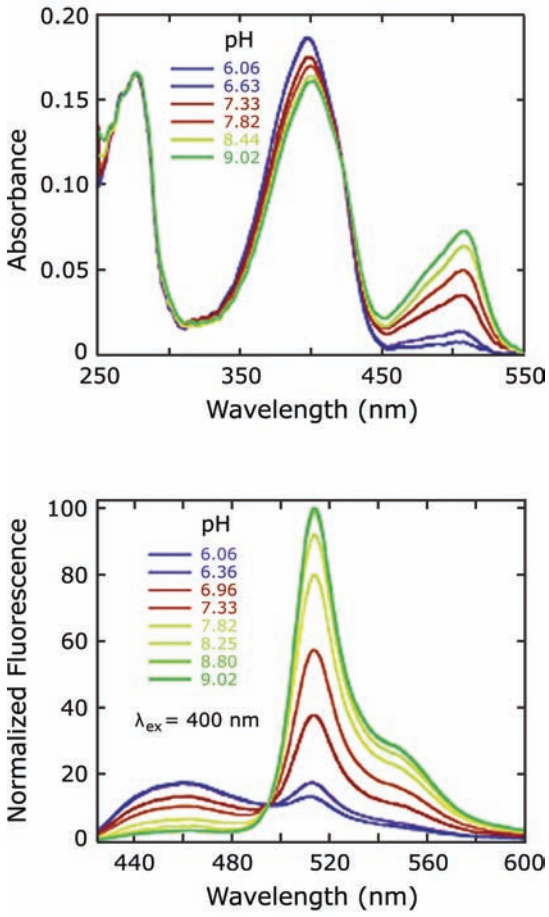

Figure 19.62. Absorption and emission spectra of a pH-sensitive GFP. Reprinted with permission from [235]. Copyright © 2000, American Chemical Society.

19.12. NEW APPROACHES TO SENSING

19.12.1. Pebble Sensors and Lipobeads

A wide variety of fluorophores are available for sensing cations and anions. These fluorophores are frequently used for measurement of intracellular ion concentration. However, these fluorophores can bind to intracellular biomolecules, which can alter the calibration curves by changing the binding constants or causing shifts in the absorption or emission spectra. The so-called Pebble sensors were developed to avoid interference due to binding of the probes to biomolecules.

Pebble sensors consist of one or more fluorophores embedded in polymer beads, typically made from polyacrylamide. The polymer is highly crosslinked and formed in the presence of the desired fluorophores, which are then trapped within the beads.[236–240] The high degree of crosslinking prevents proteins from entering the beads, so that the calibration curve is the same inside and outside the cells.

Pebble sensors have been developed for several analytes. Since the sensors are intended for intracellular use with fluorescence microscopy it is important to have ratiometric data. Figure 19.64 shows a Pebble sensor for pH. The beads were dense polymers made with 27% acrylamide and 3% N,N-methlyene-bis(acrylamide). The pH indicator

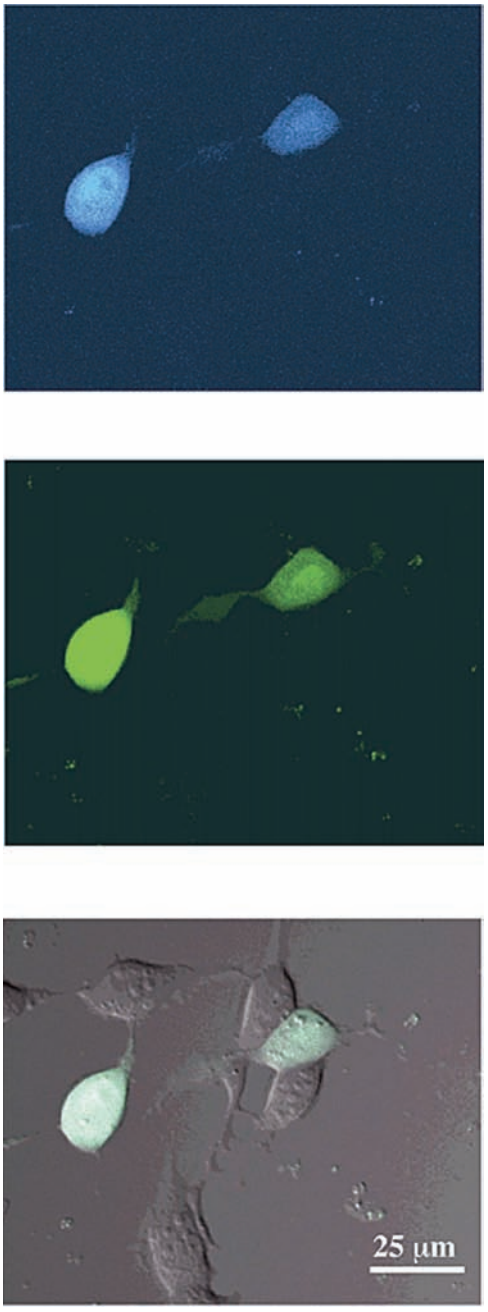

Figure 19.63. Fluorescence and light images of fibroblast cells which transiently express a pH-sensitive GFP. Top: Image at 435–485 nm. Middle: Image at 490–685 nm. Bottom: Overlay of the fluorescence images onto a light image. Reprinted with permission from [235]. Copyright © 2000, American Chemical Society.

was fluorescein, which is not practical for wavelength-ratiometric measurements. Wavelength-ratiometric measurements were made possible by inclusion of sulforhodamine, which is not sensitive to pH. Ratios of the intensities at 530 and 590 nm can be used to determine the pH without interference from biomolecules.

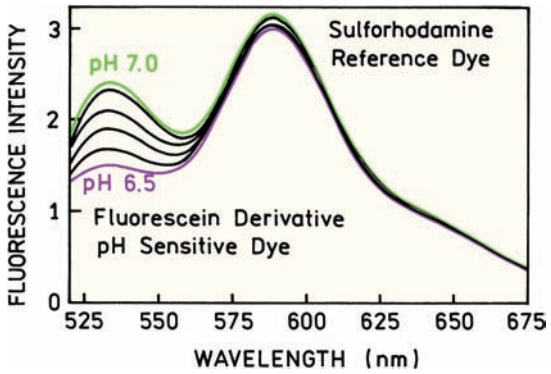

Figure 19.64. Emission spectra of a Pebble sensor, a polyacrylamide bead containing fluorescein as a pH-sensitive dye, and sulforhodamine as a pH-insensitive reference dye. Reprinted with permission from [238]. Copyright © 1999, American Chemical Society.

The intracellular use of Pebble sensors is shown in Figure 19.65. In this case the Pebbles were made by encapsulating Calcium Green and sulforhodamine in polyacrylamide beads.[239] Sulforhodamine served as a calcium-insensitive reference fluorophore. The laser scanning confocal images of human SYSY neuroblastoma cells are shown in Figure 19.65. Images were recorded using filters that transmitted the emission of sulforhodamine (right) or calcium green (left). The cells were treated with m-dinitrobenzene, which caused the release of calcium from the mitochondria, which resulted in an increase in the emission from Calcium Green but no change in the emission from sulforhodamine.

Sensors using polymer beads have also been made by coating the outer surface of polystyrene particles.[241–245] This has been accomplished by covalent attachment of probes to the outer surface. Bead sensors have also been made by coating polystyrene beads with lipids which bind the sensing fluorophores. These particles are called Lipobeads.

19.13. IN-VIVO IMAGING

In-vivo imaging is an emerging futuristic application of fluorescence technology. By in-vivo imaging we mean the creation of three-dimensional fluorescence images of the internal structures of humans or small animals. In-vivo imaging can be traced to the suggestion by Chance and coworkers that images could be obtained from the diffusive migration of photons in scattering tissues.[246–248] Tissues are strongly absorbing and strongly scattering at wavelengths below 600 nm (Figure 19.66). Tissue absorption and scattering is much

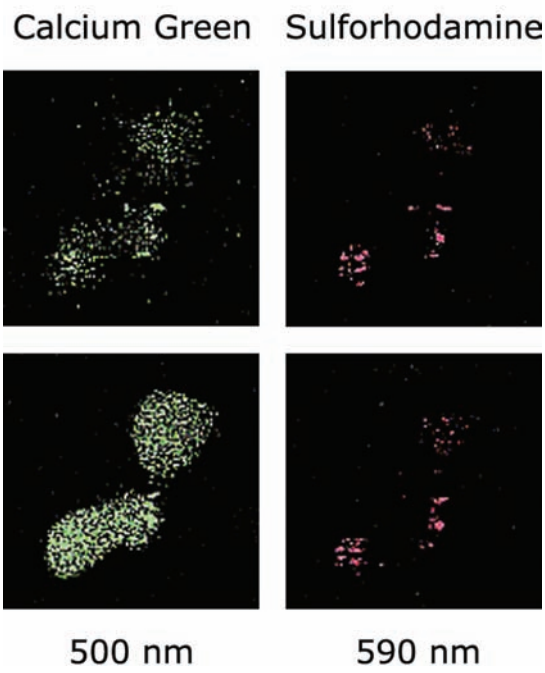

Figure 19.65. Laser scanning confocal microscopy images of human SYSY neuroblastoma C6 glioma cells containing Pebble sensors for calcium. The sensors contained Calcium Green and sulforhodamine as a reference dye. Images were recorded before (top) and after (bottom) treatment with m-dinitrobenzene. Revised and reprinted with permission from [239]. Copyright © 1999, American Chemical Society.

weaker above 650 nm, where tissues become somewhat translucent. This can be seen from the red light at 670 nm upon transillumination of a mouse.[249] When long-wavelength light passes through tissues the light migrates in a diffusive manner, similar to molecules in the gas phase. The photons move in a straight line until they are scattered, which results in a change in direction. The extent of scattering is described by a scattering coefficient μ_s that is expressed in units of reciprocal distance. Light passing through the tissue can also be absorbed, which is expressed as the absorption coefficient μ_a. Different tissues and different regions of tissues have different values of μ_s and μ_a, which affect the rate and distance over which photons can migrate in the tissue. The concept of photon migration imaging (PMI) is to measure spatially dependent transport of photons in tissues and to use the information to construct an image of the internal structure of the tissue.[246–248] This problem is much more difficult than x-ray computerized tomography because essentially none of the photons pass through the tissue without undergoing numerous scattering events.

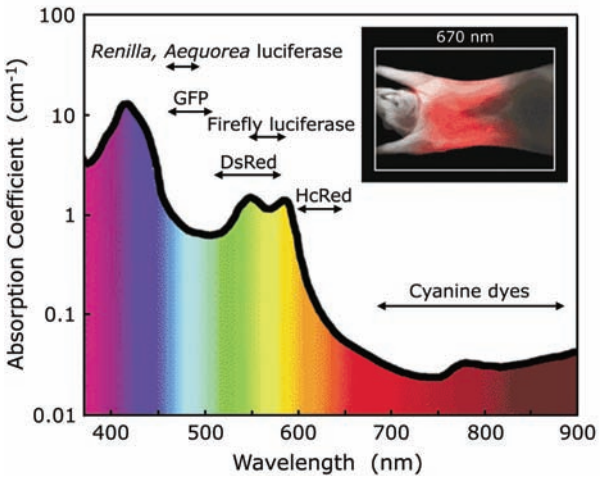

Figure 19.66. Absorption coefficient of typical tissue. The insert shows the transillumination of a mouse at 670 nm. Revised from [249].

One difficulty in PMI is the limited contrast in μ_s and μ_a between different regions of tissues. As a result there are attempts to increase the contrast by using injected dyes such as indocyanine green.[250–251] The instrumentation and algorithms developed for PMI are directly applicable to fluorescence in-vivo imaging. Figure 19.67 shows a relatively straightforward approach to in-vivo imaging. The mouse contained a tumor that overexpresses receptors for the peptide hormone somatostatin. The mouse was injected with an analogue to somatostatin labeled with a tricarbocyanine dye. The mouse was illuminated at 740 nm and imaged from the same side with a CCD camera. The location of the tumor is clearly seen from its long-wavelength emission. This tumor visualization was possible because of the weak light absorption of tissues and the absence of significant tissue autofluorescence at these long wavelengths.

Fluorescence is also being used for three-dimensional imaging of tissues.[254–255] This is accomplished by measuring the intensities or lifetimes with the light source and detector placed at a large number of locations around the animal[256–258] (Figure 19.68). Sophisticated algorithms are used to reconstruct the image from the data. An important development for in-vivo imaging is the fluorogenic probes for specific enzymes or tumors.[259–261] The image in Figure 19.68 was obtained with a peptide–polymer conjugate that was heavily labeled with Cy5.5. The fluorescence of the closely spaced Cy5.5 molecules was self-quenched due to the degree of labeling. The sequence of the peptide provided a cleavage site for a cathepsin. These enzymes degrade

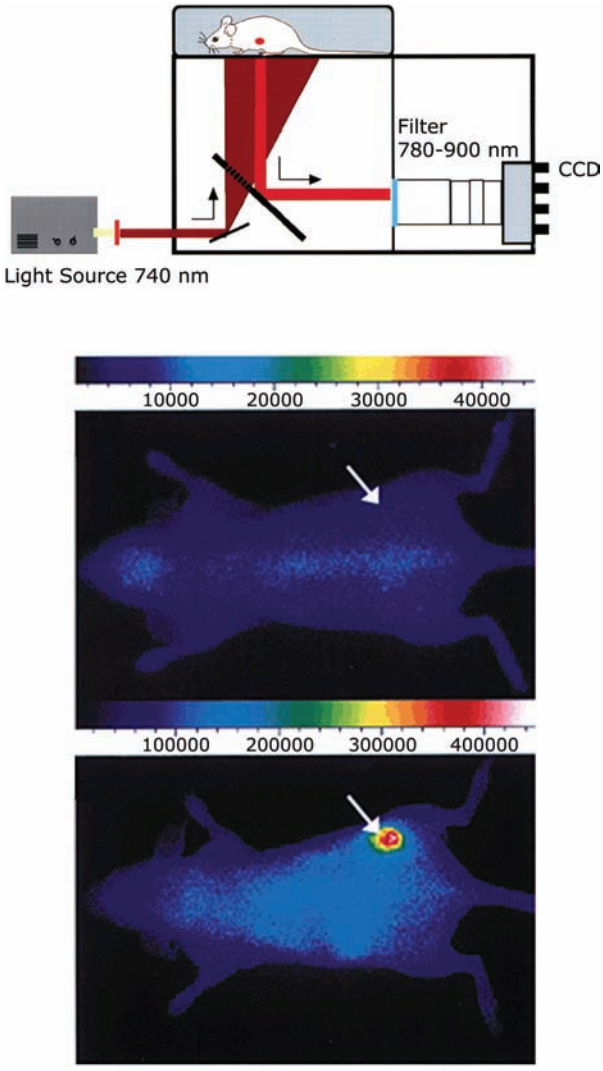

Figure 19.67. Fluorescence imaging of a labeled somatostatin analogue in a mouse tumor. The images were taken before (middle) and after (bottom) injection with the labeled peptide. The upper panel shows a schematic of the instrument. Revised from [252–253].

the extracellular matrix, and are often present at elevated levels in cancerous tissues and for other disease states.[262–264] The mouse in Figure 19.68 had a gliosarcoma surgically implanted in the brain.

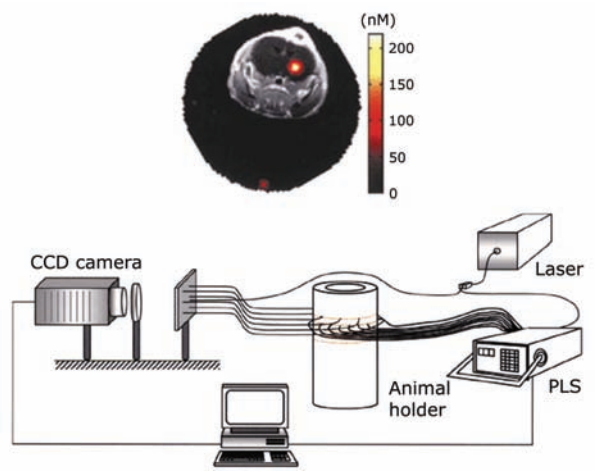

Figure 19.68. Schematic of an instrument for three-dimensional small animal imaging. PLS, programmable light switch. The image shows a sagittal section of a combined MRI and fluorescence image of a mouse injected with a cathepsin B-sensitive molecular beacon. From [258].

The labeled peptide was cleaved by a cathepsin in the tumor, resulting in increased intensity from Cy5.5 (color spot in Figure 19.68). The spot was superimposed on the MRI image of the same mouse. It is unlikely that in-vivo fluorescence imaging will provide the high spatial resolution available with MRI or CT. However, one can imagine a wide variety of labeled molecules that will localize in desired locations and be sensitive to specific enzymes. Fluorescence in-vivo imaging can add functional or physiological information to the images obtained using other modalities.

19.14. IMMUNOASSAYS

Immunoassays constitute a large and diverse family of assays that are based on many of the principles described in this book. The basic idea is to couple the association of antibody (Ab) with antigen (Ag) to some other event that yields an observable spectral change. Various mechanisms are possible, including energy transfer, anisotropy, delayed lan-

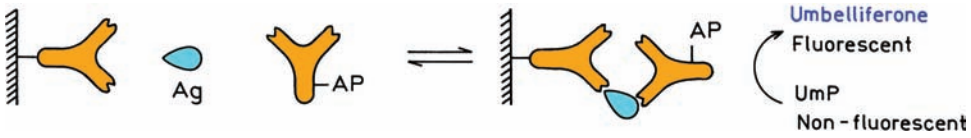

Figure 19.69. Schematic of an enzyme-linked immunosorbent assay (ELISA). AP is alkaline phosphate. Ag is an antigen, and UmP is umbelliferyl phosphate.

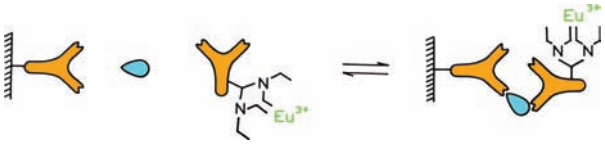

Figure 19.70. Time-resolved immunoassay based on the long-lived emission of europium.

thanide emission, or the use of enzymes to amplify the signal from a limited number of antigens.[265–270] The use of antibodies as analytical tools can be traced to the development of radioimmunoassays by Berson and Yalow,[271] which resulted in a Nobel prize. Since then immunoassays have been widely used, but are now based mainly on fluorescence detection.

19.14.1. Enzyme-Linked Immunosorbent Assays (ELISA)

The ELISA method is perhaps the most commonly used immunoassay format owing to its high sensitivity, applicability to a wide range of antigens, and the ability to remove background by washing steps. This method relies on the specific interaction between antigen and antibody. A surface is coated with an antibody specific for the antigen of interest. The sample is incubated with the surface-bound antibody, to allow the antibody to capture the antigen (Figure 19.69). The sample is then exposed to a second antibody that is covalently bound to an enzyme, typically alkaline phosphatase (AP), horseradish peroxidase, or β-galactosidase. Hence, the antigen must have more than a single antigenic site, and the second antibody must be different from the first antibody. Following adequate time for binding, the surface is washed to remove unbound enzyme-labeled antibody and the enzyme substrate is added. In the case shown in Figure 19.69 the enzyme alkaline phosphatase cleaves nonfluorescent umbelliferyl phosphate (UmP), yielding to the highly fluorescent umbelliferone. A signal is observed only when the antigen is present.

ELISA assays exist in a number of formats. In some cases the reaction product absorbs light, and in other cases the product is strongly fluorescent. The second antibody is not always labeled with enzyme but can be detected with yet another antibody that contains the bound enzyme. This procedure eliminates the need to attach probe or enzyme to a specific antibody that may be in short supply.

19.14.2. Time-Resolved Immunoassays

A variant of the ELISA method is the so-called "time-resolved immunoassay."[272–277] This type of assay also uses a polymeric support containing the capture antibody. The second labeled antibody has a covalently bound chelating group that contains a lanthanide such as europium (Figure 19.70). Detection is accomplished by addition of a so-called enhancer solution, which chelates the Eu^{3+} and has the necessary chromophore for excitation of the lanthanide by energy transfer (Figure 19.71). The enhancer solution is needed because the lanthanides absorb light very weakly, and are rarely excited directly. With the enhancer solution light is absorbed by chelators, which then transfer the excitation to the lanthanide. The chelating group is typically an EDTA derivative that strongly binds the Eu^{3+}. The Eu^{3+} can be released from the chelator at low pH. The "time-resolved immunoassays" can be performed by direct detection or in a competitive format. Direct detection is usually used for proteins which contain multiple antigenic sites.

These assays are called "time-resolved" because the sample is excited with a pulse of light, and the detector is

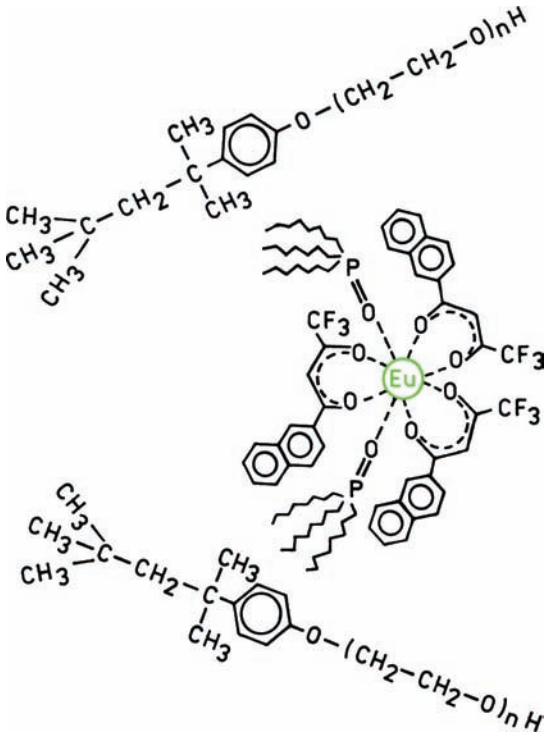

Figure 19.71. Europium in a fluorescent state following addition of enhancer solution. Structures from [274]. Copyright © 1990, CRC Press.

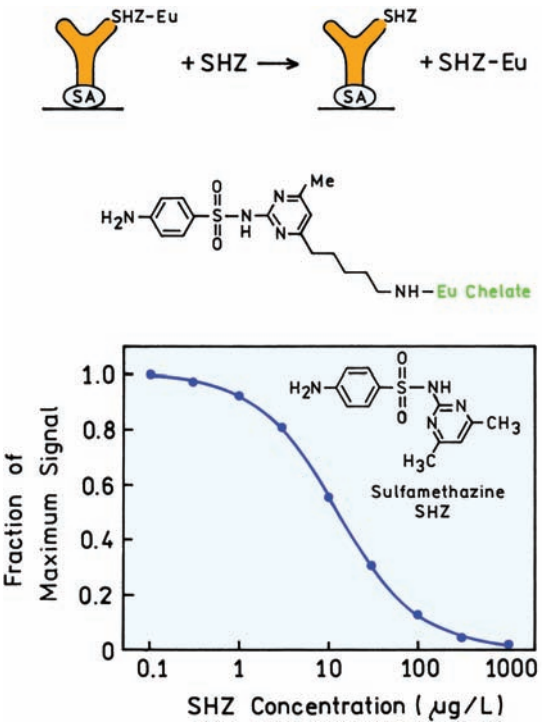

Figure 19.72. Competitive time-resolved immunoassay for sulfamethazine (SMZ). Reprinted with permission from [280]. Copyright © 2004, American Chemical Society.

gated on following decay of the prompt autofluorescence. Because the lanthanides display millisecond lifetimes, they continue to emit long after the ns interferences have decayed. The signal is integrated for a period of time, and the assay is based on measurement of integrated intensity, not a decay time. Hence, the phrase "time-resolved" should not be confused with a lifetime measurement.

Time-resolved immunoassays continue to be developed for a variety of analytes.[277–281] One example is a competitive immunoassay for the sulfa antibiotic sulfamethazine (SHZ) in food. The presence of residual antibiotics in food is of concern because of the potential health risk to humans and the development of antibiotic resistance in bacteria. This immunoassay is based on antibodies against SHZ. These antibodies are bound to streptavidin-coated microwell plates (Figure 19.72). These antibodies bind an analogue of SHZ that contains a covalently bound europium chelate (SHZ-Eu). This analogue is allowed to bind to the antibodies. The assay is performed by adding the sample to the well, allowing time for binding, washing the plate, then adding the enhanced solution and measuring the time-delayed emission. The intensity decreases as the SHZ increases because SHZ displays SHZ-Eu, and the SHZ-Eu is washed out of the well prior to addition of the enhanced solution.

19.14.3. Energy-Transfer Immunoassays

Resonance energy transfer provides an obvious approach to measuring antigen–antibody association, and was suggested for immunoassays in 1976.[282] Such an assay would typically be performed in a competitive format, and can be homogeneous (Figure 19.73). Suppose the analyte is the triazine herbicide simazine (SZ), which is shown as the open shape in Figure 19.73. An antibody against SZ is labeled with the donor Cy5 and bound to the bottom of the well.[283] The acceptor Cy5.5 is bound to BSA, which also contains a covalently bound analogue of SZ. The assay is then per-

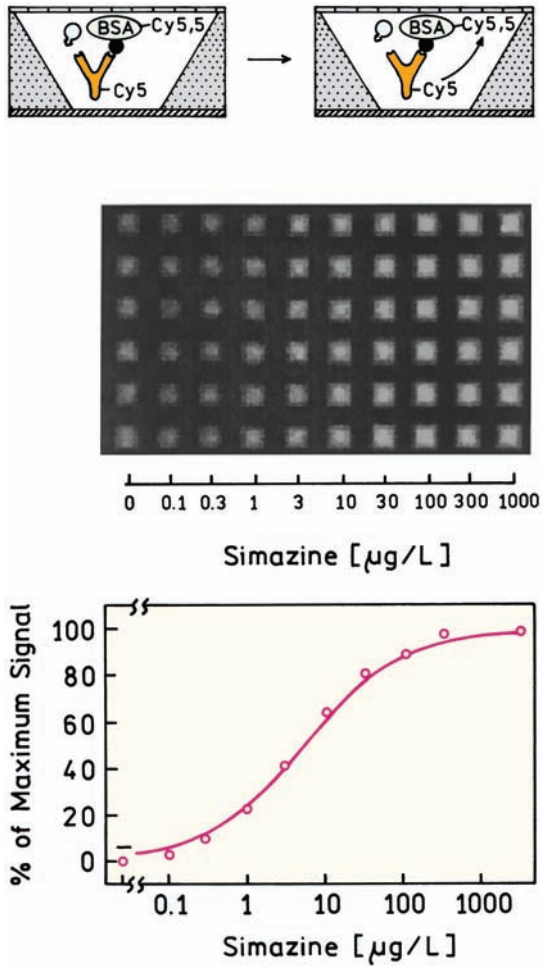

Figure 19.73. Competitive RET immunoassay for the herbicide simazine. Revised and reprinted with permission from [283]. Copyright © 2001, American Chemical Society.

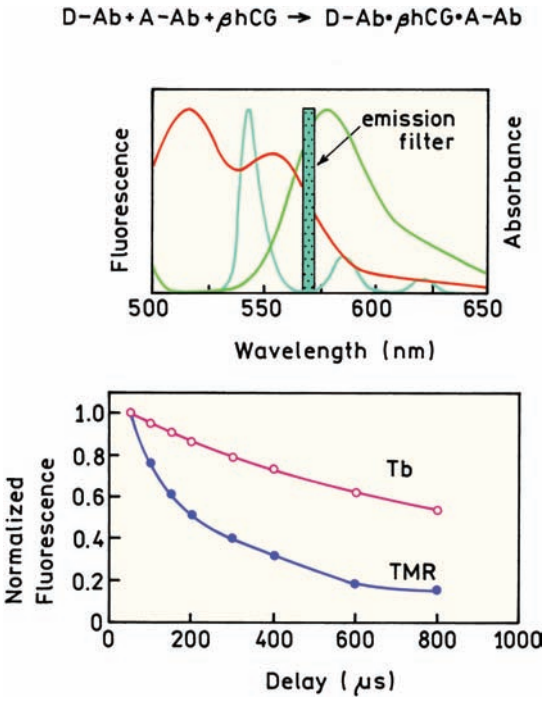

Figure 19.74. Time-resolved RET immunoassay for βhCG. The lower panel shows the intensity decay of the Tb donor and the TMR acceptor in a solution containing the complex shown in the top right. Revised from [289].

formed by adding the sample that contains SZ. As SZ increases the intensity of the surface-bound Cy5 donor increases, because the Cy5.5-BSA is displaced by SZ. This RET assay was facilitated by the large R_0 for the Cy5–Cy5.5 donor–acceptor pair,[284] which is near 75 Å. However, there is overlap in the emission spectra of Cy5 and Cy5.5. This overlap could be tolerated in this case because the unbound acceptor was washed away. Some background from Cy5.5 is acceptable because the Cy5 emission could be measured on the blue side of its emission spectrum. It is usually easier to separately measure the donor emission because the short-wavelength sides of emission spectra often drop sharply to zero, but there are almost always tails at long wavelengths. Energy-transfer immunoassays have been described for other analytes,[285–288] but it can be difficult to obtain adequate energy transfer due to the size of the proteins.

The difficulties of overlapping emission spectra of the donors and acceptors can be minimized to some extent using lanthanide donors and measurement of the sensitized acceptor emission. Figure 19.74 shows an immunoassay for the β subunit of human chorionic gonadotropin (βhCG). Two antibodies were used and directed against different epitopes of βhCG.[289] One of the antibodies was labeled with a terbium chelate as the donor, and the second antibody was labeled with TMR as the acceptor. Binding of these two antibodies to βhCG resulted in long-lived sensitive emission of the acceptor, which could be observed selectively using a 570-nm emission filter. This wavelength is near the peak of the rhodamine emission but is between peaks of the structured terbium emission.

The lower panel shows time-resolved decays of the Tb and TMR in a mixture containing the immune complex. The decay of the Tb is slower than that of TMR because of the presence of Tb-labeled antibodies that are free in solution or not near an acceptor. The intensity decay of TMR is more rapid because the long-lived acceptor emission is due to RET, so that the acceptor decay is the same as the decay of the Tb bound near the acceptor. The use of sensitized acceptor emission made it unnecessary to wash away excess reagents, so that the assay could be performed in a homogeneous format.

19.14.4. Fluorescence Polarization Immunoassays

The final type of immunoassay is the fluorescence polarization immunoassay (FPI). Assays of this type are based on anisotropy measurements of labeled antigens.[290–291] The use of the term "polarization" instead of anisotropy is historical, and now entrenched in the literature. The anisotropy of a mixture (r) is determined by the anisotropies of the free (F) and bound (B) species (r_F and r_B) and their relative fluorescence intensities (f_F and f_B):

$$r = r_F f_F + r_B f_B \qquad (19.14)$$

An FPI is a competitive assay that can be performed in a homogeneous format. Suppose that the antigen is the hormone cortisol (Cor).[292] The assay mixture would contain labeled cortisol, in this case labeled with fluorescein (Fl), and antibody specific for cortisol (Figure 19.75). Prior to addition of cortisol from the sample, the anisotropy will be

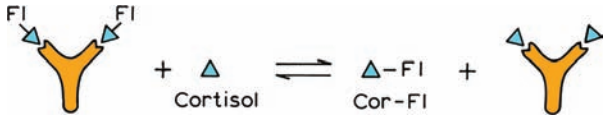

Figure 19.75. Homogeneous fluorescence polarization immunoassay for cortisol (Cor). Fl, fluorescein.

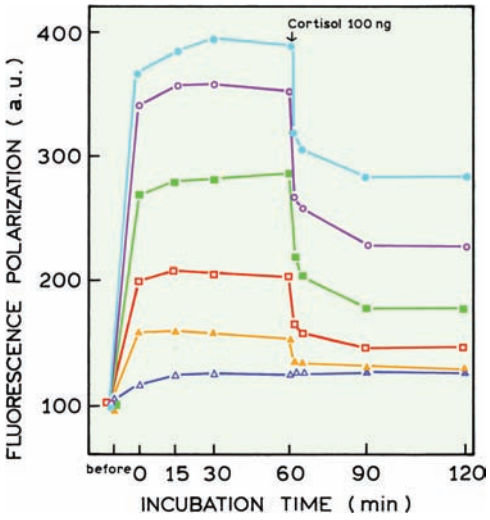

Figure 19.76. Time-dependent changes in polarization upon mixing of antibody to cortisol or nonspecific antibody (Δ) and fluorescein-labeled cortisol and upon addition, at 60 minutes, of 100 ng of unlabeled cortisol. The antibody is more dilute from top to bottom. Revised from [292].

the highest due to binding of antibody to Cor-Fl. Free cortisol from the sample will displace Cor-Fl from the antibody. The Co4Fl is now free to rotate, and the anisotropy decreases.

Typical data for a cortisol FPI are shown in Figures 19.76 and 19.77. Cor-Fl was prepared by reaction of cortisol-21-amine with fluorescein isothiocyanate (FITC). Upon mixing anti-Cor antibody (Ab) to cortisol with Cor-Fl the polarization increased, which was presumed due to specific

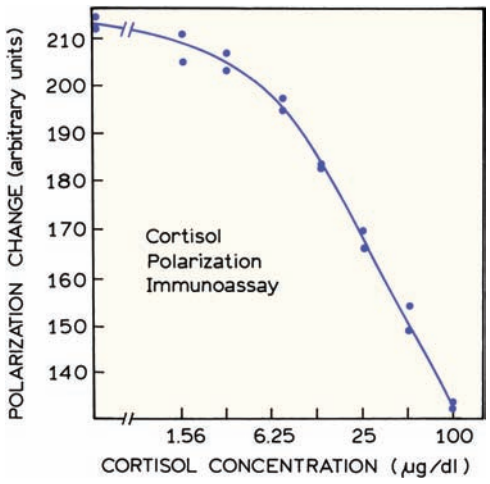

Figure 19.77. Cortisol fluorescence polarization immunoassay. Revised from [292].

binding of Ab to Cor-Fl. The specificity of the reaction was confirmed by adding unlabeled cortisol, which resulted in a decrease in polarization, and also by the absence of a change in polarization due to nonspecific antibody (Δ).

To perform the cortisol assay one uses a mixture of Ab and Cor-Fl, to which is added the serum sample. As the concentration of serum cortisol is increased, the polarization decreases (Figure 19.77). The polarization values are used to determine the cortisol concentration. Similar FPIs have been developed for a wide range of low-molecular-weight analytes, including antibiotics,[293–294] cocaine metabolites,[295–296] therapeutic drugs,[297–298] the immunosuppressant cyclosporin,[299–300] and phosphorylated proteins.[301–303] Numerous FPIs are routinely performed on automatic clinical analyzers.[304]

FPIs have advantages and disadvantages. FPIs do not require multiple antigenic sites, as is needed with heterogeneous capture immunoassays or RET immunoassays. FPIs can be performed in a homogeneous format, and may not require separation steps. However, because FPIs are usually performed with fluorescein, they are generally limited to low-molecular-weight analytes. This is because the emission must be depolarized in the unbound state, which would not occur for higher-molecular-weight fluorescein-labeled proteins.

The limitation of FPIs to low-molecular-weight analyte is illustrated by the FPI for creatine kinase-BB. Creatine kinase is a dimer, and the subunits can be from muscle (M) or brain (B). Creatine kinase MB is used as a marker for cardiac damage, and the presence of CK-BB in the blood may reflect a number of disease states, including brain trauma.[305–307] Figure 19.78 shows an FPI for CK-BB.[307] In this particular case the protein was labeled with dansylaziridine (DANZA), instead of fluorescein. The immunoassay was also performed with other probes (Table 19.6). One notices

Table 19.6. Fluorescein Polarization Immunoassay of Creatine Kinase BB[a]

Fluorophore-CK	τ (ns)	Polarization	
		No antibody	With antibody
CPM-CK[b]	~5	0.337	0.342
IAF-CK	~5	0.333	0.339
DNS-CK	~15	0.181	0.224
DANZA-CK	~15	0.170	0.242

[a]From [307].
[b]CPM, 3-(4-maleimidylphenyl)-7-diethylamino-4-methyl coumarin; IAF, 5'-iodo-acetamidofluorescein; DNS, dansyl chloride; DANZA, dansylaziridine.

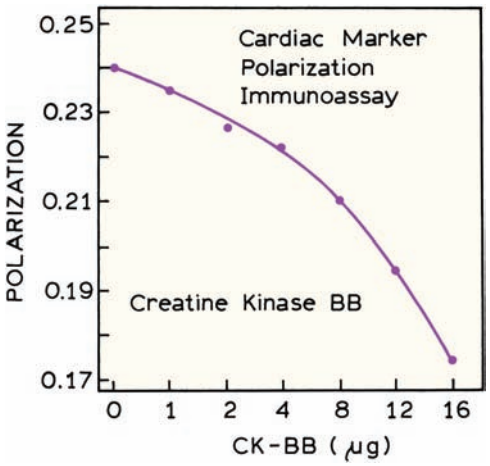

Figure 19.78. Fluorescence polarization immunoassay of creatine kinase BB. Revised from [307].

that the polarization changes are smaller with the other probes. This is because the lifetimes of these probes, the fluorescein derivative IAF, and coumarin derivative CPM are near 5 ns, while the lifetime of DANZA is near 15 ns. The longer lifetime of the dansyl-labeled protein (DNS or DANZA) allows more time for the protein to undergo rotational diffusion. This limitation of FPIs to low-molecular-weight substances can be overcome by the use of long-lifetime metal ligand probes, which is described in the following chapter.

REFERENCES

1. Wolfbeis OS. 2004. Fiber-optic chemical sensors and biosensors. *Anal Chem* **76**:3269–3284.
2. Cammann K. 2003. Sensors and analytical chemistry. *Phys Chem Chem Phys* **5**:5159–5168.
3. Rich RL, Myszka DG. 2002. Survey of the year 2001 commercial optical biosensor literature. *J Mol Recognit* **15**:352–376.
4. de Silva AP, Fox DB, Moody TS, Weir SM. 2001. The development of molecular fluorescent switches. *Trends Biotechnol* **19**(1):29–34.
5. Badugu R. 2005. Fluorescence sensor design for transition metal ions: the role of the PIET interaction efficiency. *J Fluoresc* **15**(1): 71–83.
6. Geddes CD, Lakowicz JR, eds. 2005. *Topics in fluorescence spectroscopy*, Vol. 9: *Advanced concepts in fluorescence sensing: macromolecular sensing*. Springer-Verlag, New York. In press.
7. Geddes CD, Lakowicz JR, eds. 2005. *Topics in fluorescence spectroscopy*, Vol. 10: *Advanced concepts in fluorescence sensing: small molecule sensing*. Springer-Verlag, New York. In press.
8. Lakowicz JR, ed. 1994. *Topics in fluorescence spectroscopy*, Vol. 4: *Probe design and chemical sensing*. Plenum Press, New York.
9. Undenfriend S. 1969. *Fluorescence assay in biology and medicine*, Vol 2. Academic Press, New York. (See also Vol. 1. 1962.)
10. Kricka LJ, Skogerboe KJ, Hage DA, Schoeff L, Wang J, Sokol LJ, Chan DW, Ward KM, Davis KA. 1997. Clinical chemistry. *Anal Chem* **69**:165R–229R.
11. Burtis CA, Ashwood ER. 1999. *Tietz textbook of clinical chemistry*. W.B. Saunders, Philadelphia.
12. Wolfbeis OS. 1991. Biomedical applications of fiber optic chemical sensors. In *Fiber optic chemical sensors and biosensors*, Vol. 2, pp. 267–300. Ed OS Wolfbeis. CRC Press, Boca Raton, FL.
13. Szmacinski H, Lakowicz JR. 1994. Lifetime-based sensing. In *Topics in fluorescence spectroscopy*, Vol. 4: *Probe design and chemical sensing*, pp. 295–334. Ed JR Lakowicz. Plenum Press, New York.
14. Kieslinger D, Draxler S, Trznadel K, Lippitsch ME. 1997. Lifetime-based capillary waveguide sensor instrumentation. *Sens Actuators B* **38–39**:300–304.
15. Lippitsch ME, Draxler S, Kieslinger D. 1997. Luminescence lifetime-based sensing: new materials, new devices. *Sens Actuators B* **38–39**:96–102.
16. Draxler S. 2005. Lifetime based sensors/sensing. In *Topics in fluorescence spectroscopy*, Vol. 10: *Advanced concepts in fluorescence sensing: small molecule sensing*, pp. 241–274. Ed CD Geddes, JR Lakowicz. Springer-Verlag, New York.
17. Richards-Kortum R, Sevick-Muraca E. 1996. Quantitative optical spectroscopy for tissue diagnosis. *Annu Rev Phys Chem* **47**:555–606.
18. Gouin JF, Baros F, Birot D, Andre JC. 1997. A fibre-optic oxygen sensor for oceanography. *Sens Actuators B* **38–39**:401-406.
19. Valeur B. 1994. Principles of fluorescent probe design for ion recognition. In *Topics in fluorescence spectroscopy*, Vol. 4: *Probe design and chemical sensing*, pp. 21–48. Ed JR Lakowicz. Plenum Press, New York.
20. Rettig W, Lapouyade R. 1994. Fluorescence probes based on twisted intramolecular charge transfer (TICT) states and other adiabatic photoreactions. In *Topics in fluorescence spectroscopy*, Vol. 4: *Probe design and chemical sensing*, pp. 109–149. Ed JR Lakowicz. Plenum Press, New York.
21. Czarnik AW. 1994. Fluorescent chemosensors for cations, anions, and neural analytes. In *Topics in fluorescence spectroscopy*, Vol. 4: *Probe design and chemical sensing*, pp. 49–70. Ed JR Lakowicz. Plenum Press, New York.
22. Fabbrizzi L, Poggi A. 1995. Sensors and switches from supramolecular chemistry. *Chem Soc Rev* **24**:197–202.
23. Bryan AJ, Prasanna de Silva A, de Silva SA, Dayasiri Rupasinghe AD, Samankumara Sandanayake KRA. 1989. Photo-induced electron transfer as a general design logic for fluorescent molecular sensors for cations. *Biosensors* **4**:169–179.
24. Demas JN, DeGraff BA. 1994. Design and applications of highly luminescent transition metal complexes. In *Topics in fluorescence spectroscopy*, Vol. 4: *Probe design and chemical sensing*, pp. 71–107. Ed JR Lakowicz. Plenum Press, New York.
25. Klimant I, Belser P, Wolfbeis OS. 1994. Novel metal-organic ruthenium (II) diimine complexes for use as longwave excitable luminescent oxygen probes. *Talanta* **41**(6):985–991.
26. Demas JN, DeGraff BA, Coleman PB. 1999. Oxygen sensors based on luminescence quenching. *Anal Chem News Feat* 793A–800A.
27. Bacon JR, Demas JN. 1987. Determination of oxygen concentrations by luminescence quenching of a polymer immobilized transition metal complex. *Anal Chem* **59**:2780–2785.

28. Wolfbeis OS. 1991. Oxygen sensors. In *Fiber optic chemical sensors and biosensors*, Vol. II, pp. 19–53. Ed OS Wolfbeis. CRC Press, Boca Raton, FL.
29. Mills A, Williams FC. 1997. Chemical influences on the luminescence of ruthenium diimine complexes and its response to oxygen. *Thin Solid Films* **306**:163–170.
30. Lippitsch ME, Pusterhofer J, Leiner MJP, Wolfbeis OS. 1988. Fibre-optic oxygen sensor with the fluorescence decay time as the information carrier. *Anal Chim Acta* **205**:1–6.
31. Draxler S, Lippitsch ME, Klimant I, Kraus H, Wolfbeis OS. 1995. Effects of polymer matrices on the time-resolved luminescence of a ruthenium complex quenched by oxygen. *J Phys Chem* **99**:3162–3167.
32. Simon JA, Curry SL, Schmehl RH, Schatz TR, Piotrowiak P, Jin X, Thummel RP. 1997. Intramolecular electronic energy transfer in ruthenium(II) diimine donor/pyrene acceptor complexes linked by a single C–C bond. *J Am Chem Soc* **119**:11012–11022.
33. Lakowicz JR, Johnson ML, Lederer WJ, Szmacinski H, Nowaczyk K, Malak H, Berndt KW. 1992. Fluorescence lifetime sensing generates cellular images. *Laser Focus World* **28**(5):60–80.
34. Xu W, Kneas KA, Demas JN, DeGraff BA. 1996. Oxygen sensors based on luminescence quenching of metal complexes: osmium complexes suitable for laser diode excitation. *Anal Chem* **68**:2605–2609.
35. Bambot SB, Rao G, Romauld M, Carter GM, Sipior J, Terpetschnig E, Lakowicz JR. 1995. Sensing oxygen through skin using a red diode laser and fluorescence lifetimes. *Biosens Bioelectron* **10**(6/7):643–652.
36. Papkovsky DB, Ponomarev GV, Trettnak W, O'Leary P. 1995. Phosphorescent complexes of porphyrin ketones: optical properties and applications to oxygen sensing. *Anal Chem* **67**:4112–4117.
37. Lu X, Han BH, Winnik MA. 2003. Characterizing the quenching process for phosphorescent dyes in poly[((n-butylamino)thionyl)-phosphazene] films. *J Phys Chem B* **107**:13349–13356.
38. Trettnak W, Kolle C, Reininger F, Dolezal C, O'Leary P. 1996. Miniaturized luminescence lifetime-based oxygen sensor instrumentation utilizing a phase modulation technique. *Sens Actuators B* **35–36**:506–512.
39. Kostov Y, Van Houten KA, Harms P, Pilato RS, Rao G. 2000. Unique oxygen analyzer combining a dual emission probe and a low-cost solid-state ratiometric fluorometer. *Appl Spectrosc* **54**(6):864–868.
40. Lakowicz JR, Szmacinski H, Nowaczyk K, Johnson ML. 1992. Fluorescence lifetime imaging of free and protein-bound NADH. *Proc Natl Acad Sci USA* **89**:1271–1275.
41. Lakowicz JR, Szmacinski H, Nowaczyk K, Berndt K, Johnson ML. 1992. Fluorescence lifetime imaging. *Anal Biochem* **202**:316–330.
42. Zhong W, Urayama P, Mycek MA. 2003. Imaging fluorescence lifetime modulation of a ruthenium-based dye in living cells: the potential for oxygen sensing. *J Phys D App. Phys* **36**:1689–1695.
43. Boas G. 2003. FLIM system measures long-lived, oxygen-sensitive probes. *Biophotonics Int*, September, pp. 59–60.
44. Geddes C. 2001. Optical halide sensing using fluorescence quenching: theory, simulations and applications—a review. *Meas Sci Technol* **12**:R53–R88.
45. Geddes CD. 2001. Halide sensing using the SPQ molecule. *Sens Actuators B* **72**:188–195.
46. Illsley NP, Verkman AS. 1987. Membrane chloride transport measured using a chloride-sensitive fluorescent probe. *Biochemistry* **26**:1215–1219.
47. Verkman AS. 1990. Development and biological applications of chloride-sensitive fluorescent indicators. *Am J Physiol* **253**:C375–C388.
48. Verkman AS, Sellers MC, Chao AC, Leung T, Ketcham R. 1989. Synthesis and characterization of improved chloride-sensitive fluorescent indicators for biological applications. *Anal Biochem* **178**:355–361.
49. Biwersi J, Tulk B, Verkman AS. 1994. Long-wavelength chloride-sensitive fluorescent indicators. *Anal Biochem* **219**:139–143.
50. Orosz DE, Carlid KD. 1992. A sensitive new fluorescence assay for measuring proton transport across liposomal membranes. *Anal Biochem* **210**:7–15.
51. Chao AC, Dix JA, Sellers MC, Verkman AS. 1989. Fluorescence measurement of chloride transport in monolayer cultured cells: mechanisms of chloride transport in fibroblasts. *Biophys J* **56**:1071–1081.
52. Sonawane ND, Thiagarajah JR, Verkman AS. 2002. Chloride concentration in endosomes measured using a ratioable fluorescent Cl^- indicator. *J Biol Chem* **277**(7):5506–5513.
53. Jayaraman S, Biwersi J, Verkman AS. 1999. Synthesis and characterization of dual-wavelength Cl^- sensitive fluorescent indicators for ration imaging. *Am J Physiol* 276:C747–C751.
54. Kaneko H, Putzier I, Frings S, Kaupp UB, Gensch T. 2004. Chloride accumulation in mammalian olfactory sensory neurons. *J Neurosci* **24**(36):7931–7938.
55. Wolfbeis OS, Sharma A. 1988. Fibre-optic fluorosensor for sulphur dioxide. *Anal Chim Acta* **208**:53–58.
56. Sharma A, Draxler S, Lippitsch ME. 1992. Time-resolved spectroscopy of the fluorescence quenching of a donor–acceptor pair by halothane *Appl Phys*. **B54**:309–312.
57. Omann GM, Lakowicz JR. 1982. Interactions of chlorinated hydrocarbons insecticides with membranes. *Biochem Biophys Acta* **684**:83–95.
58. Vanderkooi JM, Wright WW, Erecinska M. 1994. Nitric oxide diffusion coefficients in solutions, proteins and membranes determined by phosphorescence. *Biochim Biophys Acta* **1207**:249–254.
59. Denicola A, Souza JM, Radi R, Lissi E. 1996. Nitric oxide diffusion in membranes determined by fluorescence quenching. *Arch Biochem Biophys* **328**(1):208–212.
60. Franz KJ, Singh N, Lippard SJ. 2000. Metal-based NO sensing by selective ligand dissociation. *Angew Chem, Int Ed* **39**(12):2120–2122.
61. Kojima H, Nagano T. 2000. Fluorescent indicators for nitric oxide. *Adv Mater* **12**(10):763–765.
62. Kojima H, Hirotani M, Urano Y, Kikuchi K, Higuchi T, Nagano T. 2000. Fluorescent indicators for nitric oxide based on rhodamine chromophore. *Tetrhedron Lett* **41**:69–72.
63. Jordan DM, Walt DR, Milanovich FP. 1987. Physiological pH fiber-optic chemical sensor based on energy transfer. *Anal Chem* **59**:437–439.
64. Lakowicz JR, Szmacinski H, Karakelle M. 1993. Optical sensing of pH and pCO_2 using phase-modulation fluorimetry and resonance energy transfer. *Anal Chim Acta* **272**:179–186.

65. Sipior J, Bambot S, Romauld M, Carter GM, Lakowicz JR, Rao G. 1995. A lifetime-based optical CO_2 gas sensor with blue or red excitation and Stokes or anti-Stokes detection. *Anal Biochem* **227**: 309–318.
66. Chang Q, Randers-Eichhorn L, Lakowicz JR, Rao G. 1998. Steam-sterilizable, fluorescence lifetime-based sensing film for dissolved carbon dioxide. *Biotechnol Prog* **14**:326–331.
67. Neurauter G, Klimant I, Wolfbeis OS. 1999. Microsecond lifetime-based optical carbon dioxide sensor using luminescence resonance energy transfer. *Anal Chim Acta* **382**:67–75.
68. Marazuela MD, Moreno-bondi MC, Orellana G. 1998. Luminescence lifetime quenching of a ruthenium(II) polypyridyl dye for optical sensing of carbon dioxide. *Appl Spectrosc* **52**(10): 1314–1320.
69. von Bultzingslowen C, McEvoy AK, McDonagh C, MacCraith BD. 2003. Lifetime-based optical sensor for high-level pCO_2 detection employing fluorescence resonance energy transfer. *Anal Chim Acta* **480**:275–283.
70. Preininger C, Ludwig M, Mohr GJ. 1998. Effect of the sol-gel matrix on the performance of ammonia fluorosensors based on energy transfer. *J Fluoresc* **8**(3):199–205.
71. Mohr GJ, Draxler S, Trznadel K, Lehmann F, Lippitsch ME. 1998. Synthesis and characterization of fluorophore–absorber pairs for sensing of ammonia based on fluorescence. *Anal Chim Acta* **360**:119–128.
72. Chang Q, Sipior J, Lakowicz JR, Rao G. 1995. A lifetime-based fluorescence resonance energy transfer sensor for ammonia. *Anal Biochem* **232**:92–97.
73. Wolfbeis OS, Klimant I, Werner T, Huber C, Kosch U, Krause C, Neurauter G, Durkop A. 1998. Set of luminescence decay time based chemical sensors for clinical appointments. *Sens Actuators* **B51**: 17–24.
74. Mills A, Chang Q, McMurray N. 1992. Equilibrium studies on colorimetric plastic film sensors for carbon dioxide. *Anal Chem* **64**: 1383–1389.
75. Wolfbeis OS, Reisfeld R, Oehme I. 1996. Sol-gels and chemical sensors. *Struct Bonding* **85**:51–98.
76. Avnir D, Braun S, Ottolenghi M. 1992. A review of novel photoactive, optical, sensing and bioactive materials. *ACS Symp Ser* **499**: 384–404.
77. The Diabetes Control and Complications Trial Research Group. 1993. The effect of intensive treatment of diabetes on the development and progression of long-term complications in insulin-dependent diabetes mellitus. *New Engl J Med* **329**(14):977–986.
78. Lakowicz JR. 1994. Emerging biomedical applications of time-resolved fluorescence spectroscopy. In *Topics in fluorescence spectroscopy*, Vol. 4: *Probe design and chemical sensing*, pp. 1–9. Ed JR Lakowicz. Plenum Press, New York.
79. Schultz JS, Sims G. 1979. Affinity sensors for individual metabolites. *Biotechnol Bioeng Symp* **9**:65–71.
80. Schultz J, Mansouri S, Goldstein IJ. 1982. Affinity sensor: a new technique for developing implantable sensors for glucose and other metabolites. *Diabetes Care* **5**(3):245–253.
81. Meadows D, Schultz JS. 1988. Fiber-optic biosensors based on fluorescence energy transfer. *Talanta* **35**(2):145–150.
82. Lakowicz JR, Maliwal BP. 1993. Optical sensing of glucose using phase-modulation fluorometry. *Anal Chim Acta* **271**:155–164.
83. Tolosa L, Szmacinski H, Rao G, Lakowicz JR. 1997. Lifetime-based sensing of glucose using energy transfer with a long lifetime donor. *Anal Biochem* **250**:102–108.
84. Tolosa L, Malak H, Rao G, Lakowicz JR. 1997. Optical assay for glucose based on the luminescence decay time of the long wavelength dye Cy5™. *Sens Actuators B* **45**:93–99.
85. He H, Li H, Mohr G, Kovacs B, Werner T, Wolfbeis OS. 1993. Novel type of ion-selective fluorosensor based on the inner filter effect: an optrode for potassium. *Anal Chem* **65**:123–127.
86. Roe JN, Szoka FC, Verkman AS. 1989. Optical measurement of aqueous potassium concentration by a hydrophobic indicator in lipid vesicles. *Biophys Chem* **33**:295–302.
87. Roe JN, Szoka FC, Verkman AS. 1990. Fibre optic sensor for the detection of potassium using fluorescence energy transfer. *Analyst* **115**:353–368.
88. Mahutte CK. 1994. Continuous intra-arterial blood gas monitoring. *Intensive Care Med* 20:85–86.
89. Shapiro BA, Mahutte CK, Cane RD, Gilmour IJ. 1993. Clinical performance of a blood gas monitor: a prospective, multicenter trial. *Crit Care Med* **21**(4):487–494.
90. Yafuso M, Arick SA, Hansmann D, Holody M, Miller WW, Yan CF, Mahutte K. 1989. Optical pH measurements in blood. *Proc SPIE* **1067**:37–43.
91. Vurek GG, Feustel PJ, Severinghaus JW. 1983. A fiber optic pCO_2 sensor. *Ann Biomed Eng*. **11**:499–510.
92. Mahutte CK, Holody M, Maxwell TP, Chen PA, Sasse SA. 1994. Development of a patient-dedicated, on-demand, blood gas monitor. *Am J Respir Crit Care Med* **149**:852–859.
93. Mahutte CK, Sasse SA, Chen PA, Holody M. 1994. Performance of a patient-dedicated, on-demand blood gas monitor in medical ICU patients. *Am J Respir Crit Care Med* **150**:865–869.
94. Opitz N, Lubbers DW. 1987. Theory and development of fluorescence-based optochemical oxygen sensors: oxygen optodes. *Int Anesthesiol Clin* **25**(3):177–197.
95. Ohkuma S, Poole B. 1978. Fluorescence probe measurement of the intralysosomal pH in living cells and the perturbation of pH by various agents. *Proc Natl Acad Sci USA* **5**(7):3327–3331.
96. Thomas JA, Buchsbaum RN, Zimniak A, Racker E. 1979. Intracellular pH measurements in Ehrlich ascites tumor cells utilizing spectroscopic probes generated in situ. *Biochemistry* **18**:2210–2218.
97. Munkholm C, Walt DR, Milanovich FP. 1988. A fiber-optic sensor for CO_2 measurement. *Talanta* **35**(2):109–112.
98. Kawabata Y, Kamichika T, Imasaka T, Ishibashi N. 1989. Fiber-optic sensor for carbon dioxide with a pH indicator dispersed in a poly(ethyleneglycol) membrane. *Anal Chim Acta* **219**:223–229.
99. Yguerabide J, Talavera E, Alvarez JM, Quintero B. 1994. Steady-state fluorescence method for evaluating excited state proton reactions: application to fluorescein. *Photochem Photobiol* **60**(5): 435–441.
100. Haugland RP. 1996. *Handbook of fluorescent probes and research chemicals*. Molecular Probes Inc., Eugene, OR. (See Chapter 23, pp. 551–561.)

101. Sjoback R, Nygren J, Kubista M. 1995. Absorption and fluorescence properties of fluorescein. *Spectrochim Acta Part A* **51**:L7–L21.
102. Choi MMF. 1998. Spectroscopic behavior and proteolytic equilibrium of fluorescein immobilized in ethyl cellulose. *J Photochem Photobiol A: Chem* **114**:235–239.
103. Rink TJ, Tsien RY, Pozzan T. 1982. Cytoplasmic pH and free Mg^{2+} in lymphocytes. *J Cell Biol* **95**:189–196.
104. Clement NR, Gould JM. 1981. Pyranine (8-hydroxy-1,3,6-pyrenetrisulfonate) as a probe of internal aqueous hydrogen ion concentration in phospholipid vesicles. *Biochemistry* **20**:1534–1538.
105. Wolfbeis OS, Fürlinger E, Kroneis H, Marsoner H. 1983. Fluorimetric analysis, 1: a study on fluorescent indicators for measuring near neutral ("Physiological") pH-values. *Fresenius Z Anal Chem* **314**:119–124.
106. Schulman SG, Chen S, Bai F, Leiner MJP, Weis L, Wolfbeis OS. 1995. Dependence of the fluorescence of immobilized 1-hydroxypyrene-3,6,8-trisulfonate on sodium pH: extension of the range of applicability of a pH fluorosensor. *Anal Chim Acta* **304**:165–170.
107. Zhujun H, Seitz WR. 1984. A fluorescence sensor for quantifying pH in the range from 6.5 to 8.5. *Anal Chim Acta* **160**:47–55.
108. Uttamlal M, Walt DR. 1995. A fiber-optic carbon dioxide sensor for fermentation monitoring. *BioTechnology* **13**:597–601.
109. Whitaker JE, Haugland RP, Prendergast FG. 1991. Spectral and photophysical studies of benzo[c]xanthene dyes: dual emission pH sensors. *Anal Biochem* **194**:330–344.
110. Szmacinski H, Lakowicz JR. 1993. Optical measurements of pH using fluorescence lifetimes and phase-modulation fluorometry. *Anal Chem* **65**:1668–1674.
111. Srivastava A, Krishnamoorthy G. 1997. Time-resolved fluorescence microscopy could correct for probe binding while estimating intracellular pH. *Anal Biochem* **249**:140–146.
112. Liu J, Diwu Z, Leung WY. 2001. Synthesis and photophysical properties of new fluorinated benzo[c]xanthene dyes as intracellular pH indicators. *Bioorgan Med Chem Lett* **11**:2903–2905.
113. Adamczyk M, Grote J. 2003. Synthesis of probes with broad pH range fluorescence. *Bioorgan Med Chem Lett* **13**:2327–2330.
114. Budisa N, Rubini M, Bae JH, Weyher E, Wenger W, Golbik R, Huber R, Moroder L. 2002. Global replacement of tryptophan with aminotryptophans generates non-invasive protein-based optical pH sensors. *Angew Chem, Int Ed* **41**(21):4066–4069.
115. Kermis HR, Kostov Y, Harms P, Rao G. 2002. Dual excitation ratiometric fluorescent pH sensor for noninvasive bioprocess monitoring: development and application. *Biotechnol Prog* **18**:1047–1053.
116. Bernhard DD, Mall S, Pantano P. 2001. Fabrication and characterization of microwell array chemical sensors. *Anal Chem* **73**:2484–2490.
117. Liebsch G, Klimant I, Krause C, Wolfbeis OS. 2001. Fluorescent imaging of pH with optical sensors using time domain dual lifetime referencing. *Anal Chem* **73**:4354–4363.
118. Wolfbeis OS, Rodriguez NV, Werner T. 1992. LED-compatible fluorosensor for measurement of near-neutral pH values. *Mikrochim Acta* **108**:133–141.
119. Briggs MS, Burns DD, Cooper ME, Gregory SJ. 2000. A pH-sensitive fluorescent cyanine dye for biological application. *Chem Commun* 2323–2324.
120. Zen J-M, Patonay G. 1991. Near-infrared fluorescence probe for pH determination. *Anal Chem* **63**:2934–2938.
121. Boyer AE, Devanathan S, Hamilton D, Patonay G. 1992. Spectroscopic studies of a near-infrared absorbing pH-sensitive carbocyanine dye. *Talanta* **39**(5):505–510.
122. Wolfbeis OS, Marhold H. 1987. A new group of fluorescent pH-indicators for an extended pH-range. *Anal Chem* **327**:347–350.
123. Murtaza Z, Chang Q, Rao G, Lin H, Lakowicz JR. 1997. Long-lifetime metal–ligand pH probes. *Anal Biochem* **247**:216–222.
124. deSilva AP, Nimal Gunaratne HQ, Rice TE. 1996. Proton-controlled switching of luminescence in lanthanide complexes in aqueous solution: pH sensors based on long-lived emission. *Angew Chem, Int Ed Engl* **35**:2116–2118.
125. Kubo K, Sakurai T. 2000. Molecular recognition of PET fluoroionophores. *Heterocycles* **52**(2):945–976.
126. Bryan AJ, de Silva P, de Silva SA, Rupasinghe RADD, Sandanayake KRAS. 1989. Photo-induced electron transfer as a general design logic for fluorescent molecular sensors for cations. *Biosensors* **4**: 169–179.
127. de Silva AP, Gunaratne HQN, Habib-Jiwan J-L, McCoy CP, Rice TE, Soumillion J-P. 1995. New fluorescent model compounds for the study of photoinduced electron transfer: the influence of a molecular electric field in the excited state. *Angew Chem, Int Ed Engl* **34**: 1728–1731.
128. Kubo K. 2005. PET sensors. In *Topics in fluorescence spectroscopy*, Vol. 9: *Advanced concepts in fluorescence sensing: macromolecular sensing*, pp. 219–247. Ed CD Geddes, JR Lakowicz. Plenum Press, New York.
129. Akkaya EU, Huston ME, Czarnik AW. 1990. Chelation-enhanced fluorescence of anthrylazamacrocycle conjugate probes in aqueous solution. *J Am Chem Soc* **112**:3590–3593.
130. Fages F, Desvergne JP, Bouas-Laurent H, Marsau P, Lehn J-M, Kotzyba-Hibert F, Albrecht-Gary A-M, Al-Joubbeh M. 1989. Anthraceno-cryptands: A new class of cation-complexing macrobicyclic fluorophores. *J Am Chem Soc* **111**:8672–8680.
131. de Silva AP, de Silva SA. 1986. Fluorescent signalling crown ethers; "switching on" of fluorescence by alkali metal ion recognition and binding in situ. *J Chem Soc Chem Commun* 1709–1710.
132. Gunnlaugsson T, Davis AP, Glynn M. 2001. Fluorescent photoinduced electron transfer (PET) sensing of anions using charge neutral chemosensors. *Chem Commun* 2556–2557.
133. Snowden TS, Anslyn EV. 1999. Anion recognition: synthetic receptors for anions and their application in sensors. *Curr Opin Chem Biol* **3**:740–746.
134. Huston ME, Akkaya EU, Czarnik AW. 1989. Chelation enhanced fluorescence detection of non-metal ions. *J Am Chem Soc* **111**:8735–8737.
135. Beer PD, Gale PA. 2001. Anion recognition and sensing: the state of the art and future perspectives. *Angew Chem, Int Ed* **40**:487–516.
136. Metzger A, Anslyn EV. 1998. A chemosensor for citrate in beverages. *Angew Chem, Int Ed* **37**(5):649–652.
137. Pederson CJ. 1967. Cyclic polyethers and their complexes with metal salts. *J Am Chem Soc* **89**:7017–7036.
138. Cram DJ. 1988. The design of molecular hosts, guests, and their complexes. *Science* **240**:760–767.
139. Pederson CJ. 1988. The discovery of crown ethers. *Science* **241**: 536–540.

140. Nuccitelli R, ed. 1994. *Methods in cell biology*, Vol. 40: *A practical guide to the study of calcium in living cells*. Academic Press, New York.
141. Minta A, Tsien RY. 1989. Fluorescent indicators for cytosolic sodium. *J Biol Chem* **264**(32):19449–19457.
142. Grynkiewicz G, Poenie M, Tsien RY. 1985. A new generation of Ca^{2+} indicators with greatly improved fluorescence properties. *J Biol Chem* **260**(6):3440–3450.
143. Tsien RY. 1989. Fluorescent indicators of ion concentrations. *Methods Cell Biol* **30**:127–156.
144. Haugland RP. 1996. *Handbook of Fluorescent Probes and Research Chemicals*, 6th ed., pp. 503–584. Molecular Probes Inc., Eugene, OR.
145. Crossley R, Goolamali Z, Sammes PG. 1994. Synthesis and properties of a potential extracellular fluorescent probe for potassium. *J Chem Soc Perkin Trans* **2**:1615–1623.
146. Buet P, Gersch B, Grell E. 2001. Spectral properties, cation selectivity, and dynamic efficiency of fluorescent alkali ion indicators in aqueous solution around neutral pH. *J Fluoresc* **11**(2):79–87.
147. Szmacinski H, Lakowicz JR. 1999. Potassium and sodium measurements in blood using phase-modulation fluorometry. *Sens Actuators B* **60**:8–18.
148. Leray I, Habib-Jiwan JL, Branger C, Soumillion JPh, Valeur B. 2000. Ion-responsive fluorescent compounds, VI: coumarin 153 linked to rigid crowns for improvement of selectivity. *J Photochem Photobiol A: Chem* **135**:163–169.
149. Crossley R, Goolamali Z, Gosper JJ, Sammes PG. 1994. Synthesis and spectral properties of new fluorescent probes for potassium. *J Chem Soc Perkin Trans* **2**:513–520.
150. Golchini K, Mackovic-Basic M, Gharib SA, Masilamani D, Lucas ME, Kurtz I. 1990. Synthesis and characterization of a new fluorescent probe for measuring potassium. *Am J Physiol*, **258**:F438–F443.
151. Szmacinski H, Lakowicz JR. 1997. Sodium Green as a probe for intracellular sodium imaging based on fluorescence lifetime. *Anal Biochem* **250**:131–138.
152. Lakowicz JR, Szmacinski H. 1992. Fluorescence lifetime-based sensing of pH, Ca^{2+}, K^+ and glucose. *Sens Actuators B* **11**:133–143.
153. Meuwis K, Boens N, De Schryver FC, Gallay J, Vincent M. 1995. Photophysics of the fluorescent K^+ indicator PBFI. *Biophys J* **68**: 2469–2473.
154. Valeur B, Bourson J, Pouget J. 1993. Ion recognition detected by changes in photoinduced charge or energy transfer. *ACS Symp Ser* **538**:25–44.
155. Tsien RY, Rink TJ, Poenie M. 1985. Measurement of cytosolic free Ca^{2+} in individual small cells using fluorescence microscopy with dual excitation wavelengths. *Cell Calcium* **6**:145–157.
156. Iatridou H, Foukaraki E, Kuhn MA, Marcus EM, Haugland RP, Katerinopoulos HE. 1994. The development of a new family of intracellular calcium probes. *Cell Calcium* **15**:190–198.
157. Akkaya EU, Lakowicz JR. 1993. Styryl-based wavelength ratiometric probes: a new class of fluorescent calcium probes with long wavelength emission and a large Stokes shift. *Anal Biochem* **213**:285–289.
158. Minta A, Kao JPY, Tsien RY. 1989. Fluorescent indicators for cytosolic calcium based on rhodamine and fluorescein chromophores. *J Biol Chem* **264**(14):8171–8178.
159. Eberhard M, Erne P. 1991. Calcium binding to fluorescent calcium indicators: calcium green, calcium orange and calcium crimson. *Biochem Biophy Res Comm* **180**(1):209–215.
160. Lakowicz JR, Szmacinski H, Johnson ML. 1992. Calcium concentration imaging using fluorescence lifetimes and long-wavelength probes. *J Fluoresc* **2**(1):47–62.
161. Hirshfield KM, Toptygin D, Packard BS, Brand L. 1993. Dynamic fluorescence measurements of two-state systems: applications to calcium-chelating probes. *Anal Biochem* **209**:209–218.
162. Miyoshi N, Hara K, Kimura S, Nakanishi K, Fukuda M. 1991. A new method of determining intracellular free Ca^{2+} concentration using Quin-2 fluorescence. *Photochem Photobiol* **53**(3):415–418.
163. Lakowicz JR, Szmacinski H, Nowaczyk K, Johnson ML. 1992. Fluorescence lifetime imaging of calcium using Quin-2. *Cell Calcium* **13**:131–147.
164. Oguz U, Akkaya EU. 1997. One-pot synthesis of a red-fluorescent chemosensor from an azacrown, phloroglucinol and squaric acid: a simple in-solution construction of a functional molecular device. *Tetrahedron Lett* **38**(25):4509–4512.
165. Akkaya EU, Turkyilmaz S. 1997. A squaraine-based near IR fluorescent chemosensor for calcium. *Tetrahedron Lett* **38**(25):4513–4516.
166. Wahl M, Lucherini MJ, Gruenstein E. 1990. Intracellular Ca^{2+} measurement with Indo-1 in substrate-attached cells: advantages and special considerations. *Cell Calcium* **11**:487–500.
167. Groden DL, Guan Z, Stokes BT. 1991. Determination of Fura-2 dissociation constants following adjustment of the apparent Ca-EGTA association constant for temperature and ionic strength. *Cell Calcium* **12**:279–287.
168. David-Dufilho M, Montenay-Garestier T, Devynck M-A. 1989. Fluorescence measurements of free Ca^{2+} concentration in human erythrocytes using the Ca^{2+} indicator Fura-2. *Cell Calcium* **9**:167–179.
169. Hirshfield KM, Toptygin D, Grandhige G, Kim H, Packard BZ, Brand L. 1996. Steady-state and time-resolved fluorescence measurements for studying molecular interactions: interaction of a calcium-binding probe with proteins. *Biophys Chem* **62**:25–38.
170. Kao JPY. 1994. Practical aspects of measuring [Ca^{2+}] with fluorescent indicators. *Methods Cell Biol* **40**:155–181.
171 Morris SJ, Wiegmann TB, Welling LW, Chronwall BM. 1994. Rapid simultaneous estimation of intracellular calcium and pH. *Methods Cell Biol* **40**:183–220.
172. Scanlon M, Williams DA, Fay FS. 1987. A Ca^{2+}-insensitive form of fura-2 associated with polymorphonuclear leukocytes. *J Biol Chem* **262**(13):6308–6312.
173. Bourson J, Pouget J, Valeur B. 1993. Ion-responsive fluorescent compounds, 4: effect of cation bonding on the photophysical properties of a coumarin linked to monoaza- and diaza-crown ethers. *J Phys Chem* **97**:4552–4557.
174. Dumon P, Jonusauskas G, Dupuy F, Pee P, Rulliere C, Letard JF, Lapouyade R. 1994. Picosecond dynamics of cation-macrocycle interactions in the excited state of an intrinsic fluorescence probe: the calcium complex of 4-(N-monoaza-15-crown-5)-4'-phenylstilbene. *J Phys Chem* **98**:10391–10396.
175. Letard J-F, Lapouyade R, Rettig W. 1993. Chemical engineering of fluorescence dyes. *Mol Cryst Liq Cryst* **236**:41–46.

176. Suzuki Y, Komatsu H, Ikeda T, Saito N, Araki S, Citterio D, Hisamoto H, Kitamura Y, Kubota T, Nakagawa J, Oka K, Suzuki K. 2002. Design and synthesis of Mg^{2+} selective fluoroionophores based on a coumarin derivative and application for Mg^{2+} measurement in a living cell. *Anal Chem* **74**:1423–1428.
177. Watanabe S, Ikishima S, Matsuo T, Yoshida K. 2001. A luminescent metalloreceptor exhibiting remarkably high selectivity for Mg^{2+} over Ca^{2+}. *J Am Chem Soc* **123**:8402–8403.
178. de Silva AP, Nimal Qunaratne HQ, Maguire GEM. 1994. Off-on fluorescent sensors for physiological levels of magnesium ions based on photoinduced electron transfer (PET), which also behave as photoionic OR logic gates. *J Chem Soc Chem Commun* 1213–1214.
179. Pesco J, Salmon JM, Vigo J, Viallet P. 2001. Mag-indo1 affinity for Ca^{2+}, compartmentalization and binding to proteins: the challenge of measuring Mg^{2+} concentrations in living cells. *Anal Biochem* **290**: 221–231.
180. Illner H, McGuigan JAS, Luthi D. 1992. Evaluation of mag-fura-5: the new fluorescent indicator for free magnesium measurements. *Eur J Physiol* **422**:179–184.
181. Morelle B, Salmon J-M, Vigo J, Viallet P. 1993. Proton, Mg^{2+} and protein as competing ligands for the fluorescent probe, mag-indo-1: a first step to the quantification of intracellular Mg^{2+} concentration. *Photochem Photobiol* **58**(6):795–802.
182. Otten PA, London RE, Levy LA. 2001. A new approach to the synthesis of APTRA indicators. *Bioconjugate Chem* **12**:76–83.
183. Shoda T, Kikuchi K, Kojima H, Urano Y, Komatsu H, Suzuki K, Nagano T. 2003. Development of selective, visible light-excitable, fluorescent magnesium ion probes with a novel fluorescence switching mechanism. *Analyst* **128**(6):719–723.
184. Szmacinski H, Lakowicz JR. 1996. Fluorescence lifetime characterization of magnesium probes: Improvement of Mg^{2+} dynamic range and sensitivity using phase-modulation fluorometry. *J Fluoresc* **6**(2): 83–95.
185. Thompson RB, Peterson D, Mahoney W, Cramer M, Maliwal BP, Suh SW, Frederickson C, Fierke C, Herman P. 2002. Fluorescent zinc indicators for neurobiology. *J Neurosci Methods* **118**:63–75.
186. Walkup GK, Burdette SC, Lippard SJ, Tsien RY. 2000. A new cell-permeable fluorescent probe for Zn^{2+}. *J Am Chem Soc* **122**:5644–5645.
187. Burdette SC, Frederickson CJ, Bu W, Lippard SJ. 2003. ZP4: an improved neuronal Zn^{2+} sensor of the zinpyr family. *J Am Chem Soc* **125**:1778–1787.
188. Burdette SC, Walkup GK, Spingler B, Tsien RY, Lippard SJ. 2001. Fluorescent sensors for Zn^{2+} based on a fluorescein platform: synthesis, properties and intracellular distribution. *J Am Chem Soc* **123**: 7831–7841.
189. Nolan EM, Burdette SC, Harvey JH, Hilderbrand SA, Lippard SJ. 2004. Synthesis and characterization of zinc sensors based on a monosubstituted fluorescein platform. *Inorg Chem* **43**:2624–2635.
190. Thompson RB, Maliwal BP, Feliccia VL, Fierke CA, McCall K. 1998. Determination of picomolar concentrations of metal ions using fluorescence anisotropy: biosensing with a "reagentless" enzyme transducer. *Anal Chem* **70**:4717–4723.
191. Thompson RB, Cramer ML, Bozym R, Fierke CA. 2002. Excitation ratiometric fluorescent biosensor for zinc ion at picomolar levels. *J Biomed Opt* **7**(4):555–560.
192. Kawanishi T, Romey MA, Zhu PC, Holody MZ, Shinkai S. 2004. A study of boronic acid based fluorescence glucose sensors. *J Fluoresc* **14**(5):499–512.
193. Cao H, Heagy MD. 2004. Fluorescent chemosensors for carbohydrates: a decade's worth of bright spies for saccharides in review. *J Fluoresc* **14**(5):569–584.
194. James TD, Sandanayake KRAS, Shinkai S. 1994. Novel photoinduced electron-transfer sensor for saccharides based on the interaction of boronic acid and amine. *J Chem Soc Chem Commun* 2:477–478.
195. Yoon J, Czarnik AW. 1992. Fluorescent chemosensors of carbohydrates: a means of chemically communicating the binding of polyols in water based on chelation-enhanced quenching. *J Am Chem Soc* **114**:5874–5875.
196. DiCesare N, Lakowicz JR. 2001. Evaluation of two synthetic glucose probes for fluorescence-lifetime-based sensing. *Anal Biochem* **294**: 154–160.
197. DiCesare N, Lakowicz JR. 2001. Wavelength-ratiometric probes for saccharides based on donor-acceptor diphenylpolyenes. *J Photochem Photobiol A: Chem* **143**:39–47.
198. DiCesare N, Lakowicz JR. 2001. A new highly fluorescent probe for monosaccharides based on a donor-acceptor diphenyloxazole. *Chem Commun* **19**:2022–2023.
199. DiCesare N, Lakowicz JR. 2002. Charge transfer fluorescent probes using boronic acids for monosaccharide signaling. *J Biomed Opt* **7**(4):538–545.
200. DiCesare N, Lakowicz JR. 2001. Spectral properties of fluorophores combining the boronic acid group with electron donor or withdrawing groups: implication in the development of fluorescence probes for saccharides. *J Phys Chem A* **105**:6834–6840.
201. Badugu R, Lakowicz JR, Geddes CD. 2005. Boronic acid fluorescent sensors for monosaccharide signaling based on the 6-methoxyquinolinium heterocyclic nucleus: progress toward noninvasive and continuous glucose monitoring. *Bioorg Med Chem* **13**:113–119.
202. Badugu R, Lakowicz JR, Geddes CD. 2005. Fluorescence sensors for monosaccharides based on the 6-methylquinolinium nucleus and boronic acid moiety: potential application to ophthalmic diagnostics. *Talanta* **65**:762–768.
203. Hellinga HW, Marvin JS. 1998. Protein engineering and the development of generic biosensors. *Trends Biotechnol* **16**:183–189.
204. Sloan DJ, Hellinga HW. 1998. Structure-based engineering of environmentally sensitive fluorophores for monitoring protein-protein interactions. *Protein Eng* **11**(9):819–823.
205. Thompson RB, Maliwal BP, Fierke CA. 1999. Selectivity and sensitivity of fluorescence lifetime-based metal ion biosensing using a carbonic anhydrase transducer. *Anal Biochem* **267**:185–195.
206. Brennan JD. 1999. Preparation and entrapment of fluorescently labeled proteins for the development of reagentless optical biosensors. *J Fluoresc* **9**(4):295–312.
207. Giuliano KA, Taylor DL. 1998. Fluorescent-protein biosensors: new tools for drug discovery. *Trends Biotechnol* **16**:135–140.
208. Shrestha S, Salins LLE, Ensor CM, Daunert S. 2002. Rationally designed fluorescently labeled sulfate-binding protein mutants: evaluation in the development of a sensing system for sulfate. *Biotechnol Bioeng* **78**(5):517–526.

209. Nguyen T, Rosenzweig Z. 2002. Calcium ion fluorescence detection using liposomes containing alexa-labeled calmodulin. *Anal Bioanal Chem* **374**:69–74.
210. Marvin JS, Hellinga HW. 1998. Engineering biosensors by introducing fluorescent allosteric signal transducers: construction of a novel glucose sensor. *J Am Chem Soc* **120**:7–11.
211. Gilardi G, Zhou LQ, Hibbert L, Cass AEG. 1994. Engineering the maltose binding protein for reagentless fluorescence sensing. *Anal Chem* **66**:3840–3847.
212. Tolosa L, Gryczynski I, Eichhorn LR, Dattelbaum JD, Castellano FN, Rao G, Lakowicz JR. 1999. Glucose sensor for low-cost lifetime-based sensing using a genetically engineered protein. *Anal Biochem* **267**:114–120.
213. Marvin JS, Corcoran EE, Hattangadi NA, Zhang JV, Gere SA, Hellinga HW. 1997. The rational design of allosteric interactions in a monomeric protein and its applications to the construction of biosensors. *Proc Natl Acad Sci USA* **94**:4366–4371.
214. Brune M, Hunter JL, Howell SA, Martin SR, Hazlett TL, Corrie JET, Webb MR. 1998. Mechanism of inorganic phosphate interaction with phosphate binding protein from *Escherichia coli*. *Biochemistry* **37**:10370–10380.
215. Lundgren JS, Salins LLE, Kaneva I, Daunert S. 1999. A dynamical investigation of acrylodan-labeled mutant phosphate binding protein. *Anal Chem* **71**:589–595.
216. Wada A, Mie M, Aizawa M, Lahoud P, Cass AEG, Kobatake E. 2003. Design and construction of glutamine binding proteins with a self-adhering capability to unmodified hydrophobic surfaces as reagentless fluorescence sensing devices. *J Am Chem Soc* **125**:16228–16234.
217. Looger LL, Dwyer MA, Smith JJ, Hellinga HW. 2003. Computational design of receptor and sensor proteins with novel functions. *Nature* **423**:185–190.
218. Morii T, Sugimoto K, Makino K, Otsuka M, Imoto K, Mori Y. 2002. A new fluorescent biosensor for inositol trisphosphate. *J Am Chem Soc* **124**(7):1138–1139.
219. Quiocho FA, Ledvina PS. 1996. Atomic structure and specificity of bacterial periplasmic receptors for active transport and chemotaxis: variation of common themes. *Mol Microbiol* **20**(1):17–25.
220. Medintz IL, Anderson GP, Lassman ME, Goldman ER, Bettencourt LA, Mauro JM. 2004. General strategy for biosensor design and construction employing multifunctional surface-tethered components. *Anal Chem* **76**:5620–5629.
221. Wenck A, Pugieux C, Turner M, Dunn M, Stacy C, Tiozzo A, Dunder E, van Grinsven E, Khan R, Sigareva M, Wang WC, Reed J, Drayton P, Oliver D, Trafford H, Legris G, Rushton H, Tayab S, Launis K, Chang YF, Chen DF, Melchers L. 2003. Reef-coral proteins as visual, non-destructive reporters for plant transformation. *Plant Cell Rep* **22**:244–251.
222. Romoser VA, Hinkle PM, Persechini A. 1997. Detection in living cells of Ca^{2+}-dependent changes in the fluorescence emission of an indicator composed of two green fluorescent protein variants linked by a calmodulin-binding sequence: a new class of fluorescent indicators. *J Biol Chem* **272**(20):13270–13274.
223. Miyawaki A, Llopis J, Heim R, McCaffery JM, Adams JA, Ikura M, Tsien RY. 1997. Fluorescent indicators for Ca^{2+} based on green fluorescent proteins and calmodulin. *Nature* **388**:882–887.
224. Nagai T, Yamada S, Tominaga T, Ichikawa M, Miyawaki A. 2004. Expanded dynamic range of fluorescent indicators for Ca^{2+} by circularly permuted yellow fluorescent proteins. *Proc Natl Acad Sci USA* **101**(29):10554–10559.
225. Sato M, Ozawa T, Inukai K, Asano T, Umezawa Y. 2002. Fluorescent indicators for imaging protein phosphorylation in single living cells. *Nature Biotechnol* **20**:287–294.
226. Kawai Y, Sato M, Umezawa Y. 2004. Single color fluorescent indicators of protein phosphorylation for multicolor imaging of intracellular signal flow dynamics. *Anal Chem* **76**:6144–6149.
227. Lin CW, Jao CY, Ting AY. 2004. Genetically encoded fluorescent reporters of histone methylation in living cells. *J Am Chem Soc* **126**:5982–5983.
228. Kalab P, Weis K, Heald R. 2002. Visualization of a ran-GTP gradient in interphase and mitotic xenopus egg extracts. *Science* **295**:2452–2456.
229. Schleifenbaum A, Stier G, Gasch A, Sattler R, Schultz C. 2004. Genetically encoded FRET probe for PKC activity based on pleckstrin. *J Am Chem Soc* **126**:11786–11787.
230. Sato M, Hida N, Ozawa T, Umezawa Y. 2000. Fluorescent indicators for cyclic GMP based on cyclic GMP-dependent protein kinase Iá and green fluorescent proteins. *Anal Chem* **72**:5918–5924.
231. Cano Abad MF, Di Benedetto G, Magalhaes PJ, Filippin L, Pozzan T. 2004. Mitochondrial pH monitored by a new engineered green fluorescent protein mutant. *Biol Chem* **279**(12):11521–11529.
232. Llopis J, McCaffery JM, Miyawaki A, Farquhar MG, Tsien RY. 1998. Measurement of cytosolic, mitochondrial, and golgi pH in single living cells with green fluorescent proteins. *Proc Natl Acad Sci USA* **95**:6803–6808.
233. Kneen M, Farinas J, Li Y, Verkman AS. 1998. Green fluorescent protein as a noninvasive intracellular pH indicator. *Biophys J* **74**:1591–1599.
234. Elsliger MA, Wachter RM, Hanson GT, Kallio K, Remington SJ. 1999. Structural and spectral response of green fluorescent protein variants to changes in pH. *Biochemistry* **38**:5296–5301.
235. Hanson GT, McAnaney TB, Park ES, Rendell MEP, Yarbrough DK, Chu S, Xi L, Boxer SG, Montrose MH, Remington SJ. 2002. Green fluorescent protein variants as ratiometric dual emission pH sensors, 1: structural characterization and preliminary application. *Biochemistry* **41**:15477–15488.
236. Park EJ, Brasuel M, Behrend C, Philbert MA, Kopelman R. 2003. Ratiometric optical PEBBLE nanosensors for real-time magnesium ion concentrations inside viable cells. *Anal Chem* **75**:3784–3791.
237. Brasuel M, Kopelman R, Miller TJ, Tjalkens R, Philbert MA. 2001. Fluorescent nanosensors for intracellular chemical analysis: decyl methacrylate liquid polymer matrix and ion-exchange-based potassium PEBBLE sensors with real-time application to viable rat C6 glioma cells. *Anal Chem* **73**:2221–2228.
238. Clark HA, Hoyer M, Philbert MA, Kopelman R. 1999. Optical nanosensors for chemical analysis inside single living cells, 1: fabrication, characterization, and methods for intracellular delivery of PEBBLE sensors. *Anal Chem* **71**:4831–4836.
239. Clark HA, Kopelman R, Tjalkens R, Philbert MA. 1999. Optical nanosensors for chemical analysis inside single living cells, 2: sensors for pH and calcium and the intracellular application of PEBBLE sensors. *Anal Chem* **71**:4837–4843.

240. Tsagkatakis I, Peper S, Retter R, Bell M, Bakker E. 2001. Monodisperse plasticized poly(vinyl chloride) fluorescent microspheres for selective ionophore-based sensing and extraction. *Anal Chem* **73**:6083–6087.
241. Ji J, Rosenzweig N, Jones I, Rosenzweig Z. 2001. Molecular oxygen-sensitive fluorescent lipobeads for intracellular oxygen measurements in murine macrophages. *Anal Chem* **73**:3521–3527.
242. Ma A, Rosenzweig Z. 2004. Submicrometric lipobead-based fluorescence sensors for chloride ion measurements in aqueous solution. *Anal Chem* **76**:569–575.
243. Tsagkatakis I, Peper S, Bakker E. 2001. Spatial and spectral imaging of single micrometer-sized solvent cast fluorescent plasticized poly(vinyl chloride) sensing particles. *Anal Chem* **73**:315–320.
244. McNamara KP, Nguyen T, Dumitrascu G, Ji J, Rosenzweig N, Rosenzweig Z. 2001. Synthesis, characterization, and application of fluorescence sensing lipobeads for intracellular pH measurements. *Anal Chem* **73**:3240–3246.
245. Ji J, Rosenzweig N, Griffin C, Rosenzweig Z. 2000. Synthesis and application of submicrometer fluorescence sensing particles for lysosomal pH measurements in murine macrophages. *Anal Chem* **72**:3497–3503.
246. Chance B, Leigh JS, Miyake H, Smith DS, Nioka S, Greenfeld R, Finander M, Kaufmann K, Levy W, Young M, Cohen P, Yoshioka H, Boretsky R. 1988. Comparison of time-resolved and –unresolved measurements of deoxyhemoglobin in brain. *Proc Natl Acad Sci USA* **85**:4971–4975.
247. Franceschini MA, Moesta KT, Fantini S, Gaida G, Gratton E, Jess H, Mantulin WW, Seeber M, Schlag PM, Kaschke M. 1997. Frequency-domain techniques enhance optical mammography: initial clinical results. *Proc Natl Acad Sci USA* **94**:6468–6473.
248. Wu J, Perelman L, Dasari RR, Feld MS. 1997. Fluorescence tomographic imaging in turbid media using early-arriving photons and Laplace transforms. *Proc Natl Acad Sci USA* **94**:8783–8788.
249. Weissleder R, Ntziachristos V. 2003. Shedding light onto live molecular targets. *Nature Med* **9**(1):123–128.
250. Godavarty A, Thompson AB, Roy R, Gurfinkel M, Eppstein MJ, Zhang C, Sevick-Muraca EM. 2004. Diagnostic imaging of breast cancer using fluorescence-enhanced optical tomography: phantom studies. *J Biomed Opt* **9**(3):488–496.
251. Kuwana E, Sevick-Muraca E. 2002. Fluorescence lifetime spectroscopy in multiply scattering media with dyes exhibiting multiexponential decay kinetics. *Biophys J* **83**:1165–1176.
252. Mahmood U, Tung CH, Bogdanov A, Weissleder R. 1999. Near-infrared optical imaging of protease activity for tumor detection. *Radiology* **213**:866–870.
253. Becker A, Hessenius C, Licha K, Ebert B, Sukowski U, Semmler W, Wiedenmann B, Grotzinger C. 2001. Receptor-targeted optical imaging of tumors with near-infrared fluorescent ligands. *Nature Biotechnol* **19**:327–331.
254. Ntziachristos V, Schellenberger EA, Ripoll J, Yessayan D, Graves E, Bogdanov A, Josephson L, Weissleder R. 2004. Visualization of antitumor treatment by means of fluorescence molecular tomography with an annexin V-Cy5.5 conjugate. *Proc Natl Acad Sci USA* **101**(33):12294–12299.
255. Bremer C, Tung CH, Weissleder R. 2001. In vivo molecular target assessment of matrix metalloproteinase inhibition. *Nature Med* **7**(6):743–748.
256. Chen J, Tung CH, Mahmood U, Ntziachristos V, Gyurko R, Fishman MC, Huang PL, Weissleder R. 2002. In vivo imaging of proteolytic activity in atherosclerosis. *Circulation* **105**:2766–2771.
257. Graves EE, Ripoll J, Weissleder R, Ntziachristos V. 2003. A submillimeter resolution fluorescence molecular imaging system for small animal imaging. *Med Phys* **30**(5):901–911.
258. Ntziachristos V, Tung C-T, Bremer C, Weissleder R. 2002. Fluorescence molecular tomography resolves protease activity *in vivo*. *Nature Med* **8**(7):757–760.
259. Tung C-H, Bredow S, Mahmood U, Weissleder R. 1999. Preparation of a cathepsin D sensitive near-infrared fluorescence probe for imaging. *Bioconjugate Chem* **10**:892–896.
260. Tung C-H, Gerszten RE, Jaffer FA, Weissleder R. 2002. A novel near-infrared fluorescence sensor for detection of thrombin activation in blood. *Chem Biochem* **3**:207–211.
261. Weissleder R, Tung C-H, Mahmood U, Bogdanov A. 1999. In vivo imaging of tumors with proteas-activated near-infrared fluorescent probes. *Nature Biotechnol* **17**:375–378.
262. Hou W-S, Li Z, Gordon RE, Chan K, Klein MJ, Levy R, Keysser M, Keyszer G, Bromme D. 2001. Cathepsin K is a critical protease in synovial fibroblast-mediated collagen degradation. *Am J Pathol* **159**(6):2167–2177.
263. Suzumori N, Ozaki Y, Ogasawara M, Suzumori K. 2001. Increased concentrations of cathepsin D in peritoneal fluid from women with endometriosis. *Mol Human Reprod* **7**(5):459–462.
264. Oksjoki S, Soderstrom M, Vuorio E, Anttila L. 2001. Differential expression patterns of cathepsins B, H, K, L, and S in the mouse ovary. *Mol Human Reprod* **7**(1):27–34.
265. Hemmila IA. 1992. *Applications of fluorescence in immunoassays*. John Wiley & Sons, New York.
266. Van Dyke K, Van Dyke R., eds. 1990. *Luminescence immunoassay and molecular applications*. CRC Press, Boca Raton, FL.
267. Ozinskas AJ. 1994. Principles of fluorescence immunoassay. In *Topics in fluorescence spectroscopy*, Vol. 4: *Probe design and chemical sensing*, pp. 449–496. Ed JR Lakowicz. Plenum Press, New York.
268. Gosling JP. 1990. A decade of development in immunoassay methodology. *Clin Chem* **36**(8):1408–1427.
269. Davidson RS, Hilchenbach MM. 1990. The use of fluorescent probes in immunochemistry. *Photochem Photobiol* **52**(2):431–438.
270. Vo-Dinh T, Sepaniak MJ, Griffin GD, Alarie JP. 1993. Immunosensors: principles and applications. *Immunomethods* **3**:85– 92.
271. Berson S, Yalow R. 1959. Quantitative aspects of the reaction between insulin and insulin-binding antibody. *J Clin Invest* **38**: 1996–2016.
272. Lovgren T, Hemmila I, Pettersson K, Halonen P. 1985. Time-resolved fluorometry in immunoassay. In *Alternative immunoassays*, pp. 203–217. Ed WP Collins. John Wiley & Sons, New York.
273. Diamandis EP, 1988. Immunoassays with time-resolved fluorescence spectroscopy: principles and applications. *Clin Biochem* **21**:139–150.

274. Lövgren T, Pettersson K. 1990. Time-resolved fluoroimmunoassay, advantages and limitations. In *Luminescence immunoassay and molecular applications*, pp. 234–250. Ed K Van Dyke, R Van Dyke. CRC Press, Boca Raton, FL.
275. Khosravi M, Diamandis EP. 1987. Immunofluorometry of choriogonadotropin by time-resolved fluorescence spectroscopy, a new europium chelate as label. *Clin Chem* **33**(11):1994–1999.
276. Soini E. 1984. Pulsed light, time-resolved fluorometric immunoassay. In *Monoclonal antibodies and new trends in immunoassays*, pp. 197–208. Ed ChA Bizollon. Elsevier Science Publishers, New York.
277. Fiet J, Giton F, Auzerie J, Galons H. 2002. Development of a new sensitive and specific time-resolved fluoroimmunoassay (TR-FIA) of chlormadinone acetate in the serum of treated menopausal women. *Steroids* **67**:1045–1055.
278. Wu F-B, He Y-F, Han S-Q. 2001. Matrix interference in serum total thyroxin (T4) time-resolved fluorescence immunoassay (TRFIA) and its elimination with the use of streptavidin–biotin separation technique. *Clin Chim Acta* **308**:117–126.
279. Ohmura N, Tsukidate Y, Shinozaki H, Lackie SJ, Saiki H. 2003. Combinational use of antibody affinities in an immunoassay for extension of dynamic range and detection of multiple analytes. *Anal Chem* **75**:104–110.
280. Korpimaki T, Hagren V, Brockmann E-C, Tuomola M. 2004. Generic lanthanide fluoroimmunoassay for the simultaneous screening of 18 sulfonamides using an engineered antibody. *Anal Chem* **76**:3091–3098.
281. Korpimaki T, Brockmann E-C, Kuronen O, Saraste M, Lamminmaki U, Tuomola M. 2004. Engineering of a broad specificity antibody for simultaneous detection of 13 sulfonamides at the maximum residue level. *J Agric Food Chem* **52**:40–47.
282. Ullman EF, Schwarzberg M, Rubenstein KE. 1976. Fluorescent excitation transfer immunoassay: A general method for determination of antigens. *J Biol Chem* **251**(14):4172–4178.
283. Schobel U, Coille I, Brecht A, Steinwand M, Gauglitz G. 2001. Miniaturization of a homogeneous fluorescence immunoassay based on energy transfer using nanotiter plates as high-density sample carriers. *Anal Chem* **73**:5172–5179.
284. Schobel U, Egelhaaf H-J, Brecht A, Oelkrug D, Gauglitz G. 1999. New donor–acceptor pair for fluorescent immunoassays by energy transfer. *Bioconjugate Chem* **10**:1107–1114.
285. Qin Q-P, Peltola O, Pettersson K. 2003. Time-resolved fluorescence resonance energy transfer assay for point-of-care testing of urinary albumin. *Clin Chem* **49**(7):1105–1113.
286. Ohiro Y, Arai R, Ueda H, Nagamune T. 2002. A homogeneous and noncompetitive immunoassay based on the enhanced fluorescence resonance energy transfer by leucine zipper interaction. *Anal Chem* **74**:5786–5792.
287. Lee M, Walt DR, Nugent P. 1999. Fluorescent excitation transfer immunoassay for the determination of spinosyn A in water. *J Agric Food Chem* **47**:2766–2770.
288. Oswald B, Lehmann F, Simon L, Terpetschnig E, Wolfbeis OS. 2000. Red laser-induced fluorescence energy transfer in an immunosystem. *Anal Biochem* **280**:272–277.
289. Blomberg K, Hurskainen P, Hemmila I. 1999. Terbium and rhodamine as labels in a homogeneous time-resolved fluorometric energy transfer assay of the β subunit of human chorionic gonadotropin in serum. *Clin Chem* **45**(6):855–861.
290. Dandliker WB, de Saussure VA. 1970. Fluorescence polarization in immunochemistry. *Immunochemistry* **7**:799–828.
291. Spencer RD, Toledo FB, Williams BT, Yoss NL. 1973. Design, construction, and two applications for an automated flow-cell polarization fluorometer with digital read out: enzyme-inhibitor (antitrypsin) assay and antigen–antibody (insulin–insulin antiserum) assay. *Clin Chem* **19**(8):838–844.
292. Kobayashi Y, Amitani K, Watanabe F, Miyai K. 1979. Fluorescence polarization immunoassay for cortisol. *Clin Chim Acta* **92**:241–247.
293. Cox H, Whitby M, Nimmo G, Williams G. 1993. Evaluation of a novel fluorescence polarization immunoassay for teicoplanin. *Antimicrob Agents Chemother* **37**:1924–1926.
294. Mastin SH, Buck RL, Mueggler PA. 1993. Performance of a fluorescence polarization immunoassay for teicoplanin in serum. *Diagn Microbiol Infect Dis* **16**:17–24.
295. Ripple MG, Goldberger BA, Caplan YH, Blitzer MG, Schwartz S. 1992. Detection of cocaine and its metabolites in human amniotic fluid. *J Anal Toxicol* **16**:328–331.
296. de Kanel J, Dunlap L, Hall TD. 1989. Extending the detection limit of the TDx fluorescence polarization immunoassay for benzoylecgonine in urine. *Clin Chem* **35**(10):2110–2112.
297. Uber-Bucek E, Hamon M, Huy CP, Dadoun H. 1992. Determination of thevetin B in serum by fluorescence polarization immunoassay. *J Pharm Biomed Anal* **10**(6):413–419.
298. Klein C, Batz H-G, Draeger B, Guder H-J, Herrmann R. Josel H-P, Nagele U, Schenk R, Bogt B. 1993. Fluorescence polarization immunoassay. In *Fluorescence spectroscopy: new methods and applications*, pp. 245–258. Ed OS Wolfbeis. Springer-Verlag, Berlin.
299. Wang PP, Simpson E, Meucci V, Morrison M, Lunetta S, Zajac M, Boeckx R. 1991. Cyclosporine monitoring by fluorescence polarization immunoassay. *Clin Biochem* **24**:55–58.
300. Winkler M, Schumann G, Petersen D, Oellerich M, Wonigeit K. 1992. Monoclonal fluorescence polarization immunoassay evaluated for monitoring cyclosporine in whole blood after kidney, heart, and liver transplantation. *Clin Chem* **38**(1):123–126.
301. Turek TC, Small EC, Bryant RW, Hill WAG. 2001. Development and validation of a competitive AKT serine/threonine kinase fluorescence polarization assay using a product-specific anti-phospho-serine antibody. *Anal Biochem* **299**:45–53.
302. Martin K, Steinberg TH, Cooley LA, Gee KR, Beechem JM, Patton WF. 2003. Quantitative analysis of protein phosphorylation status and protein kinase activity on microarrays using a novel fluorescent phosphorylation sensor dye. *Proteomics* **3**:1244–1255.
303. Gaudet EA, Huang K-S, Zhang Y, Huang W, Mark D, Sportsman JR. 2003. A homogeneous fluorescence polarization assay adaptable for a range of protein serine/threonine and tyrosine kinase. *J Biomol Screening* **8**(2):164–175.
304. Fiore M, Mitchell J, Doan T, Nelson R, Winter G, Grandone C, Zeng K, Haraden R, Smith J, Harris K, Leszczynski J, Berry D, Safford S, Barnes G, Scholnick A, Ludington K. 1988. The Abbott IMx™ automated benchtop immunochemistry analyzer system. *Clin Chem* **34**:1726–1732.
305. Lang H, Wurzburg U. 1982. Creatine kinase, an enzyme of many forms. *Clin Chem* **28**:1439–1447.
306. Brayne CEG, Calloway SP, Dow L. 1982. Blood creatine kinase isoenzymes BB in boxers. *Lancet* **ii**:1308–1309.

307. Grossman SH. 1984. Fluorescence polarization immunoassay applied to macromolecules: creatine kinase-BB. *J Clin Immunol* **7**:96–100.

308. Charlesworth JM. 1994. Optical sensing of oxygen by fluorescence quenching. *Sens Actuators B* **22**:1–5.

PROBLEMS

P19.1. *Calculation of Lifetimes*: Use the data in Figure 19.13 to calculate the lifetimes of the porphyrin probe at 0 and 20.55% oxygen. The light modulation frequency is 3907 Hz.

P19.2. *Oxygen Diffusion in a Polymer*: Long-lived phosphorescent species can be used as oxygen sensors. Figures 19.79 and 19.80 show emission spectra and intensity decays of camphorquinone in poly(vinyl chloride) and poly(methyl)methacrylate (PMMA). Use the data in these figures to calculate the oxygen bimolecular quenching constant of camphorquinone. Compare this value with that expected for a fluorophore in water, which is near 1 x 10^{10} M^{-1} s^{-1}. Also calculate the diffusion coefficient of oxygen in poly(methyl methacrylate). How does this compare with the value in water, 2.5 x 10^{-5} cm^2/s? Assume that the solubility of oxygen in poly(methyl methacrylate) is the same as in water, 0.001275 M/atm.

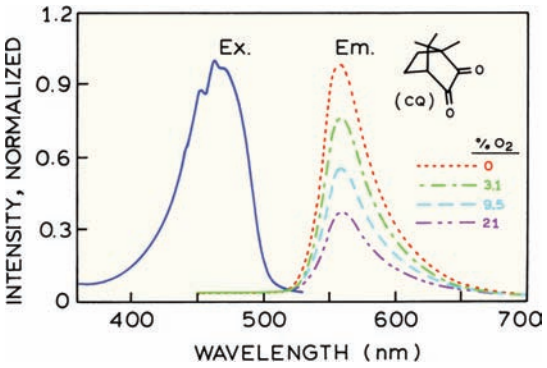

Figure 19.79. Normalized excitation and emission spectra of camphorquinone in poly(vinyl chloride) (PVC) illustrating the effect of oxygen concentration on phosphorescence intensity. Revised and reprinted from [308]. Copyright © 1994 with permission from Elsevier Science.

P19.3. *Lifetimes and Oxygen Quenching*: In Section 19.4.2, we stated that a short-lifetime probe can serve as an intensity reference in an oxygen sensor. Assume that the lifetime of the $[Ru(Ph_2phen)_3]^{2+}$ oxygen sensor is 5 μs and that the lifetime of the reference fluorophore is 5 ns. Using Figure 19.9 describe the relative extents of quenching for each probe?

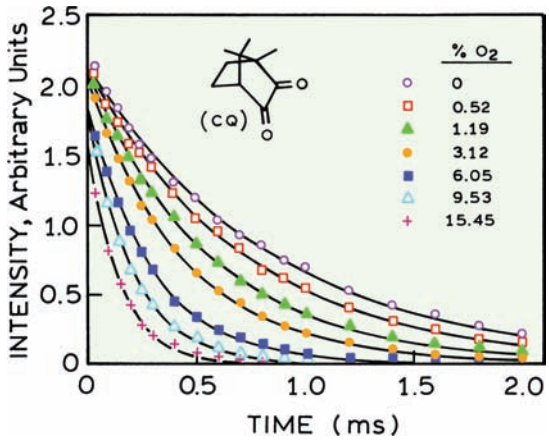

Figure 19.80. Phosphorescence lifetime measurements for camphorquinone in poly(methyl methacrylate) (PMMA), illustrating the influence of oxygen concentration on the triplet decay. The polymeric supports are different in Figures 19.79 and 19.80. Revised and reprinted from [308]. Copyright © 1994 with permission from Elsevier Science.

P19.4. *Mechanism of Sensing*: Figures 19.81 and 19.82 show data for a CO_2 sensor based on RET. Explain the changes in phase angle in response to CO_2. What are the apparent lifetimes of SR101 at 0% and 2% CO_2.

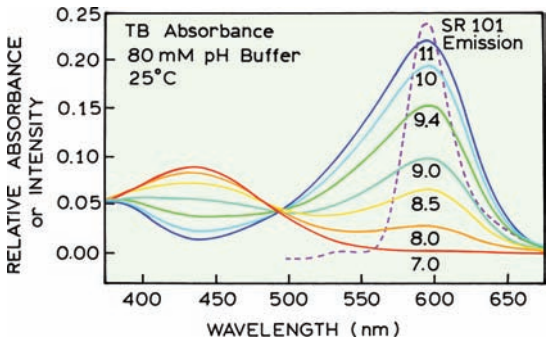

Figure 19.81. Spectral characteristics of the donor and acceptor employed in an RET pCO_2 sensor. The solid curves show the absorption spectra of the Thymol Blue (TB) acceptor at different pH values (labeled on the curves), demonstrating overlap with the emission spectrum of the SR101 donor (dashed). SR101 and TB are present in a polymer matrix, which is weakly buffered and allows penetration of CO_2. From [65].

P19.5. *Fluorescence Polarization Immunoassays and Effects of Resonance Energy Transfer*: Suppose that you are

performing a fluorescence polarization immunoassay for a small peptide with a rotational correlation time (Θ) of 1 ns, and that the peptide (P) is labeled with fluorescein (Fl) for which, $\tau = 4$ ns and $r_0 = 0.40$.

A. What is the range of anisotropy values possible? Assume the antibody (Ab) to the peptide has a rotational correlation time of 100 ns.

B. Assume that your starting assay contains Fl-P bound to Ab, and that upon mixing with the sample 10% of the Fl-P is displaced. What is the anisotropy?

C. Now assume that the antibody is labeled with rhodamine (Rh) so that Fl-P is 90% quenched by RET. What is the anisotropy when 10% of the Fl-P is displaced?

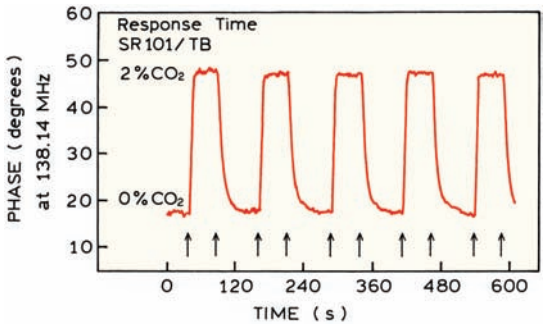

Figure 19.82. Response of an RET pCO_2 sensor employing SR 101 as donor and TB as acceptor to changes in the percentage of CO_2 between 0 and 2%. The phase-angle measurements were made at a light modulation frequency of 138.14 MHz. From [65].